

NCSL INTERNATIONAL

measure®

The Journal of Measurement Science



Vol. 8 No. 2 • June 2013

IN THIS ISSUE:

The Circle Game: The use of the Lunar Distance and Related Measurements for Celestial and Satellite-Based Navigation and Timekeeping

Two-Color One-Way Frequency Transfer in a Metropolitan Optical Fiber Data Network

Experimental and Simulation Study for a Time Transfer Service via a Commercial Geostationary Satellite

A Survey of Time Transfer via a Bidirectional Fiber Link for Precise Calibration Services

**THE VALUE OF
SIMPLIFYING
COMPLEXITY.**

With its intuitive graphics, *Flexible Standards* interface, and live customer support, SureCAL® makes it easy to calibrate a wide range of equipment. It's off-the-shelf software with always-on assistance. *That's why we're leading the way in automated calibration software.*

THE VALUE OF PERFORMANCE.

NORTHROP GRUMMAN

NCSL INTERNATIONAL

measure®

The Journal of Measurement Science



Vol. 8 No. 2 • June 2013

CONTENTS

Welcome to NCSLI Measure, a metrology journal published by NCSL International for the benefit of its membership.

FEATURES

18 SPECIAL FEATURE

The Circle Game: The use of the Lunar Distance and Related Measurements for Celestial and Satellite-Based Navigation and Timekeeping

Daniel G. Jablonski

TECHNICAL NOTES

34 Automatic Calibration of DC Low Level Current Sources and Meters

Dennis W. K. Lee, Y. C. Chau, Aaron Y. K. Yan, H. S. Lam, and Johnny C. Y. Poon

40 Implementation of an Accelerometer Transverse Sensitivity Measurement System

Christiaan S. Veldman

46 Lamp Orientation Dependence of an Integrating Sphere Response for Directional Light Sources in Luminous Flux Measurement

Cheng-Hsien Chen, Bao-Jen Pong, Yuh-Der Jiaan, and Hsiu-Lin Lin

TECHNICAL PAPERS

52 Two-Color One-Way Frequency Transfer in a Metropolitan Optical Fiber Data Network

Sven-Christian Ebenhag, Per Olof Hedekvist, and Kenneth Jaldehag

62 Experimental and Simulation Study for a Time Transfer Service via a Commercial Geostationary Satellite

Jacqueline Walker and Marco Genova

70 A Survey of Time Transfer via a Bidirectional Fiber Link for Precise Calibration Services

Wen-Hung Tseng and Shinn-Yan Lin

DEPARTMENTS

3 Letter From the Editor

4 NMI News

10 Metrology News

78 New Products and Services

80 Advertisers' Index

2014 NCSLI CALL FOR PAPERS

The 2014 NCSLI Symposium offers a great opportunity for you to be recognized by our measurement science industry. The 2014 theme is "Measurement Science and the Environment." More than ever, engineers are being called to develop measurement solutions that can help reduce energy consumption and increase energy efficiency. This includes measurement solutions for energy production and distribution, manufacturing processes and feedbacks, and environmental diagnostics and treatment - all with directly impact on environment.

We encourage engineers, mathematicians, scientists, statisticians, technicians and related personnel to present the results of their research and development work in the areas of measurement science and technology, including but not limited to: traceability, statistical process and evaluation, measurement accuracy and uncertainty analysis; laboratory management and environmental measurement.

You're also encouraged to discuss 2014 Conference topic ideas with us during the upcoming NCSLI Webinar & Symposium, July 16-18, 2013 in Louisville, KY.

GENERAL REQUIREMENTS
Abstracts are required for all proposed papers, panels and workshops.

ABSTRACT REQUIREMENTS AND DEADLINE
Abstracts must be submitted electronically using the NCSLI abstract submission system. Abstracts must be submitted by January 15, 2013. All accepted abstracts will be assigned to a session and presented at the conference. All accepted abstracts will be included in the NCSLI Technical Proceedings. Authors will be provided instructions on how to submit their full paper to the NCSLI Technical Management System. Authors will agree to the terms and conditions of the NCSLI Technical Proceedings.

MANUSCRIPT REQUIREMENTS AND DEADLINE
Manuscripts must be submitted by March 15, 2013. All papers chosen by the technical committee will be invited to submit their manuscripts to be included in the NCSLI Technical Proceedings.

CALL FOR PAPERS
www.ncsl.org/measurement/call-for-papers | **KEYNOTE SPEAKERS**
mark@ncsl.org | **SPONSORSHIP PROGRAM**
sponsorship@ncsl.org | **ADVERTISING OPPORTUNITIES**
advertising@ncsl.org

2014 NCSLI
Call for Papers

Page 32

July 14-18
2013

METROLOGY in A FAST PACED SOCIETY

Workshop & Symposium
NASHVILLE, TN
GAYLORD OPRYLAND CONVENTION CENTER



NCSL INTERNATIONAL
Serving the World of Measurement

NCSL INTERNATIONAL

measure®



The Journal of Measurement Science

NCSL Measure (ISSN #19315775) is a metrology journal published by NCSL International (NCSL). The journal's primary audience consists of practitioners and researchers in the field of metrology, including laboratory managers, scientists, engineers, statisticians, and technicians. *NCSL Measure* provides NCSL members with practical and up-to-date information on calibration techniques, uncertainty analysis, measurement standards, laboratory accreditation, and quality processes, as well as providing timely metrology review articles. Each issue contains peer reviewed metrology articles, new product and service announcements, technical notes, national metrology institute news, and other metrology information. Author instructions are available at www.ncsli.org. If you are interested in submitting new product/service announcements or purchasing advertising, please visit www.ncsli.org for more information.

Managing Editor:

Michael Lombardi, National Institute of Standards and Technology (NIST), USA,
lombardi@ncsli.org

Associate Editors:

Dr. Klaus Jaeger, Jaeger Enterprises, jaegerenterprises@comcast.net

Harry Moody, Harry J. Moody Enterprises, harryjmoody@cs.com

Dr. Leslie R. Pendrill, SP Technical Research Institute of Sweden, leslie.pendrill@sp.se

Dr. Alan Steele, National Research Council of Canada, alan.steele@nrc-cnrc.gc.ca

NMI/Metrology News Editor:

Dr. Richard B. Pettit, Sandia National Laboratories (retired), rangepettit@comcast.net

New Product/Service Announcements & Advertising Sales:

Linda Stone, NCSL International, 2995 Wilderness Place, Suite 107, Boulder, CO
80301-5404 USA, lstone@ncsli.org

Technical Support Team:

Norman Belecki, NIST (Retired), USA

Carol Hockert, National Institute of Standards and Technology (NIST), USA

Dr. James K. Olthoff, National Institute of Standards and Technology (NIST), USA

Dr. Salvador Echeverria-Villagomez, Centro Nacional de Metrologia (CENAM), MX

Dr. Seton Bennett, National Physical Laboratory (NPL), UK

Dianne Lalla-Rodrigues, Antigua/Barbuda Bureau of Standards, Antigua W.I.

Dr. Angela Samuel, National Measurement Institute (NMI), Australia

Pete Unger, American Association for Laboratory Accreditation (A2LA), USA

Dr. Michael Kühne, Bureau International des Poids et Mesures (BIPM), FR

Copyright © 2013, NCSL International. Permission to quote excerpts or to reprint any figures, tables, and/or text from articles (Special Reports/Features, Technical Papers, Review Papers, or Technical Notes) should be obtained directly from the author. NCSL International, for its part, hereby grants permission to quote excerpts and reprint figures and/or tables from articles in this journal with acknowledgment of the source. Individual teachers, students, researchers, and libraries in nonprofit institutions and acting for them are permitted to make hard copies of articles for use in teaching or research, provided such copies are not sold. Copying of articles for sale by document delivery services or suppliers, or beyond the free copying allowed above, is not permitted. Reproduction in a reprint collection, or for advertising or promotional purposes, or republication in any form requires permission from one of the authors and written permission from NCSL International.

Letter From the Editor



Have you ever wondered how clocks all over the world can be synchronized to approximately the same time? If so, you have considered the subject of time transfer. One of the authors contributing to this issue, Dr. Jacqueline Walker of the University of Limerick, aptly notes that the purpose of time transfer is “to provide

accurate time signals, synchronized to a reference clock, to locations distributed across a territory.” Time transfer systems can take many different forms, and their uncertainties can range from seconds to picoseconds. Both wireless and wired mediums are commonly utilized to transfer time. Radio signals that originate from both terrestrial stations and satellites are used to transfer time; as are signals sent via public and private telecommunication networks including the public Internet. The size of the “territory” mentioned by Walker can be as small as a single room, where a group of clocks might be synchronized via a local area network; or as large as the entire Earth and the outer space that surrounds it, as is the case with the Global Positioning System (GPS).

It seems appropriate to consider the iconic scientist Albert Einstein as the father of time transfer. As told in Peter Galison’s excellent book, *Einstein’s Clocks, Poincaré’s Maps* (W. W. Norton & Company, 2003), Einstein was fascinated with clocks. This fascination seemed to intensify when Einstein began working at the Swiss Patent Office in 1902, while still completing his doctoral thesis. In the course of reviewing the patent applications that passed his desk, Einstein was exposed to many ideas from inventors of coordinated time systems. These inventors pursued the same goal; to periodically synchronize each clock in their system to a reference clock, so that all clocks would keep the same time.

In 1905, Einstein published a paper about special relativity, which as Galison notes, became “the best-known physics paper of the 20th century.” The paper’s title when translated to English is “On the Electrodynamics of Moving Bodies” (published in German as “Zur Elektrodynamik bewegter Körper,” *Annalen der Physik*, vol. 17, p. 891, 1905). The word “clock” appears in the paper more than 100 times. Einstein describes a system where a reference clock sends its time to a group of remote clocks, who each use the signal to synchronize. The problem with this system, as Einstein explained, is that clocks close to the reference clock would synchronize before the more distant clocks; therefore true simultaneity would not be achieved. To Einstein, this was unacceptable. He argued that remote clocks should not be synchronized to the time when the reference clock signal was launched, but rather to the time when the signal was launched plus the measurement of “the time occupied in the journey,” or the path delay from clock A to clock B.

These observations form the foundation of all time transfer systems, including GPS, which in many ways is a living embodiment of Einstein’s work. The path delay measurements between clocks are always critical. Even if the reference clock is a “perfect” source of Coordinated Universal Time (UTC), the accuracy of the time transferred to the remote clock can be no better than the uncertainty of the path delay measurement. This simple fact can be thought of as the first rule of time transfer.

This issue of *Measure* includes several papers that highlight new advances in time transfer science. Dr. Walker describes a time transfer system implemented in Europe via a geostationary television satellite. Dr. Wen-Hung Tseng of Telecommunication Laboratories in Taiwan has contributed a review paper about time transfer over optical fibers, a technique that can now provide lower uncertainties than time transfer via satellite. Tseng describes the work currently being done in Taiwan and summarizes recent work performed by other national metrology institutes. Sven-Christian Ebenhag of the SP Technical Research Institute in Sweden describes a frequency transfer experiment conducted via an optical fiber data network, where the frequency signals had to coexist with data and television signals. For frequency transfer, the absolute path delay does not need to be known, but the variations in the path delay must be measured and corrected, as Ebenhag demonstrates.

One of the more captivating aspects of time metrology is its past and present link to navigation systems. GPS, for example, serves as the world’s dominant system for both navigation and high accuracy time transfer. The relationship between time and navigation is explored in a special feature contributed by Dr. Daniel Jablonski of the John Hopkins Applied Physics Laboratory in Maryland. Jablonski tells the remarkable story of how GPS combines the celestial navigation techniques and timekeeping techniques of pioneers such as the astronomer Nevil Maskelyne, the clockmaker John Harrison, the surveyors Mason and Dixon, and the explorers Lewis and Clark. He then examines the measurements collected by Lewis and Clark in 1804 and provides a new analysis of their data. The results may surprise you.

We hope you enjoy this issue, and we always welcome your comments and suggestions.

Sincerely,

A handwritten signature in black ink, appearing to read "Michael Lombardi".

Michael Lombardi
Managing Editor
lombardi@ncsli.org

► HOW TO REACH US

NCSLI Measure, 2995 Wilderness Place, Suite 107, Boulder, CO 80301-5404 USA
www.ncsli.org • measure@ncsli.org

NMI NEWS

NPL Offers Performance Verification of Articulated Arm CMMs

The National Physical Laboratory (NPL) of the United Kingdom now offers a verification service for articulate arm coordinate measurement machines (CMMs) to the *ASME B89.4.22* standard, “Methods for Performance Evaluation of Articulated Arm Coordinate Measuring Machines (CMM).”

Since articulated arm CMMs are portable, their performance must be periodically checked, especially after being transported. NPL can now provide a unique, high accuracy verification service for verifying the performance of Articulated Arm CMMs, delivered using a custom-built verification facility. The procedures are fully compliant with the *ASME B89.4.22* standard that exercises the full range of movement of the arm.

Features of the service include:

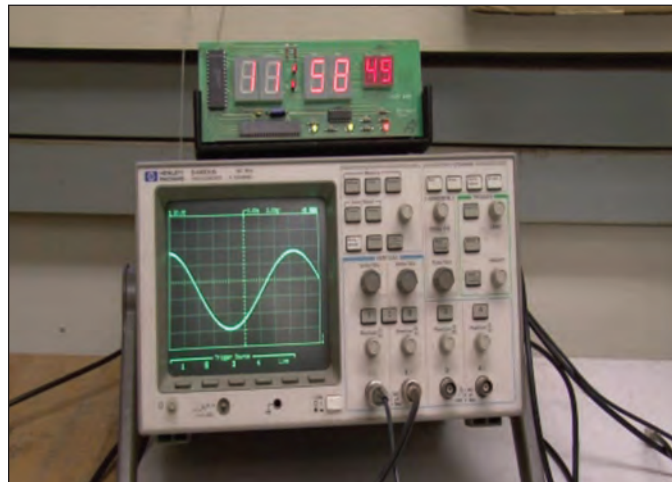
- Pre-check to assess basic performance.
 - Performance verification of all makes of Articulated Arm CMMs to the *ASME B89.4.22* standard within a temperature controlled environment.
 - Determination of effective diameter, single point articulation (SPAT) and volumetric performance.
 - Verification against manufacturer’s in-house procedures.
 - Target turnaround of five working days from delivery to return.
 - Articulated Arm CMMs up to 3.7 m can be verified using the routine service.
 - Performance of larger arms can be verified in accordance with the spirit of *ASME B89.4.22*.
- For more information, visit www.npl.co.uk, or contact Bruce Duncan: bruce.duncan@npl.co.uk

New NIST Time Code Boosts Reception for Radio-Controlled Clocks

The National Institute of Standards and Technology (NIST) is changing the way it broadcasts time signals that synchronize radio controlled clocks and watches to official United States time so that new radio controlled timepieces will be significantly more robust and reliable.

The new time code format not only improves the performance of new radio controlled clocks and watches, but will encourage the development of new timekeeping products that were not practical with the old system because of local interference or other limitations. For example, appliances such as refrigerators, microwave ovens and thermostats, as well as traffic light timers and sprinkler systems, will be able to take advantage of this new phase modulation broadcast.

Low cost radio controlled clocks are popular in the United States, and sold by many retailers. They synchronize themselves by receiving a 60 kHz signal from NIST radio station WWVB in Fort Collins, Colorado. The radio station maintains a time scale that is kept within a few nanoseconds of the official NIST time scale that is located in Boulder, Colorado so the station is able to broadcast a time code that



New changes in the 60 kHz WWVB time signal are visible on the oscilloscope. [Go to NIST website to play video showing waveform variations: nist.gov/pml/div688/wwvb-030513.cfm] Changes in the overall height of the wave are due to amplitude modulation, the method WWVB has always used to encode time information. The flipping of the wave upside down and back again as seen in the video is due to phase modulation, which is now being used to make the signal easier to detect and decode. Credit: Jim Burrus, NIST.

is closely synchronized to the official United States time. However, some radio controlled clocks have difficulty receiving the WWVB time code because of the clock’s location, local radio interference, or low signal strength due to the effects of buildings and other structure. In addition, the signal from time station MSF in the United Kingdom is also at 60 kHz, and has been known to interfere with the WWVB signal at some locations in the eastern United States.

The WWVB time code is sent by varying the amplitude of the signal, known as amplitude modulation (AM). The AM time code remains for the millions of radio controlled clocks already in operation. However, after a lengthy series of test were completed, WWVB began broadcasting a new time code that utilizes phase modulation (PM) in addition to the existing AM time code. Phase modulation encodes an additional layer of information into the broadcast by shifting the phase of the 60 kHz carrier. The inclusion of a PM time code will make it faster and easier for the next generation of radio controlled clocks to detect and decode the time, allowing clocks to work in many locations where they did not work before. Legacy clocks and watches will still continue to receive the AM time code as they have in the past, but will not benefit from the improved performance of the new PM time code. New radio controlled clocks that take advantage of the new PM time code are expected to quickly become available soon, thanks to next generation receiver chips that will begin entering the marketplace in 2013.

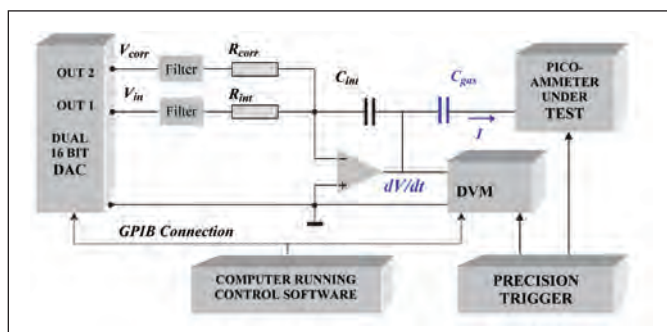
- For more how radio controlled clocks work with WWVB, visit: www.nist.gov/pml/div688/grp40/radioclocks.cfm.



VSL Supports IRMM Measurements for Radionuclide Metrology

The accurate measurement of small electrical currents is essential for the measurement of ionizing radiation as generated by radionuclides. VSL, the Dutch Metrology Institute, has been involved in current measurements as part of the development of a new well-type ionization chamber at the Institute for Reference Materials and Measurements (IRMM). This well-type chamber is meant to replace the "Système International de Référence" (SIR) which the Bureau International des Poids et Mesures (BIPM) facility uses for international comparisons of radioactivity measurements. If constructed according to specifications; this well-chamber should give reproducible results with an uncertainty of 0.1 % for radionuclides emitting gamma rays in the range from 20 keV to 2 000 keV.

To achieve this goal, accurate and traceable measurements of the ionization current are extremely important. For the prototype ionization chamber, background radiation typically produces a current of about 45 fA (10^{-15}), whereas a relatively strong gamma source results in a 1 nA (10^{-9}) current. IRMM contacted VSL to support the development of this part of the project. A generator equivalent to the VSL primary standard for small currents was duplicated and brought to IRMM. The generator generates a very stable and linear voltage ramp dV/dt that is fed to a capacitor, C , in order to convert the voltage to a current: $I = C \cdot dV/dt$. After some initial testing, a two-day training course was organized in order to discuss the details of high-precision small current measurements.



Schematic diagram of the VSL current generator used to calibrate electrometers.

For issues related to small currents, VSL will continue to be involved in the further development of the new realization of the becquerel at IRMM. In this way, VSL's expertise in electrical current measurement has provided a significant contribution to the future international traceability of the becquerel.

- ▶ For more information, contact Helko van den Brom: hvdbrom@vsl.nl

NPL's Operation Contract Will Change in 2014

The UK government has decided not to renew a contract with the private company Serco for the operation of the National Physical Laboratory (NPL) and will instead seek out academic partners to take over the laboratory.



Introducing the New CPC 8000



- 3 transducers to 6k psi & 1 barometer (all removable) ➔ Minimal down time, easy re-calibration
- Total uncertainty to 0.008% IS-33 IntelliScale ➔ Wide calibration range
- Drop-in compatibility ➔ Retrofit with minimal software changes
- Intuitive color touch screen operation ➔ It works like you think
- Precision needle valve regulator ➔ Quiet and stable control

High-End Pressure Controller

www.mensor.com * sales@mensor.com * 800.984.4200

Need a better cold-temperature calibration source?



The 9190A Ultra-Cool Field Metrology Well is the most stable cold-temperature dry-block calibrator on the market.

Don't get snowed by solutions that drift. With the 9190A, temperatures stay stable throughout your entire calibration.

You can be confident your results are accurate.

Wide temperature range from -95 °C to 140 °C
Brackets the coldest and highest temperatures required for pharmaceutical, biomedical and food processing industries

Best-in-class stability: ± 0.015 °C full range
Ideal for applications that demand strict quality control and regulatory process compliance

Get the cold hard facts about the 9190A Ultra-Cool Field Metrology Well at www.flukecal.com/snowman.

Fluke Calibration. Precision, performance, confidence.™

Electrical | RF | Temperature | Pressure | Flow | Software

©2013 Fluke Calibration. Specifications subject to change without notice. Ad 4265040A_EN

FLUKE®

Calibration

NPL is currently a government owned, contractor operated institute and has been run by Serco since 1995. The current contract expires in March 2014 and will not be renewed, according to Minister of State for Universities and Science David Willetts. According to Willetts, the change of ownership will reflect the government's aim to strengthen both fundamental research and engagement with business by applying measurement science to support innovation and growth.

The change is aimed at making better use of the existing facilities and encouraging greater interaction with businesses. Partnering with a university would also enable NPL to set up an institute dedicated to postgraduate research. It was noted that the chosen university would not necessarily have to be a UK institution.

In addition, Willetts stated that NPL Management Limited will remain the employer of staff at the laboratory, although its ownership will change; therefore the change itself will not affect jobs at NPL. It is hoped that by working with an academic partner, an increase in employment opportunities will be realized.

- ▶ For more information, visit: www.npl.co.uk/news/future-operation-of-the-national-physical-laboratory

NIST Large Mass Facility Calibrates 32 500 lb Transfer Standards



Paul Emanuel (left) and Kevin Chesnutwood carefully hoist a container off its floor mount atop the platform of the large-mass balance-beam scale. The reference masses used for the calibration are stacked at the right.

The National Institute of Standards and Technology (NIST) large-mass facility, which was originally designed to enable periodic recalibration of the numerous 50 000 lb masses used in NIST's 4.448 MN (million-pound) deadweight force machine, has quickly acquired a significant customer base from industry. (Note that very large masses are still expressed in pounds for historical reasons.)

Zeina Kubarych, leader of the Mass and Force Group in the Quantum Measurement Division, and her team recently finished calibrating a set of six nuclear waste reference containers (called replica mass standards) ranging from 1 400 lb to 32 500 lb, for U.S. Enrichment Corporation. Those containers will be used as reference calibration standards which will then be used to calibrate working units. The facility has the capability of measuring a 30 000 lb object to an uncertainty of less than 0.1 lb., which is around 3 parts per million (ppm).

Each measurement is corrected for air buoyancy, which is done using a real-time calculation of the air density, which is formulated

from the barometric pressure and relative humidity. The balance-beam scale, which has many, many knife edges, is also affected by the weather and is located in a very stable environment. The balance is rated for a maximum load of nearly 28 000 kg (almost 62 000 lb).

Nuclear canisters, however, are a comparative rarity. Much of the work in the large-mass facility consists of calibrating reference weights which are often deployed in deadweight machines, which are used to calibrate load cells. Kubarych's team calibrated a set of weights and multiple load cells from Boeing which were used as reference standards during the stress tests performed on the airframe of the 787 Dreamliner. Similar jobs have been done for the U.S. Army and the Department of Agriculture.

In 2010, NIST acquired some new standard masses which were all stainless steel that replaced the older large masses which were cast steel. The cast steel masses were not stable over time and needed to be replaced. The process of decommissioning the old masses and calibrating the new standards was finished in December of 2012! With the new standards, and the implementation of statistical process control in all measurements, the group's uncertainties have improved over the past 10 years.

- ▶ For more information, contact Zeina Kubarych at: zeina.kubarych@nist.gov

NPL Develops Portable Digitizers to Monitor the Smart Grid



NPL's SmartPQ Power Quality Analyser with real-time analysis software running on laptop computer.

The National Physical Laboratory (NPL) has ruggedized power metrology so that it can be used in the field. Its briefcase-sized digitizer addresses a need from researchers preparing to convert national power grids into smart grids, where subtle low-order effects have to be measured in the presence of large gross power flows.

The hardware is accurate to around 10 parts per million (ppm) and final accuracy is dependent on what transducer is being used. With Rogowski coils and current shunts up to about 1,000 A, the uncertainty is about 100 ppm for measurements on 415 VAC.

The digitizer has eight isolated channels: three for current, three for voltage, one for neutral, and a spare. The sampling rate is up to 32 kHz, and continuous measurements can be logging over months with no gaps. The digitizer could be left at a site to measure electrical

and power quality parameters continuously over a number of months, with control of the instrument and data collection completed remotely.

On-board power quality algorithms allow real-time continuous measurements of parameters including harmonics, flicker, dips, and swells. Other algorithms cover adaptive noise cancellation, digital filtering, and asynchronous sampling. Crucially for post-measurement analysis, a built-in Global Positioning System (GPS) receiver allows data to be accurately time-stamped. Drift is 3 ppm/°C, input impedance is 10 MΩ, and Rogowski coil integrators are built-in.

Two of the units are already deployed in Sweden to monitor power quality in SwePol, a 255 km high-voltage dc submarine cable between Sweden and Poland. SwePol delivers up to 600 MW at 450 kV and uses static inverters at each end consisting of 792 thyristors arranged in three 16 m high towers. A total of six digitizers have been made so far, with others supplied to national measurement laboratories in Belgium, Denmark, and Turkey.

Under development is the possibility of sending the digitizer to a calibration or testing laboratory and performing a remote calibration of the customer's equipment using Internet control. This will be particularly useful for power quality calibrations in testing laboratories where the circuit impedances has a significant effect on the measurements, something that cannot be taken into account when the customer sends their equipment away for a calibration.

- ▶ For more information, contact Paul Wright at: paul.wright@npl.co.uk
Or visit: www.npl.co.uk/electromagnetics/electrical-measurement/products-and-services/

NIST Tests Underscore Potential Hazards of Laser Pointers

Using a low-cost apparatus designed to quickly and accurately measure the properties of handheld laser devices, National Institute of Standards and Technology (NIST) researchers tested 122 laser pointers and found that nearly 90 % of green laser pointers, and about 44 % of red laser pointers, were out of compliance with Code of Federal Regulations (CFR) safety regulations. In addition, green laser pointers often emitted unacceptable levels of infrared radiation as well.

The NIST tests were conducted on randomly selected commercial laser devices labeled as Class IIIa or 3R and sold as suitable for demonstration use in classrooms and other public spaces. Such lasers are limited under the CFR to a maximum of 5 mw emission in the visible spectrum and less than 2 mw in the infrared spectrum. About half the devices tested emitted power levels at least twice the CFR limit at one or more wavelengths. The highest measured power output was 66.5 mw, more than 12 times the legal limit. The power measurements were accurate to within ±5 %.

Technical staff members from NIST's Laser Radiometry Project built the laser pointer test bed and collaborated with the NIST Office of Safety, Health and Environment on the tests. NIST has provided its data on laser pointer power measurements to the Food and Drug Administration, which regulates laser product safety.

Green laser radiation is generated from infrared radiation. Ideally, the device should be designed and manufactured to confine the infrared radiation within the laser housing. According to the NIST

results, more than 75 % of the devices tested emitted infrared radiation in excess of the CFR limit.

The measurement system consists of a laser power meter and two optical filters to quantify the emissions of visible or infrared radiation. The system was calibrated at NIST. Lens holders ensure repeatable laser alignment, and an adjustable aperture contains the laser radiation around the output end of the laser. The NIST test apparatus was designed so that it can be replicated easily by other institutions using off-the-shelf parts costing about \$2,000.

The results have been published: J. Hadler and M. Dowell, "Accurate, inexpensive testing of laser pointer power for safe operation," *Meas. Sci. Technol.*, vol. 24, no. 4, 045202, March 7, 2013.

- ▶ For more information, contact Joshua Hadler at: joshua.hadler@nist.gov

NPL and Cryogenic Ltd Develop New Cryogenic Current Comparator (CCC)



NPL's Cryogenic Current Comparator.

The National Physical Laboratory (NPL) and Cryogenic Ltd have designed and developed a new Cryogenic Current Comparator (CCC) that provides for the measurement of accurate current ratios. Together with the quantum Hall effect, it allows resistance to be measured to very high accuracy. The CCC is accurate to better than 1 part in 10⁹.

NPL and Cryogenic Ltd have been involved in the development of CCC technology for over two decades. The new system was originally built for NPL, and is used on a daily basis for its measurements. The CCC is now commercially available from Cryogenic Ltd for laboratories that require precise electrical measurements. Cryogenic Ltd has already signed a contract to install one at Singapore's national metrology institute (NMI), where it will underpin all their electrical measurements, including improving the accuracy of temperature measurements, analysis of the super-material graphene, and supporting fundamental physics research.

For a review of the theory, design principles and most common applications of the CCC to electrical metrology, see: J. Williams, "Cryogenic current comparators and their application to electrical metrology," *IET Sci. Meas. Technol.*, vol. 5, no. 6, pp. 211-224, November 2011.

- ▶ For more information, contact Jonathan Williams, NPL, jonathan.williams@npl.co.uk.

**DISCOVER THE
“BLUE BOX”
DIFFERENCE™**

The MI Product you've been waiting for...

FALL 2013



Measurements International
Metrology is Our Science, Accuracy is Our Business™

www.mintl.com



**Since elementary school, you've had
to show your work. Make sure your
calibration provider does too.**

When it comes to calibration, a simple pass/fail answer isn't enough. You need a full report of tests conducted—including accuracy. And if the test results were out of spec, how far? A certificate alone is not the answer to calibration. Ask to see the work.



Understand more about calibration. Scan or visit <http://qrs.ly/2y2kkco> for videos.

© Agilent Technologies, Inc. 2013

**Not all calibrations are created equal,
see why "the work" matters:
www.agilent.com/find/SeeTheWork**

u.s. 1-800-829-4444 canada: 1-877-894-4414

Anticipate — Accelerate — Achieve



Agilent Technologies

NIST/KSU Super-Nanotube Coating Tolerates High Power Laser Radiation

Researchers from the National Institute of Standards and Technology (NIST) and Kansas State University (KSU) have developed a spray-on mixture of carbon nanotubes and ceramic that has unprecedented ability to resist damage while absorbing laser radiation.

Coatings that absorb a high percentage of the energy of high-powered lasers without breaking down are essential for optical power detectors that measure laser output. The new material improves on NIST's earlier version of a spray-on nanotube coating for optical power detectors and has already attracted industry interest. [See *NCSLI Measure J. Meas. Sci.*, "NMI News," vol. 4, no. 3, p. 11, September 2009.]

The composite, which combines the optical, thermal and electrical properties of nanotubes with the robustness of the high-temperature ceramic, was developed by KSU. NIST researchers suggested using toluene to uniformly coat individual nanotubes with a ceramic shell and performed damage studies showing how well the composite tolerates exposure to laser radiation.

The new composite consists of multiwall carbon nanotubes and a ceramic made of silicon, boron, carbon and nitrogen. Boron boosts the temperature at which the material breaks down. Coatings were sprayed on copper surfaces, baked, and then exposed to far-infrared laser radiation of the type used to cut hard materials.

Analysis revealed that the coating absorbed 97.5 % of the radiation and tolerated 15 kw/cm² of laser power for 10 s. This is about 50 % higher damage tolerance than other research groups have reported for similar coatings. The nanotubes and graphene-like carbon absorb radiation uniformly and transmit heat well, while the oxidation-resistant ceramic boosts damage resistance. The spray-on material adheres well to copper surfaces and can be produced easily in large quantities.

Results were published in: R. Bhandavat, A. Feldman, C. Cromer, J. Lehman and G. Singh, "Very high laser-damage threshold of polymer-derived Si(B)CN-Carbon nanotube composite coatings," *ACS Appl. Mater. Interfaces*, vol. 5, no. 7, pp. 2354-2359, March 19, 2013.



Calibration Services You Can Count On

Your laboratory standards are the basis for your organization's most accurate measurements.

Essco is an extraordinarily diverse commercial laboratory serving many industries as well as other laboratories. Our capabilities far surpass that of most commercial laboratories.

Examples of Standards Calibrated

- | | |
|-----------------------------|--------------------------------|
| Multi-Product Calibrators | Super Micrometer™ |
| Measuring Bridges | Gage Blocks |
| Reference Multimeters | Dead Weight Tester |
| High Voltage Dividers | Torque Standards |
| Voltage Standards | Force Standards |
| Standard Resistors | Two-Pressure Humidity Standard |
| Standard Capacitors | Height Gages |
| Standard Inductors | Thread Set Plugs |
| SPRT's/PRT's/RTD's | Measuring Wires |
| Metrology Temperature Wells | Plain Plug & Ring Gages |

Super Micrometer is Trademarked to Pratt & Whitney



Accredited to ISO/IEC 17025:2005 by NVLAP (Lab Code 200972-0). Over 35 metrology technicians on staff.

www.esscolab.com/capabilities/standards

800.325.2201 • Ask about online reporting via EsscoNet

MARTEL
ELECTRONICS

BETA
CALIBRATORS



Ex ia IIB T3 Gb (Ta=-10...+45°C)
KEMA 10 ATEX 0168X 0344
Ex ia IIB T3 Gb (Ta=-10...+45°C)
II 2 G IECEx CSA 10.0013X



CALIBRATE
5X
FASTER

BETAGAUGE
[P1]
MODEL 321A-Ex
[P2] 14.710 Psi
RTD 6.0 Psi
CONFIG LOWER MORE
MARTEL ELECTRONICS

15.833°C

**Also Available in Single Sensor
BetaGauge 311A-Ex**

**BetaGauge™ 321A-Ex
Dual Sensor**

Intrinsically Safe for Use in Hazardous Areas

- Accuracy: $\pm 0.025\%$
- ClearBrite™ LCD Display
- 25 Pressure Ranges
- Single or Dual Sensor
- Pt100 RTD Connector
- Read mA
- 3 Key Martel Menu System
- NIST Traceable Calibration

Martel Electronics Corporation

Tel: 800-821-0023 / 603-434-1433

sales@martelcorp.com

www.martelcalibrators.com

Under Pressure To Calibrate Faster?



Make Connections Fast, Calibrate Faster!

- For transmitters, gauges and pressure sensing instruments
- No wrenches or thread sealants
- Eliminates thread damage
- Reduces contamination risks
- Twist-to-connect, sleeve and handle actuated connectors save time
- Leak-tight sealing from vacuum to 10,000 psi
- 1/8" to 1/2" NPT, AN37° flare, sanitary style flange and metric with additional sizes available



Improve your lab efficiency—calibration connection manifold for calibration of up to four instruments simultaneously!

www.fastestinc.com
800.444.2373

FastTest®
Your Productivity Connection



ACTUAL TYPE A MEASUREMENT
RESULTS SCREEN CAPTURE!

CPEM JULY 2012

SHOW FLOOR DEMONSTRATION

10 $\mu\Omega$ @ 1,000 ADC

<1 PPM - TYPE A RESULTS



**2.5 DAYS • 1,000 A_{DC} CONTINUOUS • 10 $\mu\Omega$ • 23°C ± LOTS
MEASUREMENT RESULTS TYPICALLY < 0.5 PPM**

YOU'D SMILE TOO WITH MEASUREMENTS LIKE THESE!

FOR MORE INFORMATION ABOUT THESE TESTS OR ANY OF OUR WORLD LEADING STANDARDS
CONTACT GUILDLINE @

WEB: WWW.GUILDLINE.COM

EMAIL: SALES@GUILDLINE.COM

TOLL FREE: (800) 310-8104

GUILDLINE
INSTRUMENTS

METROLOGY NEWS

MATHMET 2014 Set for March 2014

MATHMET 2014, an international workshop on mathematics and statistics for metrology, is a forum for statisticians, mathematicians and metrologists to present and discuss modern methods for data analysis and modeling in various applications of metrology. The workshop will be held at Physikalisch-Technische Bundesanstalt (PTB) Berlin on March 24 to 26, 2014. Topics of discussion include:

- Measurement Uncertainty
- Statistical Calibration and Regression Problems
- Modeling and Inverse Problems
- Uncertainty Quantification for Computationally Expensive Models
- Statistical Methods for Interlaboratory Comparisons and Conformity Assessment
- Statistical Methods for Biochemistry

Abstracts (up to 500 words) should be sent by email to MATHMET2014@ptb.de (with copies to the three organizers: Markus.Baer@ptb.de; Clemens.Elster@ptb.de; and Antonio.Possolo@nist.gov). The submission deadline is July 1, 2013.

- ▶ For more information, visit: www.ptb.de/cms/fachabteilungen/abt8/fb-84/mathmet-2014.html

Information on the previous workshop, MATHMET 2010, including copies of presentations, can be obtained from: www.ptb.de/cms/fachabteilungen/abt8/fb-84/mathmet-2010.html

Positive Response to EURAMET's Survey on European Metrology Research

Results from the public consultation on the future direction of European metrology research under Horizon 2020, the European framework program for research and innovation, have been published by the European Association of National Metrology Institutes (EURAMET). The survey offered individuals and organizations the opportunity to give their views on the current state of metrology research in Europe and the challenges it faces.

An analysis of the 624 responses, from 27 EU countries and 10 countries outside the EU, indicated that 97 % of the participants think that metrology research is either very relevant or relevant for addressing grand societal challenges, enhancing European competitiveness, and supporting European policies, standardization and regulations. In addition, the responses indicated a clear preference for a new, reinforced Article 185 initiative under Horizon 2020. Ninety-two percent of the respondents were of the opinion that the current research initiative, European Metrology Research Programme (EMRP), should be continued by its replacement, the European Metrology Programme for Innovation and Research (EMPIR).

Dr. Kamal Hossain, Chairperson of EURAMET and NPL's Director, Research & International, commented: "For EURAMET the evaluation was a crucial step in judging support for EMPIR. We are happy that so many of our stakeholders have supported us and we thank them for their contributions."

- ▶ For a copy of the full report, visit: <http://ec.europa.eu/research/consultations/pdf/empir-survey-final-report.pdf>

Update on GPS Jamming in the United Kingdom

The first profile of the perpetrators of Global Positioning System (GPS) jamming on British roads, presented at the recent *GNSS Vulnerabilities 2013: Countering the Threat Conference*, confirms that small devices, available online for as little as £30, rather than extreme solar weather, pose the greatest threat to navigation and timing signals in the UK. The conference was held February 13, 2013 at the National Physical Laboratory (NPL).

Data obtained from a suite of detectors deployed close to a busy airport indicate as many as 10 interference events per day. The peaks in activity during the week and a lack of hits on the weekend strongly indicate it is human activity which is the primary cause. The peaks during the times of rush hour traffic suggest the main users of jammers are commercial drivers of company vehicles rather than organized criminal gangs who have been caught with jammers. Thus, the jamming is most likely the evasion of tracking within commercial vehicles for moonlighting activities or for other non-work purposes.

In tests conducted using interference simulations on a variety of marine grade receivers used in most commercial shipping vessels, these results were obtained:

- When simulating intense solar activity, the threat only resulted in minor signal interference and no complete outages for any of the tested marine receivers.
- When using even the cheapest jammers, there were complete outages across all receivers currently on the market. Some were jammed without the users even knowing and continued to give results which were inaccurate, potentially leaving shipping at risk of grounding or collision.

In order to combat these issues, there is a new type of jamming-proof receiving system for the shipping industry under development. The new receiving system can switch automatically and seamlessly to eLoran should the GPS signal be lost.

More information on this topic was presented at the *7th GNSS Vulnerabilities and Solutions Conference* held April 18-20, 2013 in Baška, Krk Island, Croatia. The conference was cosponsored by The Royal Institute of Navigation, London, UK and the Faculty of Maritime Studies, University of Rijeka, Croatia.

Force Calibration Service

The uncertainty of the instrument calibrated is directly influenced by the measurement certainty of the calibration standard



120,000 lbf
Morehouse Dead Weight Machine

Morehouse force calibrations are performed using standards with the highest level of measurement certainty:

- ▶ Dead Weights with accuracy of 0.002% of applied force used for calibrations through 120,000 lbf
- ▶ United States National Institute of Standards & Technology (NIST) calibrated standards
- ▶ Calibrations performed in our laboratory to 2,250,000 lbf in compression and 1,200,000 lbf in tension and equivalent kgf and Newtons
- ▶ Calibrations performed in accordance with the American Society for Testing and Materials (ASTM) E74, ISO 376, and other specifications
- ▶ Calibration for Proving Rings, Load Cells, Crane Scales, Force Gauges and other force measuring instruments



ISO 17025 Accredited
American Association of Laboratory Accreditation Calibration Cert 1398.01



2,250,000 lbf
Morehouse Universal Calibrating Machine

Torque Calibrations accurate to 0.002% of applied torque to 2,000 N·m also available

MOREHOUSE FORCE & TORQUE CALIBRATION LABORATORIES

Phone: 717-843-0081 / Fax: 717-846-4193 / www.mhforce.com / e-mail: hzumbrun@mhforce.com

Morehouse INSTRUMENT COMPANY, INC.
1742 Sixth Avenue • York, PA USA

Humidity is a Tough Measurement

/VAISALA MAKES IT EASIER

Humidity measurement is called for in a wide variety of industrial applications and each application has a different set of requirements for humidity instruments. Download our toolkit for valuable utilities like a Calibration Book, Humidity Formulas, App Notes, FAQ's and more...

Download our **FREE** Humidity Measurement Toolkit:
www.vaisala.com/humiditytoolkit

Visit us at NCSL 2013 - Booth 1011



www.vaisala.com/humiditytoolkit

VAISALA

U.S. Army Developing Transportable Quantum Voltage Standard



Prototype portable QVS system under development by the U. S. Army. The equipment rack on the right contains the cryogenic refrigerator, voltage array, electronics, and control computer. Several solid state voltage standards being calibrated are on the bench behind the QVS. (Photo by J. Ball, U. S. Army)

The U. S. Army is currently testing and evaluating a compact, transportable, cryogenically refrigerated Josephson Array voltage calibration system. The system is being developed through the U. S. Army Product Director for Test, Measurement, and Diagnostic Equipment (TMDE) Calibration Sets Program.

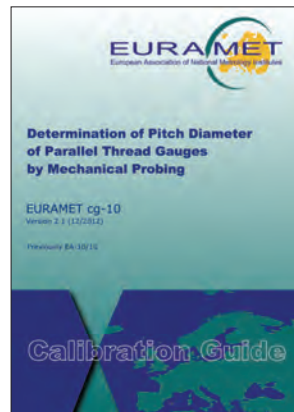
The quantum voltage standard (QVS) is based on the Josephson effect which has been used for more than two decades to generate precise DC voltages. However, the expense, delicacy and complexity of such systems have made them impractical to apply, except at national metrology institutes, primary standards laboratories, and research centers. Most QVS systems consume liquid helium to cool the Josephson Junction Array element. Helium is expensive and not always readily available.

The system shown in the photograph represents a significant step toward the development of a practical QVS system that could allow the Army to put a QVS system wherever in the world it might be needed to calibrate TMDE. The system is completely contained in a standard wheeled instrument rack, plugs into a 110 VAC receptacle, and draws only about 1,500 W. The use of cryogenic refrigeration eliminates the need for liquid helium. Everything required to perform voltage calibrations is contained in the rack, including a printer for calibration reports.

The system's operating range is from -10 V to +10 V. Preliminary performance comparisons by researchers at the US Army Primary Standards Laboratory (APSL) indicate no measurable difference between the new QVS and the Army's primary voltage standard, which is a conventional, liquid helium-cooled Josephson Voltage system. Both systems use a HYPRES all-Niobium superconducting Josephson Junction array integrated circuit as the primary element.

- ▶ For more information, contact Michael Louque at: michael.f.louque.civ@mail.mil

EURAMET Guide 10 Updated (Pitch Diameter)



European Association of National Metrology Institutes (EURAMET) Calibration Guide 10 "Determination of Pitch Diameter of Parallel Thread Gauges by Mechanical Probing" has been updated and published in Version 2.1. The document can be downloaded from the EURAMET website: www.euramet.org/index.php?id=calibration-guides

There are two changes in Version 2.1 (on pages 7 and 13): (1) A new equation for the corrections to be applied for angle deviation, under the calculation of the virtual pitch diameter; (2) the calculation of the sensitivity parameter associated with the uncertainty of measurement of the flank angle. The differences to the previous Version 2.0 are available under the *Former Versions of Calibration Guides* on the EURAMET website.

- ▶ To subscribe to receive information about updates of EURAMET Calibration Guides, visit: www.euramet.org/index.php?id=1599

CPEM 2014 to be Held in Rio de Janeiro, Brazil



The 2014 Conference on Precision Electromagnetic Measurements (CPEM 2014) will be hosted by the Instituto Nacional de Metrologia, Qualidade e Tecnologia (INMETRO) in Rio de Janeiro, Brazil, in cooperation with the Instituto Nacional de Tecnologica Industrial (INTI). The conference chairman is Humberto Brandi of INMETRO.

CPEM is devoted to topics related to electromagnetic measurements, from dc through the optical region. A major focus of CPEM 2014 will be quantum devices that relate electrical standards to fundamental constants and the International System of Units (SI).

Summary papers, consisting of two pages and two column format, describing original work should be submitted by the February 15, 2014 deadline. All papers will be reviewed and those accepted assigned for either oral or poster presentation. Authors will be notified of acceptance by April 15, 2014 and are encouraged to submit extended papers to a special issue of *IEEE Transactions on Instrumentation and Measurement*.

- ▶ For more information, visit: www2.inmetro.gov.br/cpem2014/

U. S. to Celebrate World Standards Day on October 3, 2013

Voluntary consensus standards play an essential role in promoting quality, consistency, and dependability across a vast array of industries, providing major benefits to the global economy and to the lives of people around the world. This year's U. S. Celebration of World Standards Day – "Standards for a World at Work and Play" – will focus on how standards bring confidence to businesses, governments, and consumers, impacting reliability from farm to table, manufacturer to retailer, and workplace to home.

Standards facilitate technological innovations and foster evolving social and environmental compliance practices that increase the health and safety of the world and its citizens. They are the foundation upon which developing nations build their economies and compete in the global market. Developed by collaborative bodies that act as forums for the public and private sectors to come together for a common good, standards evolve to meet the changing needs of a world at work and play.

In celebration of the critical role of standards, leaders of business, industry, academia, and government will gather in Washington, DC, on Thursday, October 3, 2013, for the U. S. Celebration of World Standards Day. The event is co-chaired each year by the American National Standards Institute (ANSI) and the National Institute of Standards and Technology (NIST). The Toy Industry Association (TIA) will serve as the administrating organization for this year's event.

- ▶ For more information, visit: gsi.nist.gov/global/index.cfm/L1-7/L2-48/A-700/



ISOTECH

The World Leader in Temperature Metrology

Isothermal Technology Limited (Worldwide)
 Web-site: www.isotech.co.uk
 E-mail: info@isotech.co.uk
 Phone: +44 (0) 1704 543830

Isotech North America (The Americas)
 Web-site: www.isotechna.com
 E-mail: sales@isotechna.com
 Phone: +(802) 863-8050

New





Key Features...

- Accuracy to 5mk (0.005°C) Over Full Range
- All Sensor Types
- USB Host: Mouse, Keyboard, Memory Stick
- Graphical Display
- 4-20mA Current Loop
- Data Logging
- Portable, Only 5 Pounds

**millisKanner
(Channel Expander)**

- Expands milliK to a maximum of 33 Channels
- Supports SPRTs, PRTs, Thermistors and TC
- Universal Inputs for Flexibility



For PRTs, TCs & Thermistors

The Circle Game: The use of the Lunar Distance and Related Measurements for Celestial and Satellite-Based Navigation and Timekeeping

Daniel G. Jablonski[†]

Abstract

The determination of a position on the Earth's surface depends critically on the mathematics and measurement of circles as functions of time, distance, and angle. The multi-century history of this topic has led us to the world's significant dependence on the Global Positioning System (GPS) and other satellite navigation systems. Based on a simple paradigm, the problem of solving three equations in three unknowns, we revisit the history of Maskelyne and Harrison and the Longitude prize; the survey of the Maryland-Pennsylvania border by Mason and Dixon; the vicissitudes of Lewis and Clark; and the development of GPS. In particular, we reanalyze the measurements made by Lewis and Clark on June 2, 1804 in light of the recent (2000) analysis of these data by Bergantino and Preston. We show that this analysis, when viewed retrospectively, provides insight into the manner in which GPS combines the techniques of Maskelyne and Harrison, Mason and Dixon, Ellicott and Patterson, and Lewis and Clark. We then re-evaluate the celestial measurements of Lewis and Clark and provide some new analyses of their data.

1. Introduction and Summary

As a result of the popular book *Longitude*, by Dava Sobel [1], there has been widespread interest in the story of John Harrison and his development of a portable chronometer suitable for celestial navigation during long voyages at sea. As recounted by Sobel and others, Harrison's efforts to win the famous Longitude Prize were foiled by the activities of Sir Nevil Maskelyne, England's Royal Astronomer.

Sir Nevil apparently favored the use of lunar distances for determining Greenwich, or Universal Time (UT), from any point on the surface of the Earth, without the need for an accurate chronometer.¹ This technique requires accurate knowledge of the motion, as functions of time, of the Sun, Moon, and stars. To this end, in 1766 Sir Nevil published the first *Nautical Almanac*. The *Nautical Almanac* is still published annually as a joint product of the United States and England, and the 1804 edition of the Almanac was recently reprinted [2].

Between 1763 and 1767, Maskelyne directed, from afar, the work by Charles Mason and Jeremiah Dixon to use astronomical observations to survey the boundary between Pennsylvania and Maryland. This put him in the interesting position of becoming an expert on three related techniques for celestial navigation and surveying:

1. Navigation using UT. This requires, for the timekeeping portion of the sextant-based celestial observations, the use of a Harrison-type chronometer that maintains its accuracy over a period of months.
2. The use of delta-time measurements for relative navigation and surveying. This requires a stopwatch that is accurate for minutes at a time. Mason and Dixon used this technique to survey the Maryland-Pennsylvania border, but only for the purpose of determining the direction of true North with high precision.

3. The use of parallax-based algorithms in conjunction with lunar observations for time-based navigation when a stopwatch accurate for several hours, but not a chronometer, is available.² This extension of method 2 is called the method of lunars; and requires simultaneous measurements of the angle subtended by the Moon and Sun (called the lunar distance) and the elevation angles of both the Moon and Sun above the horizon. This provides a means of aligning the stopwatch with UT and for correcting refraction and parallax errors associated with the optical measurements. However, the stopwatch time must also be correlated to local time. This is done typically by recording the time displayed by the watch at local noon on the day of the lunar observation.³ Using this combination of data, it is possible to derive values for both latitude and longitude.

Twenty-five years after the Mason-Dixon survey, from 1791-92, Andrew Ellicott and Benjamin Banneker used the Mason-Dixon techniques to survey the city of Washington, in the District of Columbia. Then, in 1803, Andrew Ellicott and Robert Patterson taught Maskelyne's technique for measuring lunar distances to Captain Meriwether Lewis. This was done at the request of President

[†] This contribution reflects the views solely of the author, and not those of the Johns Hopkins University or the Applied Physics Laboratory.

¹ Although a reasonably accurate stopwatch is needed.

² Parallax is the angle measurement error, with respect to a coordinate system whose origin is at the center of the Earth, caused by making the measurement at the surface of the Earth.

³ For the special case when a lunar distance can be and is measured at local noon, $\Delta t = 0$ and it could be argued that a time measurement of any sort is unnecessary. However, the determination of the local time of noon by a single measurement, at noon, is far less accurate than the determination of local noon by interpolation or extrapolation of delta-time measurements.

Jefferson. During their expedition, Lewis and his friend and associate William Clark used a hybrid combination of techniques 2 and 3 to gather the data necessary for determination of latitude and longitude. They used Mason's method of equal altitudes to determine latitude and the clock time of local noon, and measurement of the lunar distance to permit a later, post-processed determination of UT, and hence longitude. However, they did not measure the requisite elevation angles of the Sun and Moon above the local horizon.

As discussed by Preston [3], the algorithms required to reduce the data to produce a value for longitude were considered too complicated to be undertaken routinely during the course of the expedition. After the expedition, preliminary attempts to use the data were unsuccessful, with the reason historically being attributed to the lack of the necessary elevation angle measurements that are considered an essential part of the lunar distance technique.

Bergantino [4], and then Preston, show that this is not the case. They conclude that Lewis and Clark (L&C) were not negligent. Instead, they note that L&C, likely at the instruction of Ellicott, realized that these elevation measurements were not necessary. And, as noted in their journals, the need to use a double angle technique in conjunction with an artificial horizon, due to the unavailability of a clear view of the land horizon, made the elevation measurements impractical. This is because the artificial horizon technique does not work well except for measuring the Sun during broad daylight.⁴

Bergantino and Preston then demonstrated that only three data points, namely latitude, delta-time, and the lunar distance, are adequate for using a gradient descent algorithm to compute a value for longitude that is self-consistent with all of the observed data. Preston further

extended the unpublished work of Bergantino by computing latitudes and longitude values for all of the sites for which the celestial data are included in the *Journals of the Lewis and Clark Expedition* [5]. The story might end here, except that Bergantino visited these sites in order to determine their correct latitudes and longitudes to a precision of 1 minute of arc. This was possible because of the copious descriptive detail in the *Journals* of permanent geographical and historical features at each site.⁵

Based on this information, Preston tabulated the differences between the modern coordinates (latitude/longitude) of these positions and the coordinates he computed using the celestial data gathered by L&C and the members of their expedition. As expected, there are differences between the "true" latitude/longitude values and the computed values. The discrepancies are of the order of 5 minutes of arc and more, but are small enough to be attributed to ordinary measurement errors. These include the effects of cloudy or otherwise unsatisfactory measurement conditions, inaccurate values for the index errors for the instruments being used, and ordinary measurement error.

However, Preston also discusses his nagging feeling that there is a systematic bias error in the results, particularly for latitude, that is of the order of 5 minutes of arc. Yet he retires the discussion with the observation that precise measurement of lunar distances using a hand held sextant is difficult, and that the accuracy of the resulting latitude/longitude estimates are consistent with these presumed errors.

⁴ Mason and Dixon used a tripod mounted transit that could be carefully leveled in lieu of a hand-held sextant that requires a clear view of the horizon. Had Lewis and Clark had such an instrument, many of the measurement difficulties they encountered would have been avoided.

⁵ Permanent geographic features are typically described in significant detail, and historical features such as Native American burial mounds still survive.

Pressure Calibration Equipment for Laboratory and Field



- Fully automated pressure calibrator with built-in pressure generator/ controller to 375 psi (25 bar)
- 0.02%FS accuracy
- Dual pressure modules
- Portable (12 lb)



Pressure Calibrators
Ranges to 36,000 psi
24V loop power, measure mA or V with HART capability



Digital Pressure Test Gauges
Ranges to 36,000 psi
0.025%FS, 0.05%FS, 0.1%FS or 0.2%FS



Additel Pressure Test Pumps
Hydraulic or pneumatic
Handheld, portable or bench-top
Maintenance free



Documenting Process Calibrator
Multifunction Process Calibrator
User friendly interface
Smartphone-like menu

Tel: (714) 998-6899 sales@additel.com www.additel.com

22865 Savi Ranch Parkway Ste F, Yorba Linda, CA 92887, USA





Figure 1. A sextant, showing the protractor gauge, adjustable and fixed mirrors, and solar filters. This particular instrument is fitted with a “bubble horizon”, permitting its use at night in aircraft when no horizon is visible. Many modern aircraft still have “sextant ports”, windows that facilitate observations of the night sky.

Even so, the L&C data support results that are well within the half-degree, 30 minutes of arc requirement that John Harrison faced in his nearly lifelong pursuit of the Longitude Prize. The use by Lewis and Clark of a delta-time technique in lieu of a Harrison style absolute time technique, along with their adaptation of the method of lunars to eliminate the need for the additional horizon measurements, is a remarkable achievement.

Despite this, there is a feature of the results in Preston’s article [3] that hints at something more subtle. Specifically, the calculated latitude and longitude values, based on the L&C data, deviate from the correct values obtained by Bergantino [4] in a manner that is characteristic of some gradient-descent algorithms. This is particularly the case for algorithms in which “slack values” are introduced, which is the situation for the Preston algorithm.⁶

Of particular interest, Preston loads his algorithm with estimates for the unmeasured elevation values of the Sun and the Moon that are required for the traditional method of lunars. He then uses an iterative technique to find a multivariable solution that, upon iteration, reaches a stationary, self-consistent result that is plausibly correct. However, the problem is nonlinear. And, by adding slack variables, the reverse computation of time and longitude becomes under-constrained.

To explore the implications of this, a reanalysis of the problem has been conducted using Preston’s location results to recalculate his starting data. This “forward” computation is single-valued, non-iterative, and highly stable. The resulting putative values are then

compared with the actual measurements tabulated in the *Journals of the Lewis and Clark Expedition* [5] – the same values that Preston started with. The focus is on the data of June 2, 1804, when the expedition was camped at the confluence of the Osage and Missouri Rivers. This perhaps paradoxical approach doesn’t replace the Preston algorithm. Instead, it extends it by providing a methodology for pushing the algorithm harder, reducing the likelihood of artifacts, and squeezing more information from the available data.

The results suggest that Preston was too pessimistic in his assessment of Lewis and Clark’s measurement skills, and that their measurements come closer to predicting the expedition’s correct location on June 2, 1804 than has been previously realized.

To better understand this work, it is helpful to first review some of the features and mysteries of celestial navigation. Andrew Ellicott, and Benjamin Banneker, using many of the same astronomical techniques as those of Mason and Dixon and Lewis and Clark, used the stars to survey the city of Washington, D.C. The results of their work survive in plain sight for everyone to see, and illustrate some important technical points for the discussion that follows.

2. Fundamentals of Celestial Navigation

Celestial navigation is based on the location in the sky of the stars and planets, as measured by azimuth and elevation angles, as a function of date, time, and one’s location on (or above) the surface of the Earth. The stars have permanent “addresses” relative to the Earth and the Sun, namely their sidereal hour angle (SHA) and declination, whereas the planets “wander” among the stars, and their corresponding “addresses” vary with time.⁷

⁶For example, slack variables are used in the simplex algorithm for linear programming in order to provide a properly conditioned set of linear equations.

⁷The origin of the word “planet” implies such wandering.

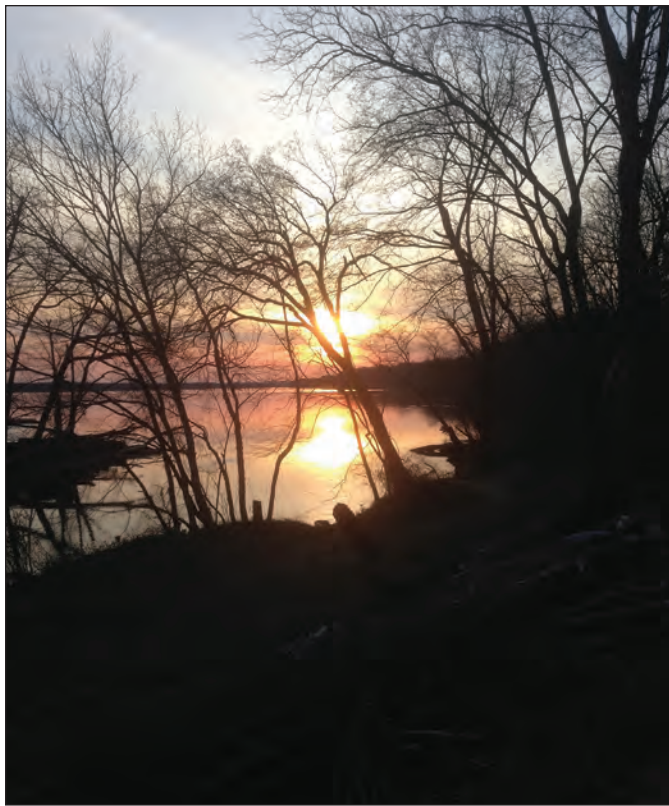


Figure 2a. Use of the Potomac River as an artificial horizon.

The location of the Sun, star, or planet as viewed from any point on Earth can be represented by its elevation angle above the local horizon, specified as H , and its azimuth angle Z , the latter measured with respect to geographic (not magnetic) north. The elevation angle is typically measured using a sextant (Fig. 1). This is nothing more than a clever mechanical protractor in which the horizon is viewed directly, and the celestial object viewed by double reflection from two mirrors. By adjusting the angle of one of the mirrors, the image of the horizon and the celestial object can be made to appear side by side.

Instead of observing the horizon, the angle between two celestial objects can be measured. Or, we can measure the angle between an object and, for instance, its reflection in a horizontally leveled mirror or a body of water. The measured angle is then divided by two before being used in computations.

This use of an artificial horizon is demonstrated in Fig. 2. Figure 2a shows the reflection of the Sun in the Potomac River. Figure 2b shows the Sun, reflected in a granite bird-bath. Figure 2c shows the direct and reflected images of the Sun as viewed through a sextant using solar filters. The Sun appears twice, with the bird-bath Sun on the left. The right-hand image comes via mirrors. The arm of the sextant, which rotates one of the mirrors, isn't properly adjusted for an accurate angle measurement; the right-hand Sun has been “brought down” below, rather than in line with, its twin.

A slightly different instrument, the octant, allows for measurement of a larger range of angles. Lewis and Clark typically used their octant for the daytime measurements of the Sun at noon for determination of latitude. A sextant was used for measurement of the lunar distance, and for morning and afternoon measurement of the Sun. As will be seen, this is an important detail.



Figure 2b. Use of a granite bird-bath as an artificial horizon.

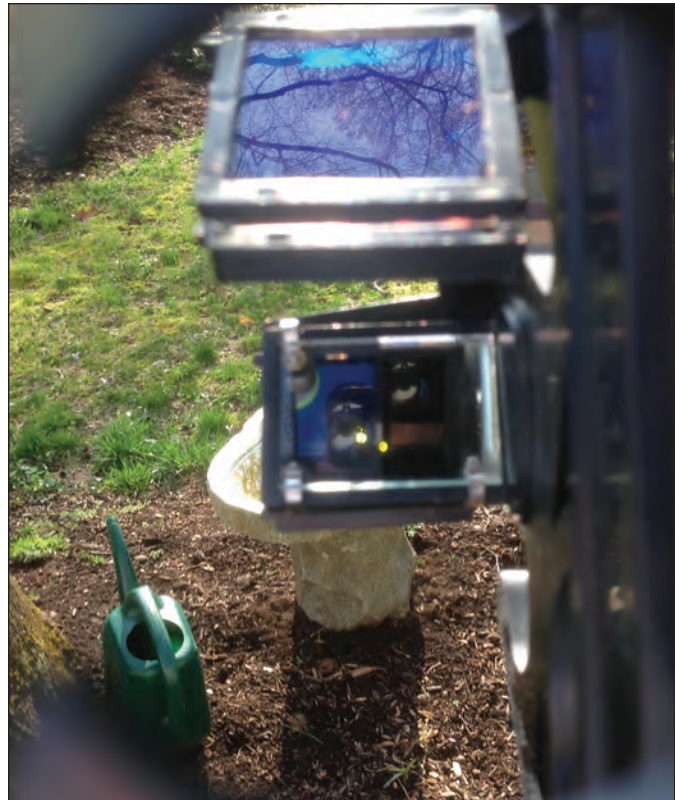


Figure 2c. Side-by-side views of the direct and reflected Sun images seen through a sextant. The tree branches are reflected from extra solar filters, which rotate out of the way when not being used.

Date of Moon to Sun Observa-tion	Latitude and Longitude			Number of Lunar Distance Readings	Error in Longitude	Probable Error of the Mean
	Modern Values	Lewis & Clark / Bergantino	Ellicott			
June 2, 1804	38° 36' 0" N 91° 57' 0" W	38° 31' N 91° 47' W	38° 35' N 91° 47' W	26	-10'	4'
June 3, 1804	38° 36' 0" N 91° 57' 0" W	38° 31' N 91° 30' W	39° 1' N 91° 36' W	36	-27'	5'
June 29, 1804	39° 7' 12" N 94° 36' 0" W	39° 5' N 94° 8' W	39° 7' N 94° 8' W	48	-28'	2'

Table 1. Results of Preston's analysis of the Lewis and Clark data for June 1804.

Azimuth angles, based on compass measurements, are difficult to obtain with the precision and accuracy afforded by a sextant. Because of this, azimuth measurements are seldom used in celestial navigation.⁸ Mathematically, the use of the covariance matrix when solving over-specified systems of linear equations demonstrates this. The weighting factors in the matrix will effectively eliminate measurements based on, in this case, compass bearings to the observed stars. Paradoxically, if angle measurements of the positions of GPS satellites made with the accuracy of a handheld sextant were included in the computation of the pseudo ranges to the satellites, the same mathematics would discard the angle measurements in favor of the more precise time measurements.

Of primary interest here are the Sun, the Moon, and the planets. Unlike their stellar counterparts, the relative positions of these celestial objects cannot be regarded as being fixed. Furthermore, when the Sun, Moon,

or "close-in" planets (e.g., Venus) are used for celestial navigation, the approach described above must be modified to account for parallax.

As noted, parallax is the angular offset that occurs when a change is made to the position from which we measure the angle to an object. However, when the distance to a celestial object is large compared to the radius of the Earth, the parallax effect becomes negligible. This leads us to the crux of the discussion. When the parallax is negligible, measurements made from the surface of the Earth are independent of our location. This makes it possible, for example, to determine UT from anywhere on Earth by observing the moons of Jupiter. Jupiter is sufficiently far from Earth that measurement versus time of the angular positions of the moons, relative to Jupiter and to each other (i.e., their "Jovian" distances), is independent of our latitude and longitude.

The Earth's moon, however, is close enough that parallax is both significant and useful. The parallax is essential for the determination of position. But it also precludes the use of lunar observations, on

⁸ However, azimuth values computed from knowledge of position and time are of considerable use.

On-site calibration and adjustment.



HygroGen2

- Generates stable humidity and temperature conditions
- Increased calibration productivity
- Stable humidity values within 5 to 10 minutes
- Calibrates up to 5 sensors simultaneously
- Integrated sample loop for use with Reference Hygrometers
- Integrated desiccant cell and digital water level monitoring
- Easy-to-use graphical user interface

Visit www.rotronic-usa.com for more information or call 631-427-3898.

ROTRONIC Instrument Corp, 135 Engineers Road, Hauppauge, NY 11788, USA, sales@rotronic-usa.com

rotronic
MEASUREMENT SOLUTIONS

their own; for the determination of UT. However, when combined with other measurements, the resulting method of lunars permits determination of both time and position.

This depends, of course, on having an accurate knowledge of the orbital parameters of the involved celestial objects, in this case the Moon and the Sun. In 1804, this knowledge of the “ephemerides” was contained in the updated version of Nevil Maskelyne’s famous 1767 almanac, which in turn built on the sixteenth century observations of Tycho Brahe. Lewis and Clark had, and used, a copy of this almanac.

Preston also used a copy, difficult to obtain in 2000 prior to its republication, of the 1804 almanac [2] for his analyses. However, for the analyses in this paper, the modern United States Naval Observatory (USNO) almanac is used [6]. It is based on updated ephemerides maintained by the Jet Propulsion Laboratory and others. Comparison of the two almanacs indicates close agreement, but the USNO data have the advantage of being available online.

3. Preston's Analysis of the data of Lewis and Clark for June 2, 1804.

Preston analyzed all of the celestial data gathered by L&C during their two year expedition. As stated earlier, we will focus on data for June 2, 1804, when the L&C expedition was camped at the confluence of the Osage and Missouri Rivers, approximately 150 miles west (upriver) from St. Louis. The observational data for this day appear to be quite good, and its documentation in the *Journals of the Expedition* [5] is relatively unambiguous. Most importantly, the position of the confluence of these two rivers provides an accurate, modern reference point for the validation of analyses.

Table 1 shows Preston’s results, compared side-by-side with the ground “truth” measurements of Begantino. Note that a variety of values, computed using variations of the standard celestial algorithms, are presented. These are discussed in great detail in Preston’s article, as are details of his gradient descent algorithm. Table 1 is an excerpt from the much larger table in Preston’s paper [3].

The modern values for latitude and longitude in column 2 differ from the values calculated by Preston in column 3, and also from the values in column 4, which were computed using a technique attributed to Andrew Ellicott. Of critical importance, L&C made a separate measurement of latitude based on the noon measurement. This was independent of the measurement earlier in the day of the lunar distance. They concluded that the latitude was $38^{\circ} 31' 6.1''$, but did not solve for the longitude for this, or any other measurement.

It should be noted that it is easier to work navigation problems backwards from an estimate of position than it is to derive the position estimate in the first place. As stated previously, the effort described here is not a substitute for Preston’s work, but rather an extension of his work. The goal is to make the case that L&C were not incapable or delinquent in any way, and that their conscious decision to not measure the altitudes of the Sun and Moon as part of the lunar distance measurement was almost two centuries ahead of its time; GPS similarly avoids horizon-based measurements. To make the corresponding case for this line of argument, the following approach is used:

- The “trade-space” for the analysis is limited to the L&C data for June 2, 1804. Analyses for other dates were performed, and support the conclusions of this paper. But, for brevity, these results are not discussed.

HIGH VOLTAGE STANDARD

- **UNIQUE MODULAR DESIGN**
 - **BUILD UP IN 50 KV SECTIONS**
- **INNOVATIVE GUARD STRUCTURE**
 - **REDUCES COUPLING ERRORS**
 - **PROVIDES METERING OUTPUT**
- **RUGGED & TRANSPORTABLE**
 - **EASY TO SHIP**
- **HIGH STABILITY, HIGH ACCURACY**
 - **STATE OF THE ART DESIGN**
- **ACCREDITED CALIBRATION INCLUDED**
 - **TO 150 KV DC**
 - **TO 100 KV AC 60 Hz RMS**



SEE WWW.OHM-LABS.COM FOR DETAILS

611 E. CARSON ST. PITTSBURGH PA 15203
TEL 412-431-0640 FAX 412-431-0649

WWW.OHM-LABS.COM



Assumed Position: 38° 53.0' N Latitude 77° 05.0' W Longitude								
Almanac Data					Altitude Corrections			
Object	Greenwich Hour Angle	Declination	H _c	Z _n	Refraction	Semi-Diameter	Parallax	Sum
Sun	77° 03.6'	N 0° 06.2'	+51 13.2'	180.0°	-0.8'	16.1'	0.1'	15.3'
Moon	335° 37.3'	N 18° 52.1'	+3 14.8'	68.3°	-16.6'	14.8'	54.4'	52.7'

Table 2a. Celestial data for local noon (17:15:35 UT) on the spring equinox, March 20, 2013, at Washington, D.C.

Assumed Position: 38° 53.0' N Latitude 77° 05.0' W Longitude								
Almanac Data					Altitude Corrections			
Object	Greenwich Hour Angle	Declination	H _c	Z _n	Refraction	Semi-Diameter	Parallax	Sum
Sun	166° 19.7'	N 0° 12.0'	+ 0 42.8'	269.7°	-----	-----	-----	-----
Moon	62° 01.3'	N 18° 26.7'	+65 44.3'	143.1°	-0.5'	15.1'	22.7'	37.3'

Table 2a. Celestial data for local sunset (23:12:35 UT) on the spring equinox, March 20, 2013, at Washington, D.C.

Using optical techniques (specifically, sightings of candlelight at night), Mason and Dixon surveyed great circles.¹⁰ They then used the mathematics of spherical trigonometry, along with some extremely tedious mechanical measurements, to convert great circle segments to a single small circle, namely the line of constant latitude that defines the border between Maryland and Pennsylvania.

Like celestial navigation, GPS also uses small circles, one for each satellite that is being measured by a GPS receiver. The receiver's position is then determined from a least squares, best estimate of the intersections of the circles defined by at least four, and often 12 or more, satellites. However, to achieve its considerable precision, GPS uses time, rather than angle measurements, with time being converted to distance by using the speed of light as a scale. It is now possible to compare and contrast GPS to the method of lunars and its L&C variant:

- Both GPS and lunar methods depend on parallax. A critical feature of GPS is that the orbital radii are of the same order of magnitude as the Earth's radius (14 000 miles versus 4 000 miles). Indeed, it is more appropriate to refer to GPS satellites as navigation moons, rather than navigation stars, or NavStars, which is the name they often go by.
- Both methods rely on having accurate almanac information. However, the GPS almanac must be updated on a daily or more frequent basis, whereas a 1767 celestial almanac can be used to determine one's position, even in 2013, within approximately 60 m.¹¹
- Intersecting sections of the circles on the surface of the Earth are modeled, for computation purposes, as straight line segments, thus permitting the copious use of linear algebra techniques, including Kalman filters.
- Both methods require an extra measurement in order to "solve for time". In the case of lunars, the measurement is used to align

local stopwatch time to UT. For GPS, the measurement is used to correct the frequency offset error of the internal oscillator that a GPS receiver uses as its timing reference.

- For two-dimensional navigation on the surface of the Earth, GPS and celestial techniques thus require three independent measurements:

1. For GPS, these are the time differences of arrival between the signals of each of three satellites. Using trigonometry and repeated use of the vector dot product operation, these times, when converted to distances, can be further converted to the angular distances between the satellites. This underscores the close connection between GPS and the method of lunars.
2. For Maskelyne's traditional method of lunars, the requirements are for simultaneous measurement of one lunar distance and two elevation angles.
3. For Lewis and Clark, the required three measurements are one elevation measurement made at noon, one lunar distance measurement made with no regard for the horizon, and a precise measurement of the time difference between local noon and measurement of the lunar distance.

It is useful to note that, as functions of time, the small circles move. Thus, one circle can be used, at multiple points in time, to create a running fix. Related to this, a combination of satellites and/or land-based transmitters, as the case may be, can be regarded as defining multiple, intersecting position circles. The resulting time difference of arrival (TDOA) contours form hyperbolas. The Omega and LORAN radio navigation systems (both now turned off in the United States) were based on this concept.

When reviewing the L&C data for the lunar distances as functions of time for June 2, 1804, features of both circles of position (i.e., the small circles) and TDOA contours are evident. However, when viewed for short time intervals, plots of these data appear as families of almost parallel lines. The position information is contained in the values of both the intercepts and the slopes of these lines.

¹⁰ By Fermat's principle, light travels in great circles, as do radio waves. For the latter case, aviation charts based on radio navigation beacons are printed using a projection for which straight lines correspond to great circles. This is in contrast to nautical charts, which typically use Mercator projections. On a Mercator map, a straight line corresponds to a line of constant bearing.

¹¹ The precision of celestial almanac data leads to position computations that are accurate to tens of meters, while sextant inaccuracies limit position measurements to hundreds of meters.



Figure 5. The “correction analemma” at the sundial at the Center for Computing Sciences in Bowie, Maryland.¹²

However, multiple plots of straight lines are not particularly inspiring until put into context. The L&C expedition, operating under less than favorable conditions, took two years to trudge across the country and back. They wrote down everything they saw, and spent a considerable amount of time recording what seem to be extremely prosaic and uninspiring numbers. To do their work justice, it is helpful to explore some of these numbers in terms of what we actually see when going outside and “looking up”.

3.2 Stonehenge on the Potomac

The city of Washington, D.C. was surveyed by Andrew Ellicott and Benjamin Banneker using the celestial techniques of Mason and Dixon. As a result, many of the numbered streets are lines of

¹² The analemma is part of the sculpture “Sunwork,” by John Van Alstine, granite and stainless steel, 12 in × 40 in × 30 in, 1989. This photograph is used with permission of the artist. A photograph of the entire sculpture can be found at www.johnvanalstine.com. Dr. Neil Coletti provided significant input and guidance with respect to the astronomical accuracy of the sundial and analemma during its design and installation.



Figure 6a. The Sun above the Washington Monument shortly before local noon on the spring equinox, March 20, 2013.



Figure 6b. The Sun, viewed through a solar filter, a few minutes later post meridian (or P.M.) on March 20, 2013.

constant longitude (great circles) while the corresponding lettered streets are lines of constant latitude (small circles). This makes the city a convenient place from which to make solar observations during the course of daily activities. However, in contrast to its circular British predecessors, such as Stonehenge and Avebury, the District of Columbia is a square, with sides of length 10 miles.¹³ The naming of numbered and lettered streets follows a Cartesian system whose origin is the U. S. Capitol building.

To continue, it is useful to show what some of the data in a *Nautical Almanac* look like. For comparison, an excerpt of a page from the 1804 *Almanac* is shown in Fig. 3 for the date of June 2. This is followed in Fig. 4 by an excerpt from the 2013 *Nautical Almanac* for the same date.¹⁴

Despite being more than two centuries old, the 1804 *Almanac* is surprisingly easy to use. It also provides lunar distances, which aren't included in modern almanacs. However, the distances are easily computed using the equation for the vector dot product.

The 1804 *Almanac* provides data for noon, UT, for each day. Note that the declination of the Sun, which is its elevation relative to the equator at, is $22^{\circ} 12' 26''$ in the 1804 table, and $22^{\circ} 14.4'$ on the same day in 2013. The declination varies between -23.5° and 23.5° degrees over twelve months due to the tilt of the Earth's axis.

The 1804 *Almanac* has a column for the equation of time. Because the Earth's orbit around the Sun is elliptical, not circular, Kepler's third law dictates that magnitude of the Earth's orbital velocity around the Sun over the course of a year varies with the Earth's distance from the Sun. But, UT or Greenwich time is, for convenience, Greenwich Mean Time (GMT). The correction shown in the equation of time

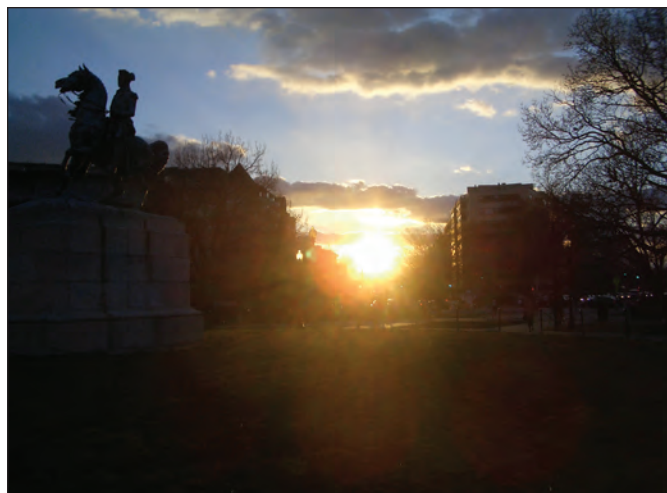


Figure 7. Sunset at Washington Circle along K St. In Washington, D.C. a few days after the equinox. This shows that K Street is a line of constant latitude. A statue of George Washington, lined up with Pennsylvania Avenue and pointing directly at the White House, is on the left.

column is the difference between mean time and the un-averaged value of time that reflects Kepler's third law. This corrected value is needed in order to accurately compute celestial based positions.

¹³ The requirements for this are specified in the United States Constitution.

¹⁴ The *Nautical Almanac* is one of several available versions of almanacs.

For example, the *Air Almanac* provides data that are tabulated for smaller increments in time, reflecting the fact that aircraft travel faster than ships.

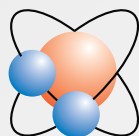
Thunder's Calibration Laboratory Offers Accredited Humidity Calibration Services

Thunder Scientific provides instrument calibration for virtually any humidity measurement device or dew-point hygrometer with as found and as left data with uncertainties.



NVLAP Lab Code 200582-0

Humidity Parameter	Range	Uncertainty
Volume ratio, V (PPM)	0.1 to 3 PPM	4.0% of value
	3 to 200 PPM	2.0% of value
	200 to 400000 PPM	0.1% of value
Dew/Frost Point Temperature	-90 to -70 °C	±0.2 °C
	-70 to -20 °C	±0.1 °C
	-20 to 70 °C	±0.05 °C
Relative Humidity (0 °C to 70 °C)	0% to 99%	0.3% RH



Humidity Generation and Calibration Equipment
THUNDER SCIENTIFIC®
CORPORATION The Humidity Source

Ph: 505-265-8701 ✪ Fax: 505-266-6203

www.thunderscientific.com
sales@thunderscientific.com

Sales ✪ Service ✪ Support
 800-872-7728

Model 1200 Humidity Generation System

Mini/Mobile "Two-Pressure" Humidity Generator Self contained humidity calibration standard NIST traceable certificate of calibration certified at ±0.5%RH accuracy.



Model 2500 Humidity Generation System

Benchtop/Mobile "Two-Pressure" Humidity Generator self contained humidity calibration standard NIST traceable certificate of calibration certified at 0.5%RH accuracy ControLog® automation software.



Model 3900 Low Humidity Generation System

"Two-Pressure Two-Temperature" Low Humidity Generator. NIST traceable certificate of calibration, certified at 0.1 °C Frost Point, over the range of -95 °C FP to +10 °C DP.



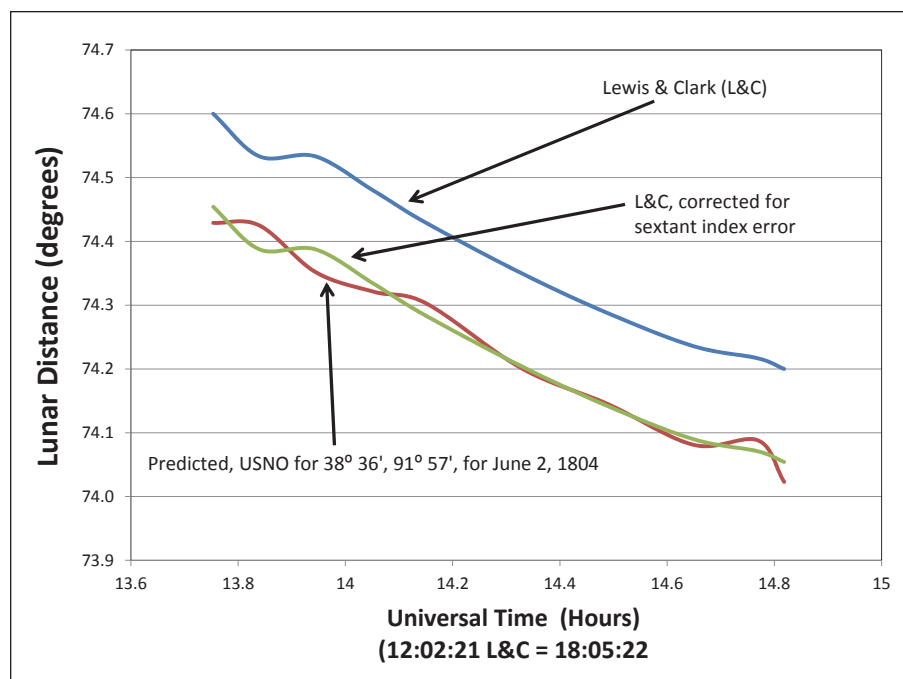


Figure 8. The lunar distance measurements of Lewis and Clark compared with theoretical computations based on the known correct position of the expedition on June 2, 1804.¹⁵

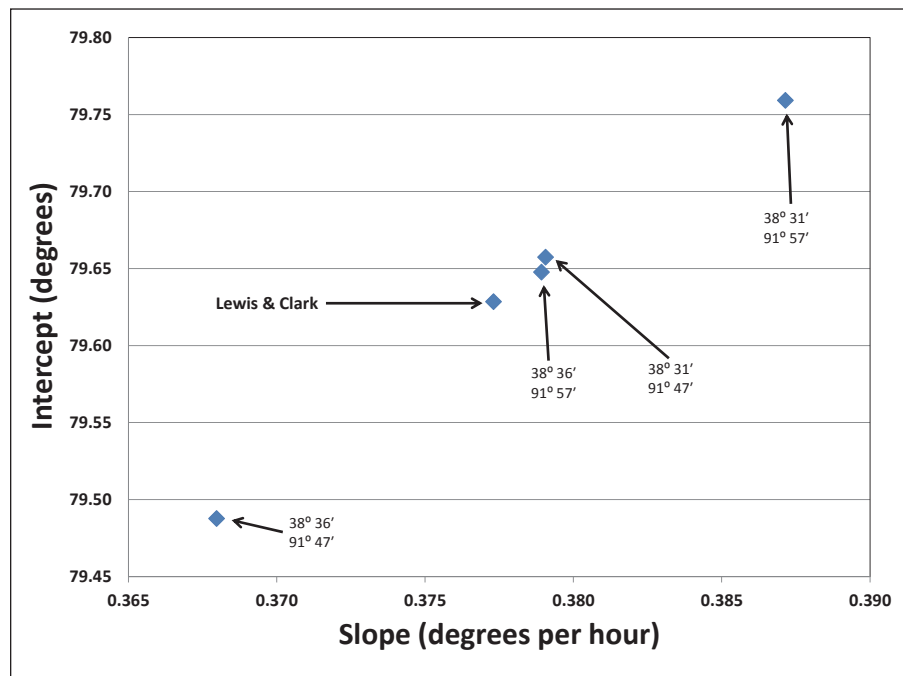


Figure 9. Slope/intercept combinations for the four putative latitude/longitude combinations.¹⁶ Note that the L&C measurements are in close agreement with two of the combinations, including the correct position.

The 2013 Almanac illustrates this correction in the variable known as Greenwich Hour Angle (GHA). At local noon, when the Sun is due south, the GHA is zero as the sun goes from Ante Meridian to Post Meridian, or from A.M. to P.M. But, this does not coincide precisely with the value of

GMT for this instant. That is, GMT is not precisely aligned to 12:00:00 at local noon. However, there are four days per year when GMT is approximately equal to unaveraged time. On these days, the sign of the equation of time correction changes from plus to minus or vice versa.

At this point, the GHA and declination are just numbers. But, Fig. 5 shows a plot, embedded in stone as part of a rather large, functional, and astronomically correct sundial, of the equation of time. The equation of time is a graph of the Sun's declination versus the difference between "actual" time and mean time at noon for each day of the year. The figure-eight plot, known as an analemma, shows that on June 15th, for example, the equation of time passes through zero and changes sign. The Sun's declination goes to zero a few weeks earlier, on the equinox.

Fortunately, the USNO has provided several online applications that allow us to browse conveniently through the numerous permutations of GHA, declination, parallax, equation of time, and so on, that characterize significant events. Using one such application, it is possible to connect numerical values for these parameters to photographs shown below. For example, Table 2a [6] shows data for the Sun at local noon for the March 20, 2013 equinox. Note the low value of declination, meaning that the noon Sun has just crossed the equator, spring having "arrived" four and three-quarters hours earlier. The latitude can be inferred from the elevation angle of the Sun above the horizon, H_c , since the azimuth angle Z_n to the Sun is 180.0 degrees, meaning that the Sun is due south. The latitude is computed by subtracting the declination from H_c , and subtracting this result from 90 degrees.

The longitude is approximated by the value of GHA, subject to the correction due to the equation of time. Note the provision of corrections for refraction, semi-diameter, and parallax. The parallax of the Sun is small, but that of the Moon quite large. From a timekeeping perspective, it would be useful for the Moon to "travel" among the stars without the parallax error, thus making the lunar angle a function of time, but not position. However, this would make the lunar distance less useful for determining position.

Table 2b shows the corresponding celestial data for approximately six hours later. Note that the Sun is almost due west ($Z_n \sim 270$ degrees) and at very low elevation angle. The GHA has advanced by approximately 90°, representing the quarter of a day rotation of the Earth.

¹⁵ The lunar distances were measured in the morning, before local noon. The reading of 12:02:21 on the expedition's chronometer corresponds to 18:05:22 Universal Time.

¹⁶ The plotted value of slope is the negative of the actual numerical value.

Figures 6 and 7 illustrate the meaning of the numbers in Tables 2a and 2b. Figures 6a and 6b show the Sun, a few minutes from local noon, “touching” the top of the Washington Monument as it transits the sky. Note that the use of a solar filter dramatically changes the Sun’s apparent diameter. Numerically, as viewed from the Earth, the Sun and Moon have about the same apparent diameter. Scattering of sunlight in the atmosphere makes the Sun look larger than the Moon, except at low elevation angles, when refraction and psychometric effects combine to make each body appear, to the human eye, larger than they really are.¹⁷ Figure 7 shows sunset on K Street, a segment of a small circle of constant latitude, a few days after the equinox.

4. Updated Analysis of the Lewis and Clark Results

Now that we have reviewed the basics, we can address the specifics of the data for June 2, 1804, its analysis by Preston, and an updated analysis using the approach summarized in Section 3. First, it is important to ask the obvious question - was the chronometer used by L&C, if properly wound,¹⁸ adequate for navigation using the traditional sight reduction method (technique 1 in the earlier list)?

The simple answer is “no”. Comparison of the local time of noon as measured by L&C on June 2, 1804 with the same measurement performed on June 29, 1804, indicates that the known drift rate of the chronometer of 15.5 seconds per day is insufficient to account for the clock uncertainty that accumulated over these 27 days. In particular, over this period, the difference between the time of noon as measured with the chronometer, corrected for drift, and that predicted using location and almanac information, is about 5.5 minutes of time, or 1.4 degrees of arc.

Sobel [1] notes that the figure of merit for the Harrison chronometer, in order to win the Longitude prize, was that its accumulated uncertainty in time be no more than 3 seconds per day, or about 1.3 minutes over a 27 day period, so that after several weeks, longitude could be determined to 0.5 degrees of arc. Despite not meeting this requirement, the expedition’s chronometer was sufficient for measuring delta-times over a period of 6 hours with a time accuracy of 3 seconds, corresponding to 45 seconds of arc.

The next question is whether it is possible for Preston’s algorithm to provide a self-consistent position fix that is supported by the measured data, but nevertheless incorrect. To address this question, lunar distances were computed for 10 values of time for each of the four presumed position latitude/longitudes for June 2, 1804. These were then “de-corrected” for parallax, semi-diameter, and refraction error. A plot of lunar distance versus time for the presumed correct position of $38^{\circ} 36' / 91^{\circ} 57'$ is shown in Fig. 8.

The corresponding lunar distance measurements by members of the expedition for this date are also plotted in Fig. 8, both with and without the $8' 45''$ index error of the sextant. This precise value for the sextant error is stated in many *Journal* [5] entries over the course of the expedition.

The fluctuations in the experimental data are presumably due to measurement error. For the computed data, the fluctuations are a dithering error caused by the limited resolution (6 minutes) of the numerical data for predicted azimuth from the USNO website [6].

¹⁷ To eliminate the psychometric enlargement of a full moon located near the horizon, one can supposedly turn his or her back to the Moon, then duck forward so as to view the Moon upside down between their legs.

¹⁸ Which, according to the editors of the *Journals*, was not always the case.

To correct for this, the computed lines for all four of the putative latitude/longitude combinations and for the actual measurements were averaged, using a linear regression, to produce values for slope and intercept. This averaging hopefully reduces the 6 minute dithering noise by a factor of $1/\sqrt{10}$, thus reducing the error to approximately 2 minutes of arc.

In Fig. 9, the slopes and intercept points for the Lewis and Clark data, the correct position of $38^{\circ} 36' / 91^{\circ} 57'$, the incorrect position $38^{\circ} 31' / 91^{\circ} 47'$, and the two “half-correct” positions, $38^{\circ} 36' / 91^{\circ} 47'$ and $38^{\circ} 31' / 91^{\circ} 57'$, are plotted. The results are striking. First, when corrected for index error, the lunar distance measurements seem to be accurate to about 2 minutes of arc, which is much better than Preston suggests. Second, the postulated location fixes of the half-correct positions, used as control values in the analysis, are clearly not consistent with the L&C measurements. However, the presumed values of $38^{\circ} 36' / 91^{\circ} 57'$ and $38^{\circ} 31' / 91^{\circ} 47'$ are both consistent with the lunar measurements of Lewis and Clark.

This demonstrates the problem with algorithms that involve circles. In addition to intersecting at two points, the circles move as functions of time. For the case at hand, it is the incorrect measurement of latitude that drives the rest of the solution. This underscores the need to have at least one additional measurement to cross-check the validity of a position solution. Further analysis indicates that had a measurement been made of the elevation of the Moon above the horizon at the time of even one lunar measurement, it would have been possible to distinguish between the correct and incorrect solutions.

Table 3 illustrates the situation in greater detail. The correct value of latitude, $38^{\circ} 36'$, is assumed. Computed lunar distances are then listed as functions of local “clock time”, not UT, for several values of longitude. These values differ by 10 minutes of arc, or 40 seconds of clock time. To determine UT, the L&C measurements are convolved with the table entries. Note that the lunar values are strong functions of time, but weak functions of longitude. However, since the delta time from noon, when the value of latitude was measured, is accurately known, it is possible to determine that the highlighted column, for $91^{\circ} 57'$, is the only plausible solution. However, if the presumed latitude was $38^{\circ} 31'$, the corresponding table would indicate that the value of $91^{\circ} 47'$ is the only plausible value.

Stated differently, although the lunar distances are not a strong function of longitude, the rows and the columns in the table are both strong functions of time. Provided that we have an accurate measurement of latitude with which to calculate the table entries for an arbitrarily large combination of time and longitude values, a sliding correlation of the measured data with the calculated data isolates a single cell in the table as the best estimate of longitude and UT. Note that this use of a two dimensional search bin is analogous to the operation of the code tracking loop in a GPS receiver.

Finally, it’s worth taking a more detailed look at the data for June 2, 1804. Two features stand out. First the conclusion that the latitude was $38^{\circ} 31'$ seems to be based on the assumption by Clark, stated in a *Journal* entry dated June 2nd, that the index error for the octant, the instrument that was used for the noon measurement, was $2^{\circ} 0' 0''$. However, there are two ways to make a measurement using an octant, a fore observation and a back observation. The back observation was always used for the noon measurements, but the quoted index error on June 2nd is for the forward observation. In an

Hypothetical chronometer time for (-6:03:01) offset from UT	91° 37'	91° 47'	91° 57'	92° 07'	92° 17'	L&C lunar measurement	L&C chronometer time used to calculate (-6:03:01) offset
13:30	74.567	74.555	74.543	74.478	74.465		
13:45	74.442	74.476	74.457	74.441	74.424	74.429	13:45:13
14:00	74.345	74.322	74.346	74.325	74.353	74.321	14:03:11
14:15	74.259	74.277	74.246	74.264	74.235		
14:30	74.166	74.130	74.137	74.146	74.154	74.145	14:29:22
14:45	74.042	74.086	74.082	74.082	74.038	74.088	14:46:10
15:00	73.988	73.977	73.963	73.998	73.989		
Relative Δt for (-6:03:01) offset from UT	-80	-40	0	40	80		

Table 3. The time/longitude search bin for a presumed latitude of 38° 36'. If the presumed latitude is correct, knowledge of the delta times between the noon latitude measurement and the lunar measurements is adequate for determining both UT and longitude.

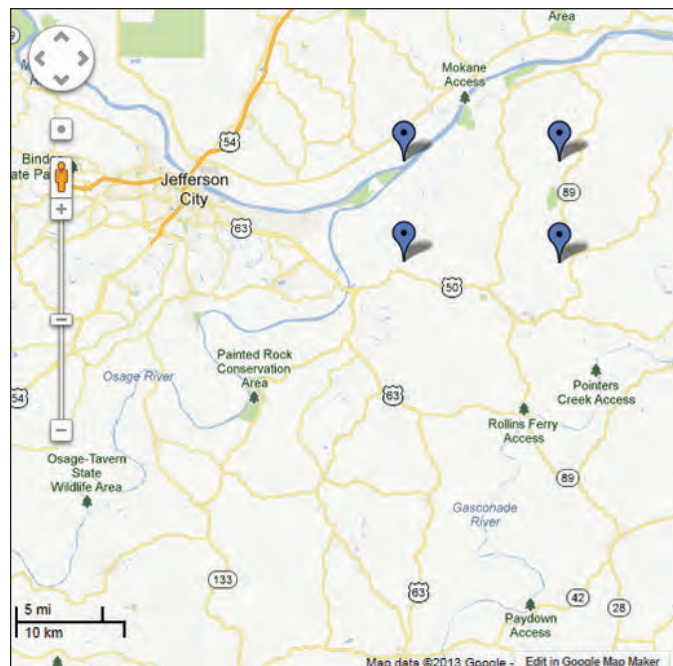


Figure 10. The four putative locations used in the analysis. The correct position of the L&C expedition on June 2, 1804 is at the upper left marker.

entry dated July 22, 1804, Lewis provides the correct index error for the back observation, namely 2° 11' 40.3".

For a measurement made using an artificial horizon, the latitude is computed as

$$\text{Latitude} = 90 + \text{declination} - (1/2) \times (\text{measured elevation} - \text{index error}). \quad (1)$$

The increased value of index error thus increases the corresponding value of latitude, in this case by almost 6 minutes of arc. Furthermore, when performing the morning and afternoon equal altitude measurements, when the Sun is lower in the sky than at noon, Lewis and Clark used their sextant. They recorded not only the clock time, but the elevation of the Sun above the horizon.



Figure 11. The Missouri River near Ft. Benton, Montana.

For the two putative values of position for June 2nd, the predicted values of the Sun's elevation angle for the morning equal altitudes measurement are 47° 50' 18" for the correct position of 38° 36' / 91° 57', and 47° 58' 48" for the incorrect position of 38° 31' / 91° 47'. For June 2, 1804, the measured value of the Sun's elevation above the horizon, corrected for index error and the use of an artificial horizon, was 47° 51' 0". Thus, both the sextant and octant measurements of Lewis and Clark support the correct position of 38° 36' / 91° 57'.

5. Conclusion

Figure 10 shows the map locations of the four position fixes used in the analysis. Note that $38^{\circ} 36' / 91^{\circ} 57'$ is the only plausible result for a measurement made at the confluence of the Osage and Missouri Rivers. The four locations differ by 5 minutes of latitude and/or 10 minutes of longitude. Thus, the ~2 minute accuracy demonstrated by the analyses above is more than adequate for distinguishing the correct from the incorrect positions. For reference, 2 minutes of latitude is approximately 2.2 miles, comparable to the length of a runway at a major airport.

Furthermore, there exists a set of documents, known as Codex's, that contain material that was sometimes, but not always, copied "into the text of the journals proper" [7]. Codex "O", written by Lewis, describes a set of astronomical observations he made prior to the expedition. As noted by Preston [3], these measurements include a single computation of both latitude and longitude, but provide no details of the computation itself. Lewis then compares his results with the known latitude and longitude of the position, and concludes that his longitude observations "may with safety be depended on to two or three minutes of a degree."

Figure 11 shows a modern day view of the Missouri River, showing why accurate measurement of elevation angles requires the use of an artificial horizon. By order of President Clinton, significant portions of the Upper Missouri River, just east of this location, are now protected wilderness. Since 1804, other major stretches of the Missouri

also remain essentially unchanged. As part of the world's fourth longest river system, this is a remarkable fact.

It is perhaps even more remarkable to note that the Earth has orbited the Sun 209 times since Lewis and Clark's 1804 measurements, while rotating through more than 1.8 million hourly lines of nautical almanac. The precession of the equinoxes, noted by Nevil Maskelyne as being measurable over the course of a year, has travelled through almost 1 % of its 26,000 year period. And, the 19 year repeat period of the tides has passed through 11 cycles.

In any case, it appears that navigation is about time, but that time is about circles. Perhaps Joni Mitchell captured the essence of this when she wrote:

*"And the seasons they go 'round and 'round
And the painted ponies go up and down
We're captive on the carousel of time
We can't return we can only look behind
From where we came
And go round and round and round
In the circle game."¹⁹*

6. References

- [1] D. Sobel, *Longitude: The True Story of a Lone Genius Who Solved the Greatest Scientific Problem of His Time*, Walker & Company, reprint edition, 2007.
- [2] *The Nautical Almanac and Astronomical Ephemeris for the year 1804. Published by order of the Commissioners of Longitude*, Gale ECCO, Print Editions, 198 p., June 1, 2010.
- [3] R. Preston, "The Accuracy of the Astronomical Observations of Lewis and Clark," *P. Am. Philos. Soc.*, vol. 144, no. 2, June 2000.
- [4] R. Bergantino and K. Sandau, *The route and campsites of Lewis and Clark in Montana: a geologic perspective*, Montana Bureau of Mines and Geology, Butte, Montana, 2001.
- [5] G. Moulton, ed., *The Journals of the Lewis and Clark Expedition*, University of Nebraska Press, 1st/2nd edition, August 1999.
- [6] USNO, "Celestial Navigation Data for Assumed Position and Time, <http://aa.usno.navy.mil/data/docs/celnavtable.php>, accessed May 2013.
- [7] R. Thwaites, ed., *Original Journals of the Lewis and Clark Expedition, Scientific Data Accompanying the Journals of Lewis and Clark: Geography, Ethnology, Zoology*, vol. 6, parts 1 and 2, Codex O, pp. 6–52, Dodd, Mead, and Company (New York), 1905.

Daniel G. Jablonski

Johns Hopkins University
Applied Physics Laboratory
11100 Johns Hopkins Road
Laurel, MD 20723
dan.jablonski@jhuapl.edu

¹⁹ "Circle Game, The," words and music by Joni Mitchell, © 1966 (Renewed) CRAZY CROW MUSIC, All rights administered by SONY/ATV MUSIC PUBLISHING, 8 Music Square West, Nashville, TN 37203.

August 3 - August 7, 2014
Walt Disney World Swan & Dolphin
Orlando, Florida

WORKSHOP SYMPORIUM

and

MEASUREMENT SCIENCE AND THE ENVIRONMENT



2014 NCSLI CALL FOR PAPERS

The 2014 Workshop & Symposium will offer a great opportunity for you to be recognized for your measurement science related work. The 2014 theme is "Measurement Science and the Environment." More than ever, engineers are being called on to develop new measurement techniques, lower system tolerances and produce higher quality results to support advancements in such areas as energy production and distribution, manufacturing processes and techniques, and healthcare diagnostics and treatment - all of which directly impact our environment.

We welcome papers from engineers, metrologists, scientists, statisticians, technicians and related personnel to expand the understanding of their work. Potential topics include new test and measurement techniques, measurement standards and traceability, statistical process and evaluation, measurement accuracy and uncertainty analysis, laboratory management and accreditation and new advances in measurement science.

You're also encouraged to discuss 2014 Conference topic ideas with us during the upcoming NCSLI Workshop & Symposium, July 14-18, 2013 in Nashville, TN.

GENERAL REQUIREMENTS

Abstracts are required for all proposed papers, panels and workshops.

ABSTRACT REQUIREMENTS AND DEADLINE

Abstracts must be 350 words or less and be submitted electronically using the NCSLI Abstract Management System on the NCSLI website no later than November 1, 2013. Submitters may edit and track their abstract using the NCSLI Abstract Management System. Speakers will return to this page to upload their manuscripts once accepted.

ABSTRACT ACCEPTANCE DATE

Speakers will be notified on or before November 30, 2013 if their abstract has been accepted. Once abstracts are selected for the NCSLI Technical Program, authors will be provided manuscript instructions.

MANUSCRIPT REQUIREMENTS AND DEADLINE

All manuscripts must be uploaded by February 17, 2014. All papers received by the manuscript deadline will be included in the NCSLI Conference Proceedings CD.

SPEAKER DISCOUNTS

- All speakers who upload their abstract by the November 1, 2013 deadline (and are accepted) will receive a \$150 discount off of registration.
- All speakers who upload their manuscript by the February 17, 2014 deadline will receive a \$350 discount off of registration.
- All deadlines must be met to receive the speaker registration discount of \$500.

BEST PAPER AWARDS

A Best Paper Award will be presented in each track. The overall Best Conference Paper will then be awarded to the paper which receives the overall highest point total. To be considered for the Best Paper Award, all deadlines must be met please.

CALL FOR PAPERS

www.ncsl.org>conference>call for papers

EXHIBIT SALES

exhibits@ncsl.org

SPONSORSHIP PROGRAMS

larcher@ncsl.org

ADVERTISING OPPORTUNITIES

lstone@ncsl.org

Automatic Calibration of DC Low Level Current Sources and Meters

Dennis W. K. Lee, Y. C. Chau, Aaron Y. K. Yan, H. S. Lam, and Johnny C. Y. Poon

Abstract: An automated system has been developed at SCL for the calibration of low level dc current sources and meters, including electrometers and femtoammeters, from 100 picoamperes (pA) down to 100 femtoamperes (fA). The system is comprised of in-house developed control software, ramping voltage generation circuitry, and a set of precision air capacitors. For measurement at the 100 pA level, expanded measurement uncertainties of 0.1 % and 0.3 % for generating test currents and calibrating meters, respectively, can be achieved by this system.

1. Introduction

DC current sources and meters at the femtoampere level are essential for low-level current applications, such as leakage current measurements for electrical/electronic components, current measurements for mass spectrometers, measurements of test probe current in electrochemistry, and the calibration of precision medical equipment. The conventional method of generating test currents using high-valued resistors (1 GΩ or above) lacks the precision and accuracy necessary to support these applications. Therefore, a new method that utilizes a capacitor charging technique for generating low level currents has been developed [1, 2, 3, 4, 5].

SCL has developed an automatic system (Fig. 1) to calibrate dc current ranging from 100 pA to 100 fA based on the capacitor charging technique. The system consists of a precision low level dc current generator (which is composed of a linear ramping voltage generator and an air dielectric capacitor), a function generator, a digital voltmeter, a calibrator, and a notebook computer.

2. System Description

The basic method of generating dc low level current is to apply a linear ramping voltage, V , to the air dielectric capacitor, C , as

$$I = C \frac{dV}{dt}. \quad (1)$$

A constant test current, I , can be generated if the voltage ramping rate, dV/dt , is constant and the capacitance, C , is stable. The value of this test current is determined by the product of the capacitance and the ramping rate of the ramping voltage.

The major components of the current generation system include (a) a linear ramping voltage generator; (b) a precision digital voltmeter and (c) a programmable voltage source (i.e. a voltage calibrator).

Figures 2 and 3 show a photograph and circuit diagram, respectively, of the SCL developed ramping voltage generator. The ramping rate can be set from ± 0.01 V/s to ± 0.1 V/s. It is an operation amplifier based circuit (IC1, C1 and R1 in Fig. 3) that generates ramping dc voltages, under the control of a programmable voltage source (multifunction calibrator). A feedback circuit (IC2, R2 to R4) is used to compensate leakage in C1 in order to maintain linearity (variation within 50×10^{-6} in ramping rate of 0.1 V/s). The ramping rate of the output voltage is measured by a precision digital voltmeter (DVM) with a sampling time that is accurately controlled by external trigger signal; a 1 Hz square-wave from a precision function generator. The entire system is controlled by software written in Visual Basic.

Figure 4 shows the schematic diagram of the calibration setup. Electrometers and femtoammeters are calibrated by the test current generated. The calibration system

is powered from a single AC outlet with one Earth point at the ramping voltage generator. This arrangement is to eliminate ground loops due to physically distant AC mains outlets on different branch circuits. To deal with unavoidable ground voltages at the same AC mains branch circuit, the op-amp circuitry is housed in a metal enclosure, shown in Fig. 2, which is connected to the system's single Earth point for noise shielding.

Authors

Dennis W. K. Lee
wklee@itc.gov.hk

Y. C. Chau
scl_dc@itc.gov.hk

Aaron Y. K. Yan
ykyan@itc.gov.hk

H. S. Lam
hslam@itc.gov.hk

Johnny C. Y. Poon
cypoony@itc.gov.hk

The Government of the Hong Kong Special Administrative Region
Standards and Calibration
Laboratory (SCL)
36F Immigration Tower
7 Gloucester Road
Wan Chai, Hong Kong

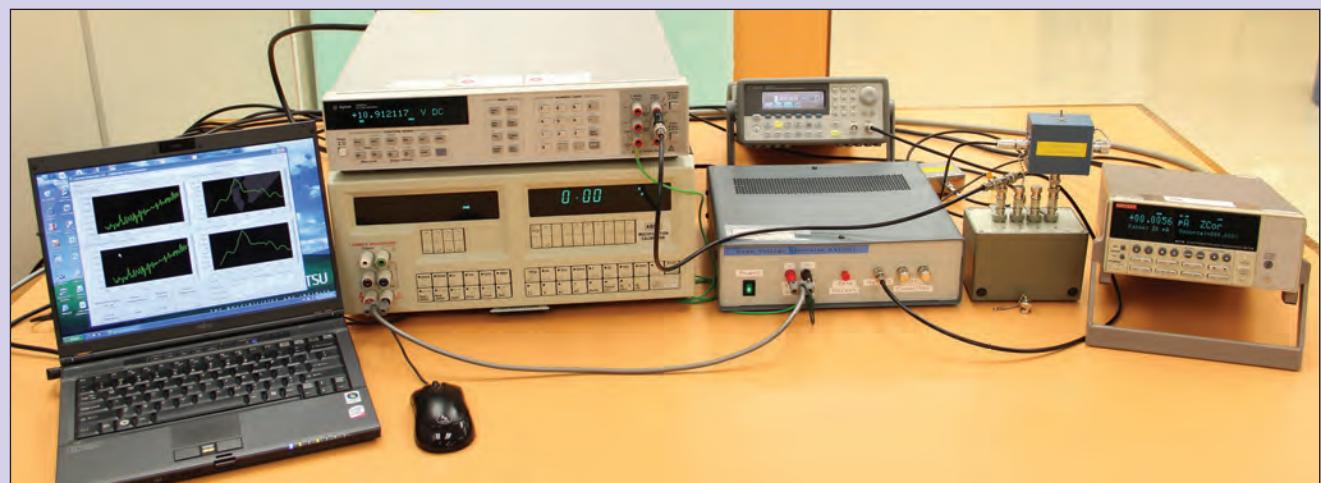


Figure 1. The low level dc current calibration system.

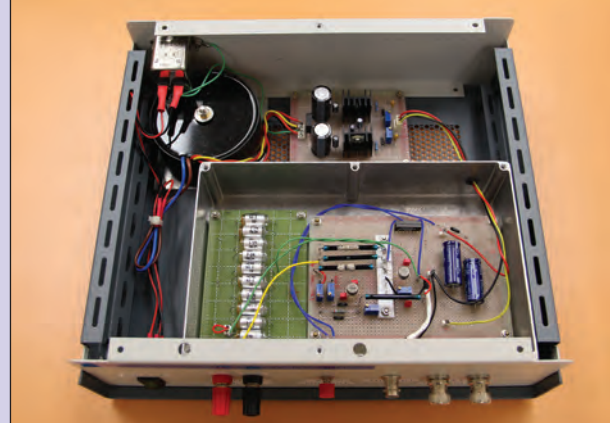


Figure 2. Photograph of the ramping voltage generator.

To guard against noise signals, in particular common-mode errors, the system is configured so that “local guard” is selected for the voltage calibrator (i.e. tying the Guard and Lo terminals together) and “remote guard” is used for the DVM (i.e. connecting the Guard terminal only to the system’s single Earth point). Lastly, co-axial and tri-axial cables are used for connections among the ramping voltage generator, system DMM, and the electrometer under test. The outer conductors of these cables are tied to the system’s single Earth point.

3. Calibration of Low Level Current Meters

The calibration of low level current meters is performed by completing the following steps:

Step 1 - Compensation of meter offset

Before the commencement of calibration, the operator is required to disconnect the high potential (Hi) terminal of the air capacitor, C , from the output of the ramping voltage generator. Then, a BNC shorting cap is used to short the Hi terminal to ground for a “zeroing” condition. When the unit under test (UUT) meter reading has been stabilized, the meter’s Relative function is activated to subtract the offset from the subsequent readings (equivalent to “zeroing” in a general engineering

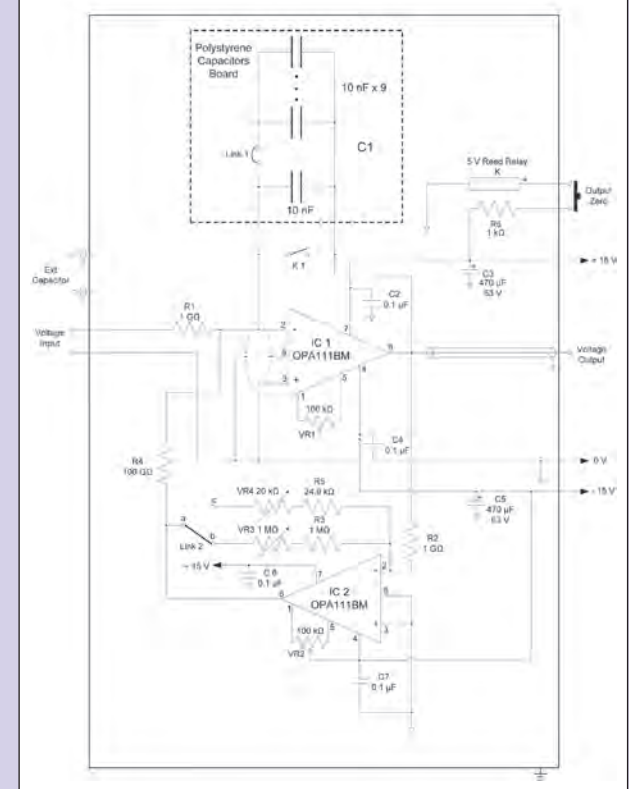


Figure 3. Circuit diagram of the ramping voltage generator.

sense). The capacitor, C , will be re-connected back to the ramping voltage generator afterwards.

Step 2 - Generation of DC ramping voltage

A ramping voltage V is generated based on programming the voltage output of the calibrator, V_{in} , as

$$V = \frac{V_{in} \times t}{R_1 C_1} \quad (2)$$

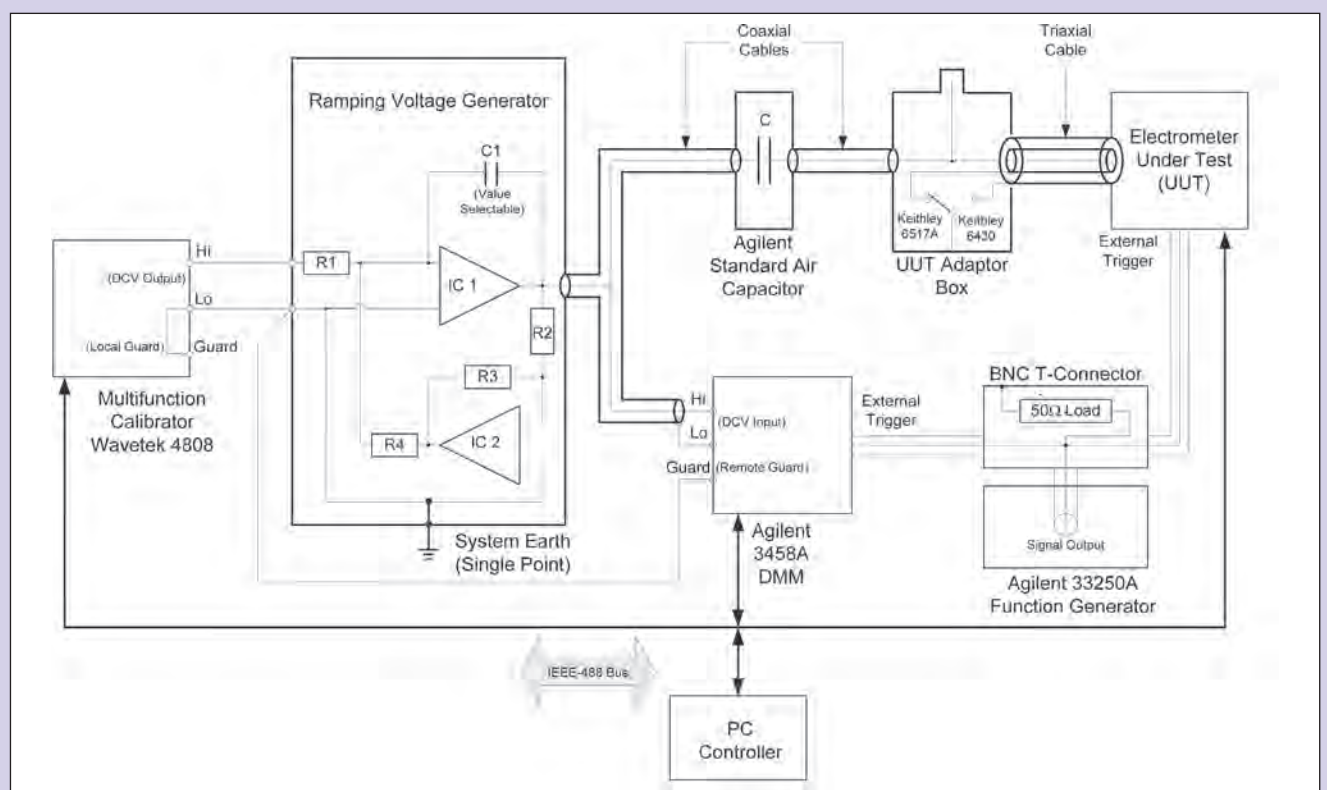


Figure 4. Schematic diagram of the system.

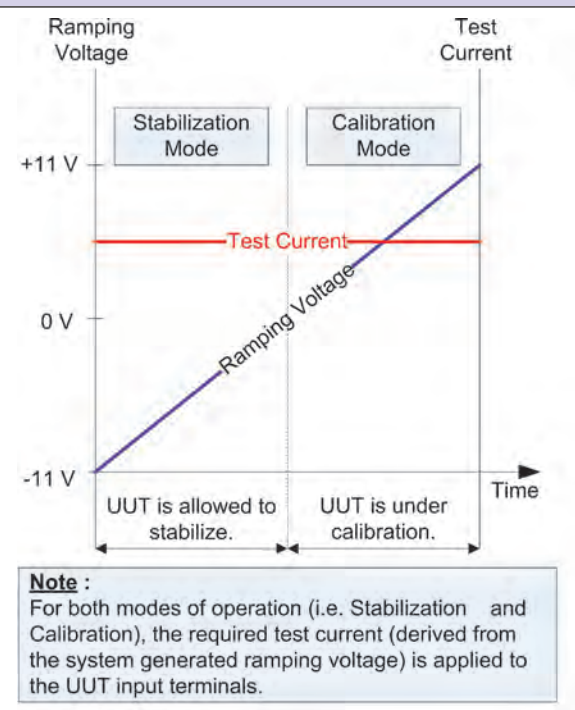


Figure 5. The two operating modes used in calibrating electrometers.

The ramping rate is set by the value of V_{in} and is determined by measuring the output voltage of the ramping voltage generator using

the system DVM at intervals of 1 s (through a 1 Hz triggering signal from the function generator). The instantaneous ramping rate is calculated as

$$\frac{dV}{dt} = \frac{V_{t(n)} - V_{t(n-1)}}{t_{(n)} - t_{(n-1)}}, \quad (3)$$

where $V_{t(n)}$ and $V_{t(n-1)}$ are voltages measured at times $t_{(n)}$ and $t_{(n-1)}$, respectively.

Step 3 - Generation of low level DC current

The ramping voltage is applied to the air dielectric capacitor. The instantaneous value of the generated test current, $I_{t(n)}$, is

$$I_{t(n)} = C \frac{dV}{dt} = C \frac{V_{t(n)} - V_{t(n-1)}}{t_{(n)} - t_{(n-1)}}, \quad (4)$$

where C is an air dielectric capacitor of value 1 pF, 10 pF, 100 pF or 1000 pF depending on the required test current. The value of C is determined by using an Andeen-Hagerling AH 2500A capacitance bridge at 1 kHz. The difference in capacitance between dc and 1 kHz is assumed to be negligible due to their air dielectric construction [1].

For a period from $t_{(1)}$ to $t_{(m)}$, the average test current is

$$I_{avg} = \frac{\sum_1^m I_{t(n)}}{m}. \quad (5)$$

Step 4 - Determination of error in the meter reading

With the test current applying to the meter, the meter instantaneous reading error is determined as

$$E_{t(n)} = \frac{I_{meter_t(n)} + I_{meter_t(n-1)}}{2} - C \frac{V_{t(n)} - V_{t(n-1)}}{t_{(n)} - t_{(n-1)}}. \quad (6)$$

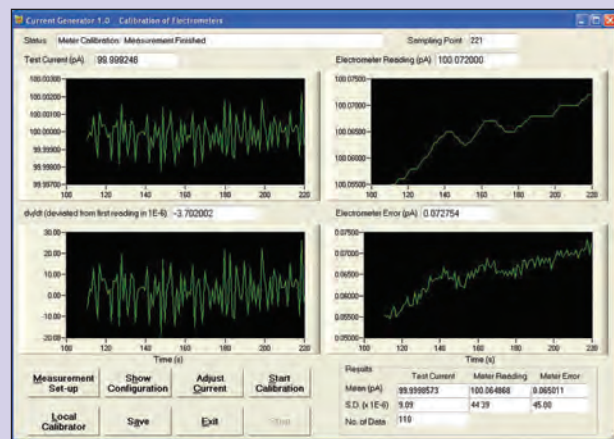


Figure 6. The graphical interface of the control software.

	Quantity	Expanded Measurement Uncertainty ($k = 2$)
Generation of Current	100 pA	10.0 fA (0.01 %)
	10 pA	2.0 fA (0.02 %)
	1 pA	1.0 fA (0.1 %)
	100 fA	0.1 fA (0.1 %)
Calibration of Meter	100 pA	11.0 fA (0.011 %)
	10 pA	2.0 fA (0.02 %)
	1 pA	1.0 fA (0.01 %)
	100 fA	0.3 fA (0.3 %)

Table 1. Estimated measurement uncertainty of the system.

Source of Uncertainty	Type	Standard Measurement Uncertainty (%)		Degrees of Freedom	
		100 fA	100 pA	100 fA	100 pA
Uncertainty due to the Standard Air Capacitor, C					
Calibration uncertainty in C [using capacitance bridge AH2500A]	B	0.018	0.00075	∞	∞
Allowance for drifts in the value of C	B	0.00289	0.00289	∞	∞
Temperature effect on C [over the range of $(23 \pm 1)^\circ\text{C}$]	B	0.00289	0.00289	∞	∞
Uncertainty due to the System DMM, Agilent 3458A					
DMM non-linearity	B	0.000577	0.000577	∞	∞
Uncertainty due to the System Waveform Generator					
Errors in the time intervals generated	B	0.0002	0.0002	∞	∞
Uncertainty in the Indicated Value of the Test Current Generated					
Linearity error in the ramping voltage due to imperfections in the operation amplifier circuitry (namely R_1 , C_1 , IC_1 & IC_2)	B	0.00289	0.00289	∞	∞
Random variations	A	0.0001	0.0001	109	109
Combined Relative Standard Measurement		0.019	0.0051		
Coverage Factor		2	2		
Relative Expanded Measurement Uncertainty		0.038	0.010	1E11	7E8
Quoted Relative Expanded Measurement Uncertainty		0.1	0.01		

Table 2. Uncertainty budget for generation of test current at 100 fA and 100 pA.

To allow the meter readings to settle before making measurements, the system has two modes of operation, namely the Stabilization and Calibration Modes as shown in Fig. 5.

In the Stabilization Mode, the test current is applied to the electrometer unit under test (UUT) and the UUT is allowed to settle for stabilized meter readings. In the Calibration Mode, the test current is applied and the UUT meter reading is captured by the PC Controller. After data acquisition, the PC Controller will compute the

mean value for the acquired data and report it as the measured value. The experimental standard deviation of the mean value is calculated, taken as the Type A measurement uncertainty, and then evaluated and included in the uncertainty budget table.

The control software allows the operator to choose the time intervals for the two operation modes. The default values are 110 data points for both Stabilization and Calibration Modes. (Typically, there are 220 total data points for generating ramping voltage from -11 V to 11 V,

Source of Uncertainty	Type	Standard Measurement Uncertainty (%)		Degrees of Freedom	
		100 fA	100 pA	100 fA	100 pA
Uncertainty due to the Standard Air Capacitor, C					
Calibration uncertainty in C [using capacitance bridge AH2500A]	B	0.018	0.00075	∞	∞
Allowance for drifts in the value of C	B	0.00289	0.00289	∞	∞
Temperature effect on C [over the range of $(23 \pm 1)^\circ\text{C}$]	B	0.00289	0.00289	∞	∞
Uncertainty due to the System DMM, Agilent 3458A					
DMM non-linearity	B	0.000577	0.000577	∞	∞
Uncertainty due to the System Waveform Generator					
Errors in the time intervals generated	B	0.0002	0.0002	∞	∞
Uncertainty in the Test Current					
Linearity error in the ramping voltage due to imperfections in the operation amplifier circuitry (namely R_i , C_i , IC_1 & IC_2)	B	0.00289	0.00289	∞	∞
Uncertainty in the Displayed Value of the Meter Reading					
Uncertainty due to UUT meter resolution	B	0.029	0.00029	∞	∞
Random variations	A	0.1	0.0005	109	109
Combined Relative Standard Measurement		0.11	0.00513	159	1E6
Coverage Factor		2	2		
Relative Expanded Measurement Uncertainty		0.22	0.010		
Quoted Relative Expanded Measurement Uncertainty		0.3	0.011		

Table 3. Uncertainty budget for calibration of electrometer at 100 fA and 100 pA.

during a period of 220 s.) The entire calibration process is software controlled. The ramping voltage, test current, meter readings, and meter errors are displayed for real-time monitoring as shown in Fig. 6.

4. Measurement Uncertainties

To estimate the uncertainty of the generated test current a measurement model based on Eqs. (4) and (5), as in step 3 of Section 3, was used. The overall reading error was determined by instantaneous UUT displayed meter values. To estimate the measurement uncertainty in the reported error, a measurement model based on Eq. (6) as in step 4 of Section 3 was used.

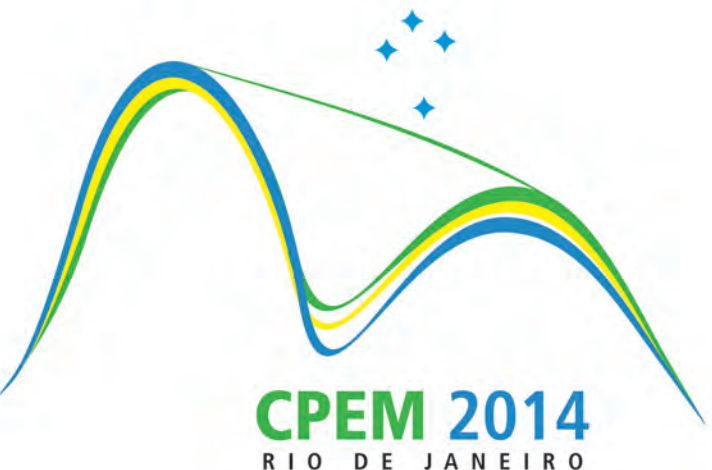
The measurement uncertainty evaluation was carried out in accordance with the guidelines in [6]. Table 1 lists the overall measurement uncertainties from 100 fA to 100 pA. Detailed uncertainty budgets are listed in Tables 2 and 3.

5. Conclusions

A low level dc current generation and measurement system for the calibration of electrometers, femtoammeters, and precision medical equipment has been developed. As a result, SCL has been accredited to perform calibration of low level dc current from 100 fA to 100 pA with measurement uncertainties of 0.3 fA to 11 fA ($k = 2$).

6. References

- [1] N. Fletcher, S. Giblin, J. Williams, and K. Lines, "New Capability for Generating and Measuring Small DC Currents at NPL," *IEEE T. Instrum. Meas.*, vol. 56, no. 2, pp. 326-329, April 2007.
- [2] L. Callegaro, V. D'Elia, P. Capra, and A. Sosso, "Techniques for Traceable Measurements of Small Currents," *IEEE T. Instrum. Meas.*, vol. 56, no. 2, pp. 295-298, April 2007.
- [3] L. Callegaro, V. D'Elia, and B. Trinchera, "A Current Source for Picoammeter Calibration," *IEEE T. Instrum. Meas.*, vol. 56, no. 4, pp. 1198-1201, August 2007.
- [4] G. Willenberg and H. Tauscher, "Novel Digital Voltage Ramp Generator for Use in Precision Current Sources in the Picoampere Range," *IEEE T. Instrum. Meas.*, vol. 58, no. 4, pp. 756-760, April 2009.
- [5] I. Iisakka, K. Kalliomäki, J. Seppälä, and A. Manninen, "Subpicoampere Current Source Based on a Digital-to-analog converter," *IEEE Conference on Precision Electromagnetic Measurements (CPMEM) Digest*, pp. 352-353, June 2008.
- [6] JCGM, "Evaluation of measurement data – Guide to the expression of uncertainty in measurement," *JCGM 100*, 2008.



29th Conference on Precision Electromagnetic Measurements

Rio de Janeiro, Brazil
August 24 - 29, 2014

<http://www.inmetro.gov.br/cpem2014>

Realization



INTI



Implementation of an Accelerometer Transverse Sensitivity Measurement System

Christiaan S. Veldman

Abstract: The National Metrology Institute of South Africa (NMISA) has implemented a system to measure the transverse sensitivity of accelerometers. The system is in compliance with *ISO 16063-31*. As a mechanical device, the principle sensing axis of an accelerometer is not 100 % perpendicular to the mounting axis. This gives rise to the effect that the accelerometer will produce an electrical output even when a mechanical input perpendicular to the principle measurement axis is applied. The quantification of this “defect” parameter is of importance when high accuracy acceleration measurements are performed using accelerometers. This paper describes the system implemented by the NMISA to measure the transverse sensitivity of vibration transducers.

1. Introduction

Accelerometers are widely considered as the vibration sensor of choice, due to their ease of use and low cost. Unfortunately, a variety of different models are required to cover the extremely large number of vibration measurement applications. To select the accelerometer best suited for a specific application, the user will typically scrutinize the manufacturer’s specifications. Apart from the most obvious and most relevant specifications such as size, sensitivity, frequency range, and acceleration range, the manufacturer also specifies the relative transverse sensitivity (RTS) of an accelerometer.

For specialized applications, the transverse sensitivity is important. Depending on the application, the nominal transverse sensitivity value specified by manufacturer could be sufficient. However for some specialized applications, a more accurately known value of the magnitude of the transverse sensitivity is often required [1, 2, 3]. In addition, knowledge of the angle is required.

As part of the NMISA’s research in vibration metrology, it needed to have access to a facility to accurately measure the transverse sensitivity of accelerometers. The existing low frequency accelerometer calibration system was modified to accommodate the transverse sensitivity measurement of accelerometers. Once

fully implemented and validated, this new capability will be offered to industry as a calibration service.

ISO (the International Organization for Standardization), through its Technical Committee, ISO/TC 108, “Mechanical vibration and shock, Subcommittee SC 3, Use and calibration of vibration and shock measuring instruments,” has developed and published a series of methods for the calibration of vibration and shock transducers. The standard, *ISO 16063-31* [4], specifies the instrumentation and procedure(s) to be used for performing transverse sensitivity measurements. It prescribes procedures and minimum requirements for the instrumentation to be used. The aim of this work is to evaluate the implementation of one of these described methods, using the instruments specific to the NMISA.

2. Transverse Sensitivity

In *ISO 2041* [5], the transverse sensitivity of an accelerometer is defined as the sensitivity to acceleration applied at right angles to its geometric axis. The sensitive axis of the transducer is not necessarily aligned with the geometric axis, as shown in Fig. 1. As a result, any motion not in line with the geometric axis will produce an output.

If the transducer is placed in a rectangular co-ordinate system, as shown in Fig. 1, the vector, S_{\max} , representing the maximum

transducer sensitivity can be resolved into the components: the geometric axis sensitivity, S_N , and the maximum transverse sensitivity, $S_{T,\max}$.

The theoretical transverse sensitivity curve is shown in Fig. 2. The transverse sensitivity is expressed as a percentage of the geometric axis sensitivity (it is dependent on the excitation angle).

For high quality accelerometers, manufacturers supply devices with low transverse sensitivities, typically $\leq 1 \%$, and with the direction of the lowest transverse sensitivity, $\beta_{T,\min}$, indicated with a red dot on the accelerometer. The manufacturer supplies these low transverse sensitivity devices through selection, that is, they physically measure the transverse sensitivity and select the units that meet the required RTS specification.

Author

Christiaan S. Veldman
csveldman@nmisa.org

Acoustics, Ultrasound and Vibration Laboratory
National Metrology Institute of South Africa
Private Bag X34, Lynnwood Ridge, 0040, South Africa

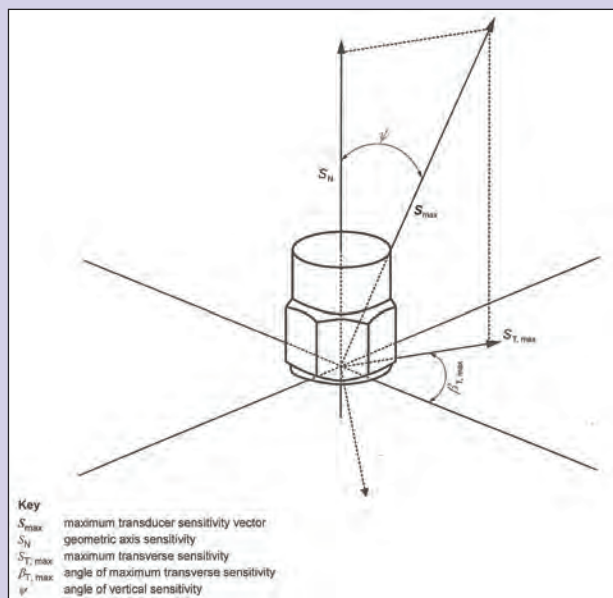


Figure 1. Graphical illustration of transverse sensitivity.

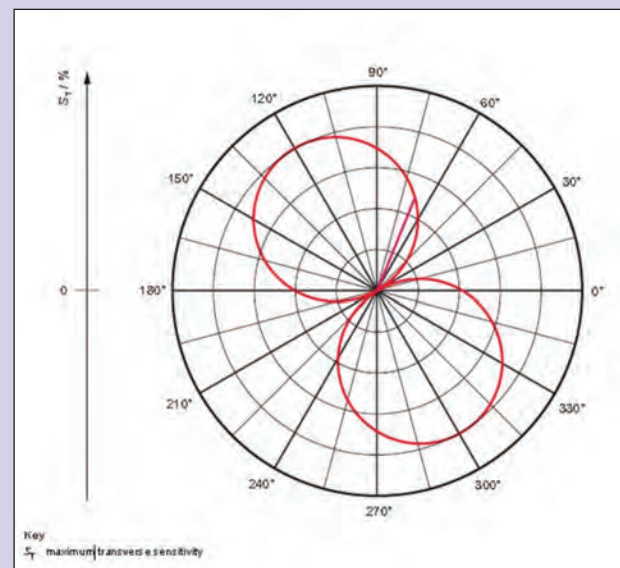


Figure 2. Theoretical transverse sensitivity curve for an accelerometer.



Figure 3. Turntable mounted on top of air-bearing translation stage.

Vibration frequency range	5 Hz to 20 Hz
Transverse acceleration range	5 m/s ² to 50 m/s ²
Analog inputs	Four simultaneously sampled 12 bit channels
Sampling frequency	500 kHz
Turntable rotation angle	0° to 360°
Reference	Heterodyne laser interferometer system

Table 1. Parameters of the NMISA transverse sensitivity calibration system.

3. System Description

The transverse sensitivity calibration system of the NMISA was developed in compliance with *ISO 16063-31* [4]. The transverse sensitivity capability was developed as an extension of the existing primary low frequency accelerometer calibration system. The system utilizes the existing long stroke (152 mm peak-to-peak) electrodynamic exciter, connected to an air bearing linear translation stage (ABT). A stepper motor controlled turntable is mounted on top of the ABT (Fig. 3). Table 1 provides the system parameters.

3.1 Measurement Procedure

ISO 16063-31 describes four apparatus that can be used for testing the transverse vibration sensitivity of an accelerometer:

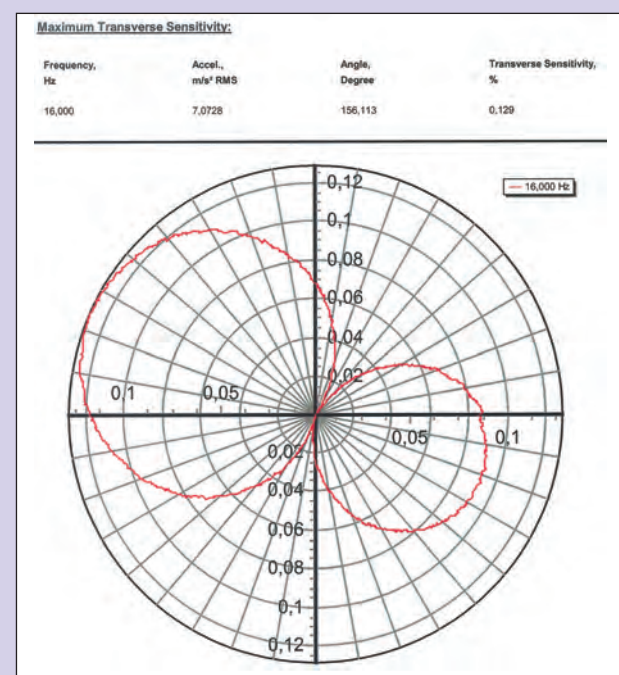
- A vibration exciter with an octahedron to obtain eight different excitation angles
- A vibration generator with turntable
- Using a test system with X- and Y-vibration generators
- Using a test system with a tri-axial vibration generator

For the vibration generator with turntable system implemented by the NMISA, once the unit under test (UUT) is mounted on the turntable and all the hardware and cable connections are completed, the control software developed in-house is run. The desired reference transducer (REF) and UUT are selected from Microsoft™ Excel database files. Then, the desired vibration frequency and angle step size are selected.

Depending on the UUT, the metrologist has the option of employing a Brüel & Kjær, model 2525, or Brüel & Kjær, model NEXUS, amplifier, or a power supply unit (PSU) dedicated for a specific accelerometer. These amplifiers are software controlled, allowing the metrologist to perform the amplifier setup with ease.

The software performs a set of procedural steps as part of each transverse sensitivity measurement per turntable angular position:

- Move the turntable to the angular position of interest, (from 0° to 350° in 10° steps)
- Ramp the exciter to the selected vibration level, in frequency and amplitude
- Sample all four analog inputs, streaming the data (time series data) directly to computer storage

**Figure 4.** Certificate issued with device.

- Apply the sine approximation method (SAM) [6] to the REF and UUT output voltages time series to calculate acceleration amplitude and the UUT voltage output
- Calculate the relative transverse sensitivity (RTS) using Eqs. (1) and (2)
- Record the RTS in the result sheet
- Plot the RTS on a polar diagram

These steps are executed for each angular position from 0° to 360° using the selected step size, without the need of any intervention by the metrologist. The calculation for transverse sensitivity, S_T , is

$$S_T = \frac{\hat{u}_{out}}{\hat{a}_T}, \quad (1)$$

where S_T is the transverse sensitivity; \hat{u}_{out} is the amplitude of the output signal of the transducer vibrating perpendicularly to its sensitivity axis; and \hat{a}_T is the amplitude of the acceleration in the test direction.

The calculation for the relative transverse sensitivity, S_T^* , is

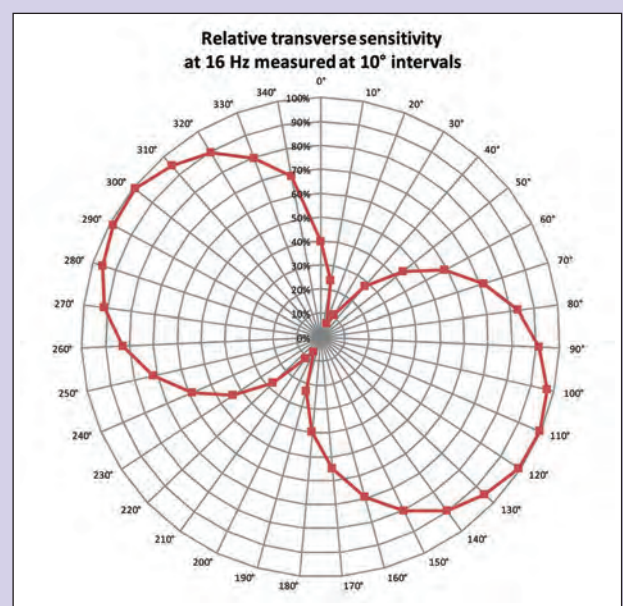
$$S_T^* = \frac{S_T}{S} \times 100, \quad (2)$$

where S is the sensitivity of the transducer on the geometric axis of sensitivity.

Once all of the measurements have been completed, the results are saved using an Excel template file. The result sheet also displays the RTS in graphical format.

4. Transverse Sensitivity Measurements

A transverse sensitivity calibration system has been implemented at the NMISA with success. Some detailed performance evaluations still need to be conducted. However, the operation principle has been established and the preliminary results support the operating principle and validate the calculations performed.

**Figure 5.** Polar plot of a tri-axial accelerometer's X-axis.

4.1 Validation Methodology

With system validation in mind at the conception stage of the project, an accelerometer with an accompanying transverse sensitivity certificate was purchased. The PCB, model 3701G2FA3G (PCB UUT) accelerometer is designated as a laboratory standard (VS-Std-08) and is supplied with a dedicated PSU.

The new system will be validated against this accelerometer as part of the implementation validation. Once the new system is fully characterized, periodic verification will be performed using this accelerometer as a reference.

4.2 Measurement Results

Initial measurement using the PCB UUT did not produce the expected measurement results. The certificate supplied with the unit (Fig. 4) specified a maximum RTS of 0.129 %, while a maximum RTS of 0.03 % was measured by the NMISA.

On closer investigation, it would seem that the device either has a very small RTS, which could indicate a possible error on the supplied certificate, or an error in the measurement setup with the PCB UUT. In a systematic approach to isolate the problem, the output signals were analyzed with an oscilloscope. Only noise could be measured on the PCB UUT output. Even with an acceleration level of 50 m/s² applied, no indication of a discernible vibration signal (transverse output signal) from the PCB UUT could be observed. This result appeared highly unlikely as the PCB UUT has a sensitivity of 102 mV/m/s². Taking the small RTS of 0.13 %, it should result in the PCB-UUT having an S_T of 0.13 mV/m/s². With an applied acceleration of 50 m/s², an output signal of 6.5 mV is expected.

As an alternative and in order to confirm the principle operation of the system, a tri-axial accelerometer was used as the UUT. The X-axis of the accelerometer was selected as the transverse sensitivity axis. It was expected that the RTS measurement result would be 100 %. The results obtained are shown in Fig. 5. As demonstrated in the graph, a maximum RTS of 100 % was recorded at 120° and 300°. These

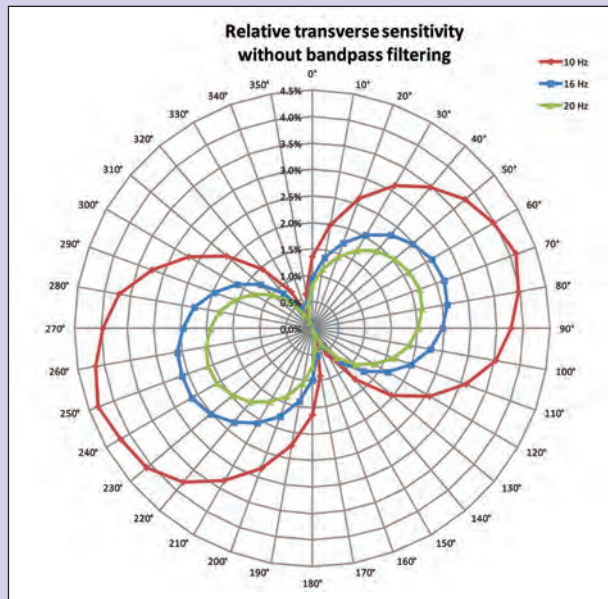


Figure 6. Relative transverse sensitivity values at three frequencies without the use of an analog band-pass filter.

results validated both the measurement system and the calculations performed by the software.

Following these promising results, the transverse sensitivity of a PCB model 301M15 laboratory standard accelerometer was measured. The RTS was measured at three vibration frequencies of 10 Hz, 16 Hz, and 20 Hz (Fig. 6). A maximum RTS of 4.3 % was measured at 10 Hz, and a maximum RTS of 2.2 % was measured at 16 Hz, a difference of more than 2 %. Such a large difference in RTS was indicative of a measurement problem, as the linearity of this accelerometer is better than 1 % over this frequency range. Again, the investigation was focused on the influence of the signal-to-noise ratio (SNR) and how it can be improved.

The recommendation by the ISO 16063-31 standard [4] to use a 24 dB/octave narrow analog band-pass filter was implemented. The 10 Hz to 16 Hz measurements for the PCB 301M15 accelerometer were repeated, with an analog band-pass filter. The results obtained using this setup are reported in Fig. 7 and indicate a huge improvement. The maximum RTS measured, with the analogue band-pass filter, was 0.8 % at all three frequencies, emphasizing the need for a high SNR.

4.3 Analog Versus Digital Filtering

From the measurement results reported in the previous section, the requirement for a high SNR was identified and highlighted. This was evident, even when using the accurate SAM [7, 8] for determining the signal amplitude. To allow an informed decision on the suitability of implementing digital filtering techniques, instead of adding to the instrument count by using analog filters, some comparison measurements were performed. Table 2 reports RTS results for three different makes and models of accelerometers using analog or digital filtering.

Some analysis of the results reveals that the measurement procedure requires a certain level of SNR in order to measure the RTS reliably. The application of some filtering is therefore required to improve the SNR. For accelerometers with a high RTS, such as the PCB 301M15, the difference in RTS obtained with and without filtering is substantially

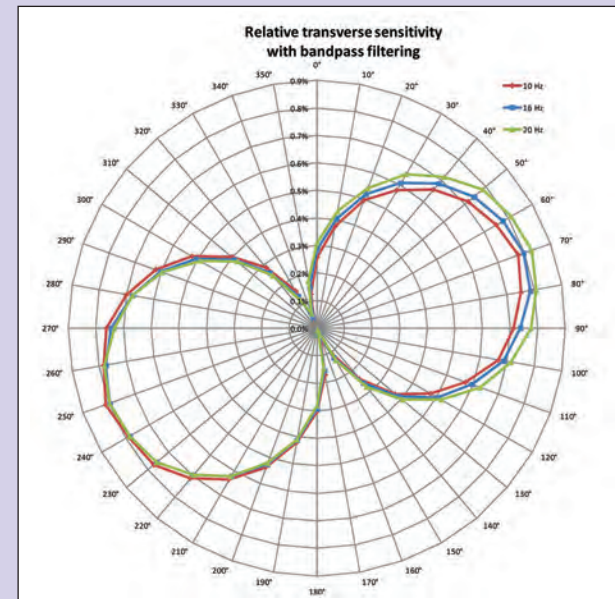


Figure 7. Relative transverse sensitivity values at three frequencies with the use of an analog band-pass filter.

Accelerometer	RTS (no filtering)	RTS (analog filter)	RTS (digital filter)
PCB 3701G2FA3G # 8790	0.014 %	0.064 %	0.066 %
Endevco 2270M8 # 13229	-	-	0.37 %
PCB 301M15	2.7 %	0.8 %	0.8 %

Table 2. Relative transverse sensitivity results using digital and analog filtering.

Accelerometer	Nominal Sensitivity	NMISA RTS	SPEKTRA RTS	RTS _{SPEKTRA} - RTS _{NMISA}
PCB J353B01	2 mV/(m/s ²)	0.94 %	0.81 %	-0.13 %
PCB 3701G2FA3G # 8353	100 mV/(m/s ²)	0.24 %	0.25 %	0.01 %
Endevco 2270M8 # 16194	0.2 pC/(m/s ²)	0.78 %	0.95 %	0.17 %

Table 3. Comparison of measurement results.

less, due to the accelerometer's higher RTS and therefore higher SNR. For the PCB 301 accelerometer, which has a much lower RTS, the SNR requires improvement by using filtering techniques. It is evident that the type of filtering, be it analog or digital, is not of significant importance, because both types of filters perform the same function.

4.4 Validation by Comparison Measurements

When the system is running, proper operation cannot be assumed. To adequately validate the system, comparison measurements were performed with SPEKTRA, an accredited laboratory from Germany. Three makes and models of accelerometers were compared. The RTS of the accelerometers were first measured by SPEKTRA and the accelerometers were then hand carried to the NMISA by a member of the Physikalisch-Technische Bundesanstalt (PTB). Two of the accelerometers were of the same make and model as those used to compare the analog and digital filter results. For clarification, the serial numbers of the devices are listed in Table 2 and Table 3. The results from this comparison are reported in Table 3.

Both NMISA and SPEKTRA performed RTS measurements for all three accelerometers at a vibration frequency of 16 Hz. For a variety of accelerometer types, including charge and ICP type devices, the results compare favorably. However, the associated uncertainties of measurement were not available, preventing the author from performing a sound metrological comparison. All three accelerometers are of laboratory standard quality. Accelerometer 2 has the highest sensitivity of the three, and the results indicate that the RTS measurements agree much better when the device has a good SNR. Even so, there is not a systematic offset in the RTS results obtained by the laboratories for accelerometers with low sensitivities, or poor SNR.

5. Conclusions

A transverse sensitivity calibration system was implemented in compliance with *ISO 16063-31* by the NMISA. The transverse motion is generated using an electro-dynamic vibration exciter with a stepper motor controlled turntable for the angular positioning control.

Comparative results using a laboratory standard accelerometer indicated non-agreement between the NMISA results and the results specified on the supplied certificate. However, the system operation with respect to the data processing and RTS calculation could be validated using a tri-axial accelerometer.

The RTS values obtained using a laboratory standard accelerometer was indicative of an acceptable measurement system. However, the requirement for a good SNR was highlighted, making the use of narrow band-pass filtering a requirement.

A comparison of RTS measurement results with a calibration laboratory for three different types of accelerometers produced acceptable results. Without statements of the associated uncertainty of measurement, metrological sound evaluation of the measurement results were not possible. However, there is again a strong indication that an adequate SNR is required to produce reliable RTS measurements.

6. References

- [1] T. Petzsche, "Determination of the transverse sensitivity using a mechanical vibration generator with turntable," *ISO TC 108/SC 3/WG 6 Doc. N153*, 2007.
- [2] J. Dosch and M. Lally, "Automated testing of accelerometer transverse sensitivity," *Proceedings of the International Modal Analysis Conference (IMAC)*, Kissimmee, Florida, USA, pp. 1-4, 2003.
- [3] R. Sill and E. Seller, "Accelerometer transverse sensitivity measurement using planar orbital motion," *Proceedings of the 77th Shock and Vibration Symposium*, Monterey, California, USA, pp. 8-12, November 2006.
- [4] ISO, "Methods for the calibration of vibration and shock transducers -- Part 31: Testing of transverse vibration sensitivity," *ISO 16063-31*, 2009.
- [5] ISO, "Mechanical vibration, shock and condition monitoring – Vocabulary," *ISO 2041*, 2009.
- [6] ISO, "Methods for the calibration of vibration and shock transducers -- Part 11: Primary vibration calibration by laser interferometry," *ISO 16063-11*, 1999.
- [7] J. Zhang, Z. Xinmin, H. Xiao, and S. Jinwei, "Sinewave Fit Algorithm Based on Total Least-Squares Method with Application to ADC Effective Bits Measurement," *IEEE T. Instrum. Meas.*, vol. 46, no. 4, pp. 1026-1030, August 1997.
- [8] K. Chen, X. Cao, and Y. Li, "Sine wave fitting to short records initialized with the frequency retrieved from Hanning windowed FFT spectrum," *Measurement*, vol. 42, no. 1, pp. 127-135, January 2009.

16th

| measure |
| innovate | perform |

INTERNATIONAL CONGRESS OF METROLOGY

| 7 | 8 | 9 | 10 | OCTOBER | 2013 |
| | | | | | | | | | | | | | | | | | | | | |



COLLÈGE FRANÇAIS DE
MÉTROLOGIE

www.metrologie2013.com | info@cfmetrologie.com



A⁺ métrologie



Held jointly with



Lamp Orientation Dependence of an Integrating Sphere Response for Directional Light Sources in Luminous Flux Measurement

Cheng-Hsien Chen, Bao-Jen Pong, Yuh-Der Jiaan, and Hsiu-Lin Lin

Abstract: Integrating spheres are widely used for the photometric (or luminous flux) measurement of light sources. Their size and geometry influence the measurement uncertainty; including the baffle geometry inside the sphere, which avoids the first incident light from the light source. Different set-up conditions of the directional light source, including the light emitting diode (LED) light-bar and surface light source, result in different luminous flux. We have simulated directional light sources mounted at the center of sphere to advance the feasibility study of directional light sources in different mounting conditions. By varying the types of directional light sources, the geometry of the integrating sphere, the baffle condition, the size of the sphere, and the absorptivity of the light source, we have found the optimal measurement conditions. This study provide knowledge about the limitations of an integrating sphere when measuring a directional light source, and this knowledge can be applied to reduce the measurement uncertainty.

1. Introduction

Due to the rapidly increasing demand of more efficient lighting that saves energy, LEDs have recently become more popular. The LED light-bars and LED surface light sources are widely used for display and lighting applications. Therefore, the luminous flux measurement of these lighting sources has become increasingly important so that lighting quality can be accurately characterized.

In general, there are two standard methods for surface emitting light sources (SLSs) and LED light-bar measurements: the gonio-photometer method, and the integrating sphere method. The gonio-photometer method consists of utilizing a standard photometer, rotating the light source to measure the spatial luminous intensity, and then analyzing the data to determine the total luminous flux. However, it is not always convenient to build and maintain a gonio-photometer, because they require a large dark room, a long measurement time, and high precision movements. In addition, for some designs, the gonio-photometers must rotate the lamp, which can cause errors due to the sensitivity of the lamp with regard to the burning position and draft. Some lamp mounting mechanisms of the gonio-photometer can also create the shadow in the measured luminous

flux. The integrating sphere method utilizes an integrating sphere that consists of a baffle, a detector port, an auxiliary lamp, and a photometer or spectrometer. By use of the substitution method, the output signal from the test lamp is compared to the signal from the standard lamp in an integrating sphere to calculate and obtain the total luminous flux. The limitations of the test lamp are subject to the effects of sphere size and the coating inside the sphere. In addition, the sensitivity of the photometer and the reflectance inside the sphere are the key issues for large spheres, and some geometric designs inside the sphere will cause different results. The integrating sphere method takes less time to complete than the gonio-photometer method.

For ideal operation of an integrating sphere, the following geometric and optical characteristics are required [1]:

- (1) small detector or external port when compared to sphere diameter,
- (2) small components (a test light source, a baffle, and a lamp mount) inside the sphere with their influences on optical radiation neglected after its first reflection,
- (3) a spectrally neutral, spatially uniform Lambertian sphere surface.

Normally, the sphere size is chosen based on the test sample size and economical purposes. However, there are many questions to consider which are discussed in this paper. For example, how should we select the size of the sphere for the SLSs or LED light-bar? How should we select the size of baffle and geometry inside the sphere? What are the limitations of the sphere?

Authors

Cheng-Hsien Chen
chrischchen@itri.org.tw

Bao-Jen Pong
bjpong@itri.org.tw

Yuh-Der Jiaan
yuhder@gmail.com

Hsiu-Lin Lin
hsiulin@itri.org.tw

Center for Measurement Standards
Industrial Technology Research
Institute (ITRI)
Hsinchu, Taiwan, 300, Republic
of China

As noted, the integrating sphere method requires a standard lamp, and the substitution method is utilized to calculate the total luminous flux of a test lamp. There are some important devices inside the integrating sphere to consider. One such device is the baffle. The size of the baffle used to avoid incident light from reaching the detector depends upon both the size of the detector and the distance between the lamp and the detector. A second device to consider is the auxiliary lamp, which provides absorption between the standard lamp and the test lamp.

In the integrating sphere method, the equation of luminous flux Φ_t is

$$\Phi_t = \frac{I_t}{I_s} \cdot \frac{A_s}{A_t} \cdot \Phi_s, \quad (1)$$

where I_t is the signal of the test lamp, I_s is the signal of the standard lamp, A_s is the signal of the auxiliary lamp with the standard lamp mounting, and A_t is the signal of the auxiliary lamp with the test lamp mounting. A photo-detector (photometer) commonly shows some deviation of its spectral responsivity from the spectral luminous efficiency function, which introduces an error if the spectral distribution of a test lamp does not match to that of a standard lamp. For directional light sources, the spatial non-uniformity of the integrating sphere response also introduces an error, whose originates from finite size of a baffle and nonuniform coating of sphere surface.

By introducing two factors to correct the spectral mismatch and the spatial mismatch, the equation of luminous flux Φ_t can be expressed as

$$\Phi_t = \frac{I_t}{I_s} \cdot \frac{A_s}{A_t} \cdot ccf \cdot scf \cdot \Phi_s, \quad (2)$$

where ccf is the spectral mismatch correction factor, and scf is the spatial response distribution function (SRDF) of the integrating sphere [2, 3, 4].

If we want to correctly measure directional light sources whose spatial distribution of illumination is considerably different from that of the standard lamp, we need to evaluate scf based on the spatial response distribution function (SRDF) of an integrating sphere. Note that the SRDF is a function of sphere geometry such as sphere size and baffle size.

In this work, we can use the point source in the center of sphere and measure the light distribution of the DUT to calculate the SRDF. In addition, we can use the same method to evaluate the SRDF to measure the directional

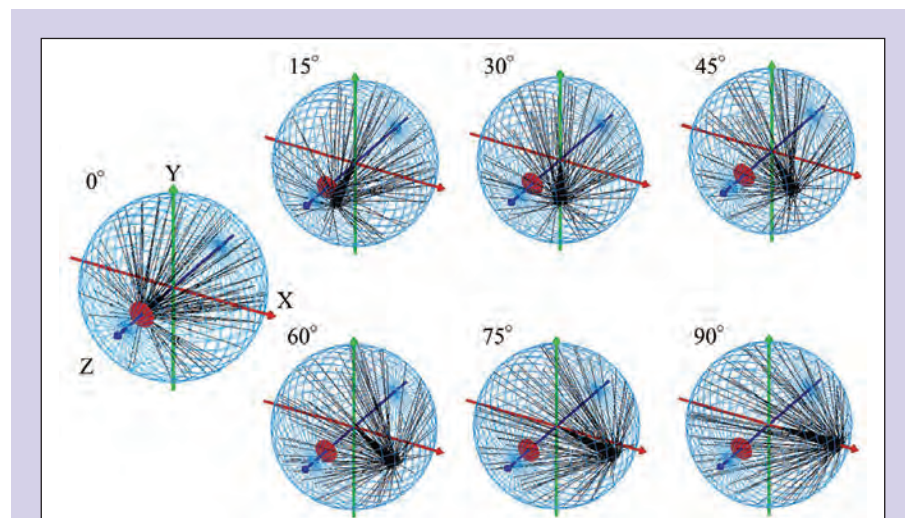


Figure 1. The beam scanning (rotation around y-axis) in the integrating sphere.

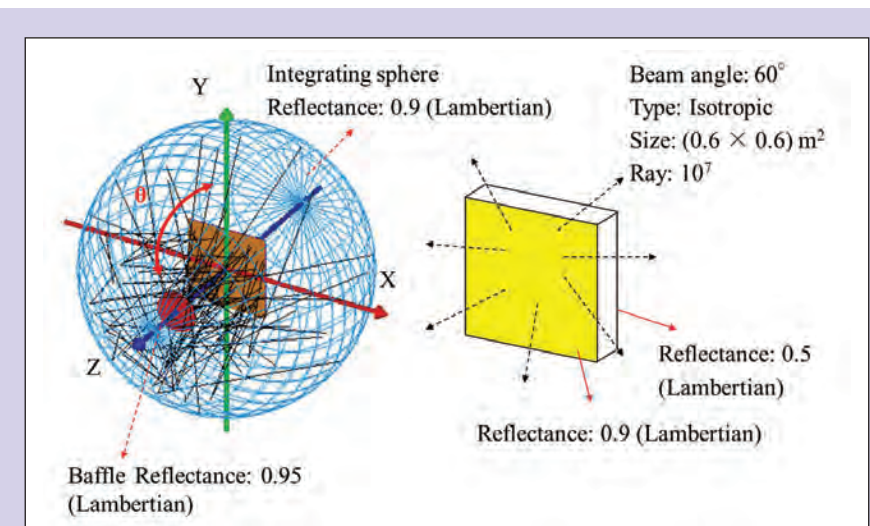


Figure 2. SLSS simulation setup conditions.

light source in the center of integrating sphere. As we will demonstrate, by knowing the limitation of the integrating sphere we can measure the directional light source, and decrease the measurement uncertainty.

2. Simulation Method and Experiment

We use the Monte-Carlo ray-tracing method implemented with the commercial simulator ASAP® to simulate the total luminous flux of SLSSs and LED light-bar. The Monte Carlo technique is a flexible method for simulating light propagation in material. The simulation is based on the random paths of rays when they travel through material, and is chosen by statistically sampling the probability distributions for step size and angular deflection per scattering event. After

propagating many photons, the net distribution of all the photon paths yields an accurate approximation to reality [5]. We assumed that the ray hit the Lambertian surface of sphere and scattered more rays. For an accurate simulation, the number of rays is determined by the convergence result of Ref. [5].

We use the 1.5 m integrating sphere to measure the SLSSs of two tablet computers that display a white pattern. We then rotate the SLSSs inside the sphere to measure the signal with the photo-detector, and analyze the results.

3. Results and Discussions

The following sections describe the simulation, and the associated measurements and results.

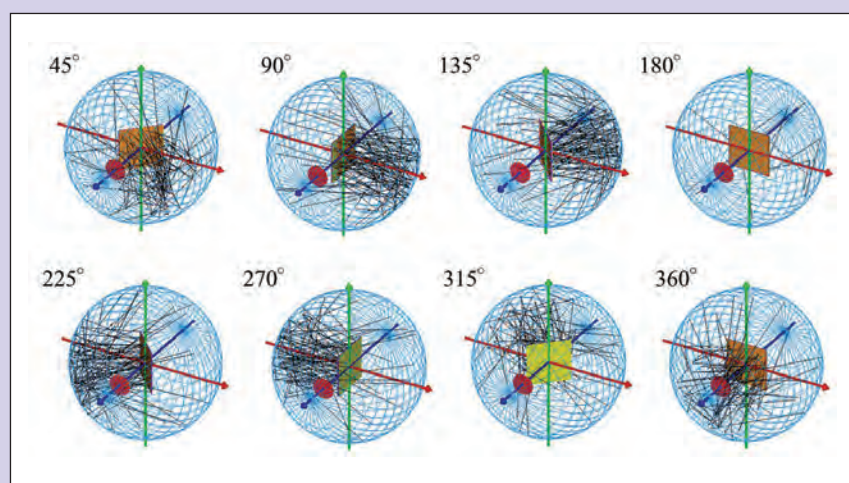


Figure 3. Rotation of SLSs in the center of the integrating sphere.

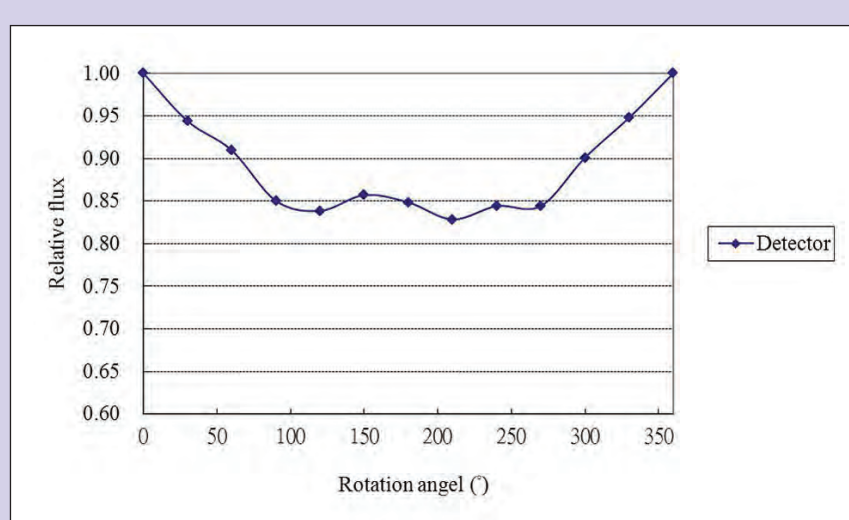


Figure 4. The result of SLSs by rotating around the y-axis.

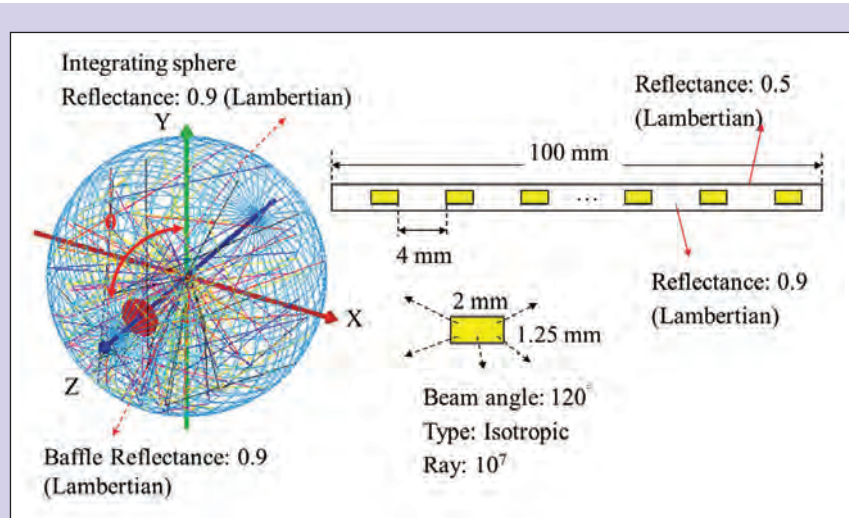


Figure 5. LED light-bar simulation setup conditions.

3.1 Simulation of the Single-Baffle Integrating Sphere for SLSs Simulation

We set the single-baffle integrating sphere for simulation. The diameter of the baffle is 0.3 m, and we define its surface as a Lambertian surface with a reflectance factor of 0.95. The integrating sphere also has a Lambertian surface type with a diameter of 2 m, with a detector positioned 0.3 m in front of the baffle. The isotropic point source and shape into a 5° beam angle is located at the center of the integrating sphere. The scanning beam is set up to rotate such as to simulate the spatial response distribution function (SRDF) of integrating sphere, as shown in Fig. 1. Increasing the number of rays used in the simulation results in a higher accuracy when using the Monte-Carlo method. Therefore, for an accurate simulation, more than 10^7 rays were necessary to get the convergence result.

The SLSs have two surfaces. The front surface is the emitting surface that has an isotropic distribution with a 60° beam angle. The rear surface is the Lambertian surface with a reflectance factor of 0.5. The size of the SLSs is defined as $(0.6 \times 0.6) \text{ m}^2$, which is at the center of the integrating sphere (Fig. 2). We assumed that the detector was calibrated by use of an isotropic luminous flux standard lamp. By rotating the SLSs along the y-axis (Fig. 3), we found that the signal from the detector depends upon the orientation of SLSs, as shown in Fig. 4. The lower signal area is from 100° to 250°, which is also the local uniform area.

3.2 Simulation of the Single-Baffle Integrating Sphere for LED Light-Bar Simulation

The LED light-bar consists of two surfaces. The front surface is the emitting surface, which includes 11 LEDs. The rear surface is the Lambertian surface with a reflectance factor of 0.5. The emitting area of the LED is $(2 \times 1.25) \text{ mm}^2$ with a beam angle of 120°, and we regard it as an isotropic source. The size of the LED light-bar is defined as $(100 \times 2.5) \text{ mm}^2$, which is in the center of the integrating sphere (Fig. 5). We assumed that the detector was calibrated by use of a isotropic luminous flux standard lamp. By rotating the LED light-bar along the y-axis, we found that the signal from the detector is dependent upon the orientation of LED light-bar, as shown in Fig. 6. The signal became even lower when rotating the source from

100° to 250°. This is due to the smaller light source.

3.3 Analysis of the Single-Baffle Integrating Sphere for SLSs and LED Light-Bar Simulation

To analyze the effects caused by different light sources, we rotated the isotropic point source, as shown in Fig. 7. By correcting the SRDF of the integrating sphere, we found that the source effect caused the different behavior of its orientation result between SLSs and LED light-bar, as shown in Fig. 8. If we did not correct the SRDF and the source effect, the error reaches 10 to 20 %.

3.4 Simulation of the Single-Baffle Integrating Sphere for Varied Conditions of SLSs

We generally mount the DUT in the center of sphere to measure the luminous flux and set the baffle between the detector and the DUT to avoid the light directly incident to the detector. We want to simulate the different conditions that offset the baffle to show the effects of SLSs. The SLSs have two surfaces, the front one is the emitting surface that has isotropic distribution with a 60° beam angle, and the rear one is the Lambertian surface with 0.5 of reflectance. The area of SLSs are from (100 × 100) mm² to (500 × 500) mm², which are in the center of the integrating sphere (Fig. 9). We assumed that the detector was calibrated by use of an isotropic luminous flux standard lamp. By rotating the SLSs along the y-axis, we found that the signal from the detector depends upon on the orientation of SLSs, shown in Fig. 10. The intention of this simulation is to find the limitation of the integrating sphere when measuring the SLSs luminous flux, and to find the relation between the source effect and the source size. As shown in Fig. 10, the SLSs area about (0.5 × 0.5) m² will cause 30 % deviation at 200° compared with the location at 50°. However, the SLSs area below (0.3 × 0.3) m² shows a small deviation below 10 %. Using the SRDF correction from Fig. 7, we can obtain the result by source effect shown in Fig. 11.

We change the conditions of reflectance of the rear SLSs, where the reflectance is defined as 0, 0.3, 0.5, and 0.95, respectively. The intent of the simulation is to find the baffle effect of different reflectance, and to find the effect caused by source surface absorption. We assumed that the detector was

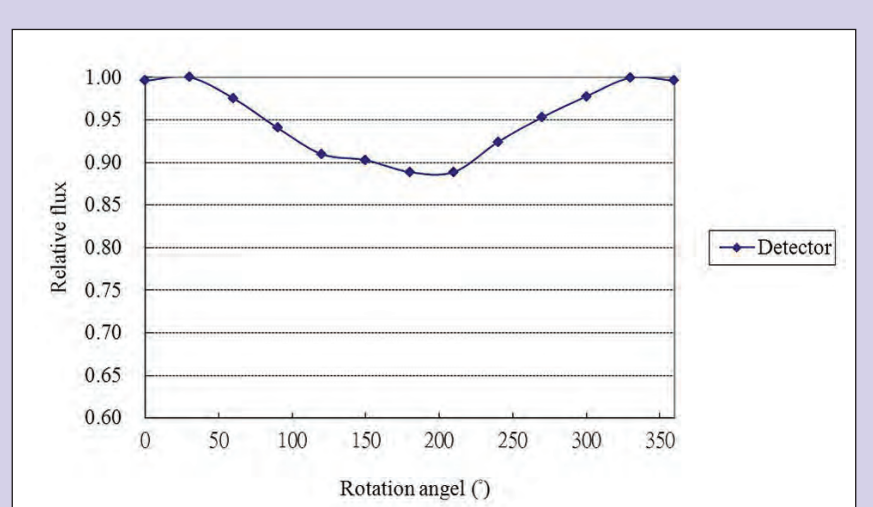


Figure 6. The results of the LED light-bar simulation when rotating along the y-axis.

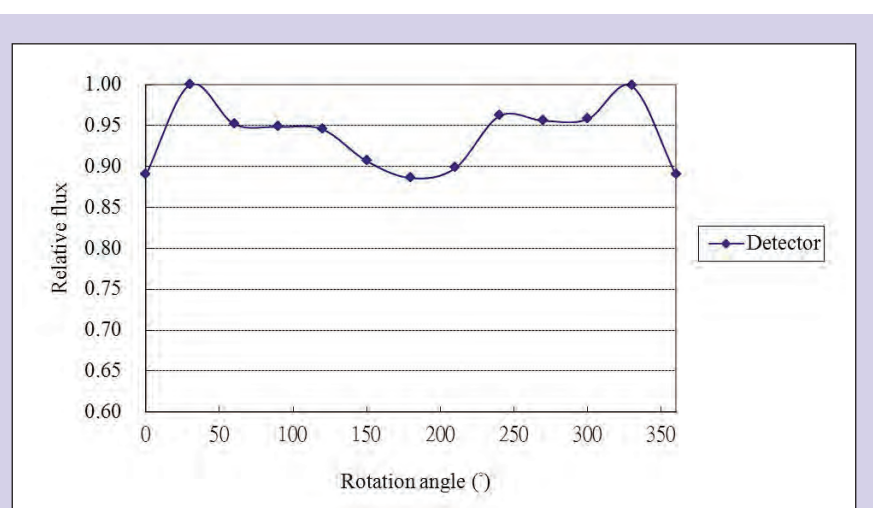


Figure 7. The SRDF of the integrating sphere.

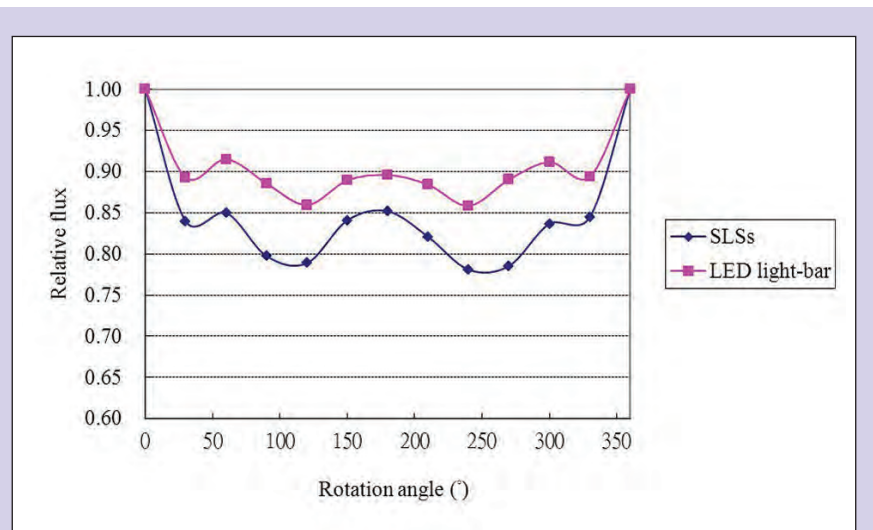


Figure 8. The source effects between the SLSs and the LED light-bar.

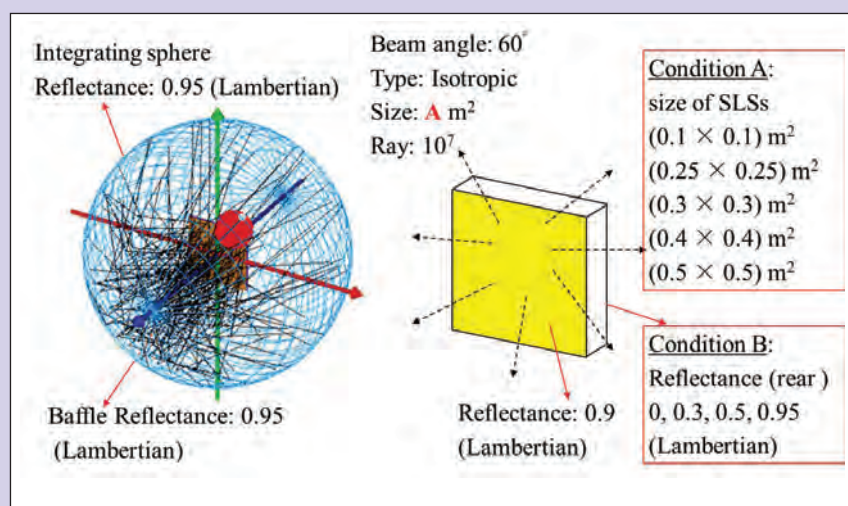


Figure 9. The varied area of SLSs simulation setup conditions.

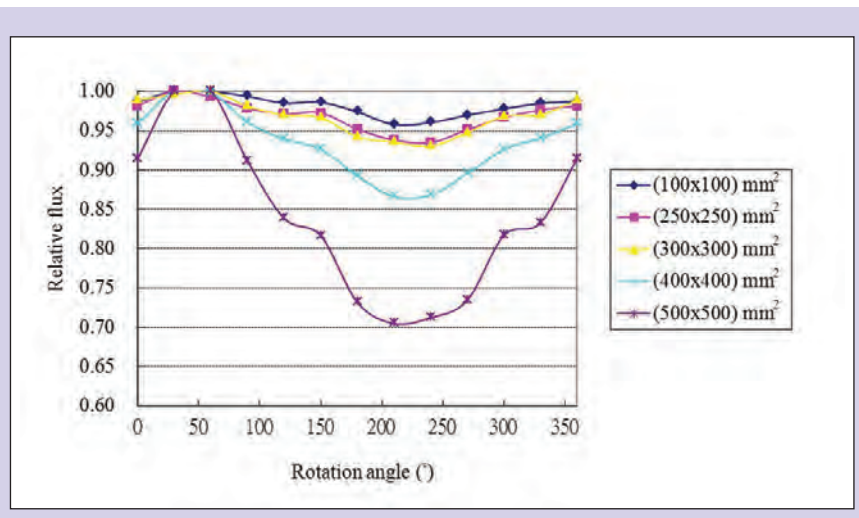


Figure 10. Results for different SLSs area.

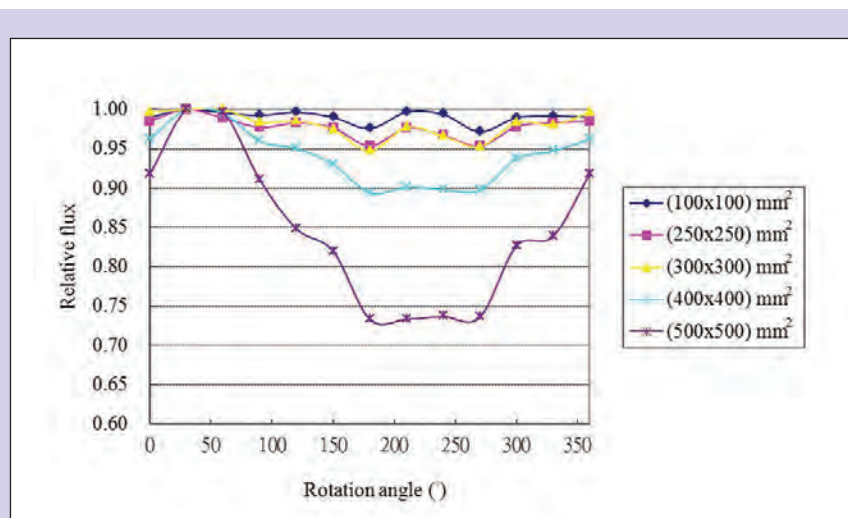


Figure 11. The SRDF correction for different SLSs area.

calibrated by use of a isotropic luminous flux standard lamp. Figure 12 shows the result of different reflectance conditions at the $(0.25 \times 0.25) \text{ m}^2$ SLSs area. Perhaps the smaller area of SLSs does not cause the large variation of non-uniformity effect, because it seems that there is no relationship between reflectance and the source effect at an SLS area of $(0.25 \times 0.25) \text{ m}^2$.

3.5 Experiment of the Single-Baffle Integrating Sphere for a Tablet Computer

We performed an actual measurement for two tablet PCs using a single-baffle integrating sphere. The diameter of the baffle is 0.2 m, and the surface is Lambertian with a reflectance of 0.95. The integrating sphere also has a Lambertian surface type, and its diameter is 1.5 m with a 0.03 m detector in front of the baffle. Tablet 1 has a $(0.15 \times 0.19) \text{ m}^2$ LED backlight display and tablet 2 has a $(0.11 \times 0.14) \text{ m}^2$ AMOLED (active-matrix organic light emitting diode) display.

To measure each tablet computer, we display the full white pattern at the center of sphere. The data are recorded when the tablet computer is rotated, which produces the result shown in Fig. 13. In Fig. 14, the smaller SLSs indicate a smaller deviation compared with the normal location (0°). If we set the SLSs in the non-uniform region, we find a measurement error of up to 20 %. The rule-of-thumb of the integrating sphere is that the diameter of the light source must be 10 times smaller than that of the sphere. However, we need to consider the geometry inside the sphere, such as the direction of the SLSs incident to the uniform region, and the reflectance and size of the SLSs.

4. Summary

We simulated the situation of integrating sphere measurement for two types of directional light sources such as SLSs and LED light-bars using a commercial Monte-Carlo ray tracing simulator, and verified the simulation results through actual measurements. The simulation results showed that the orientation of the directional light sources can increase measurement uncertainty if there is not well designed geometry or correction in the sphere. Even if we use SRDF to correct the spatial mismatch for SLSs and LED light-bars, different types of directional light sources have different results in the same orientation inside the sphere. Therefore, we can use simulation to check the limitations of

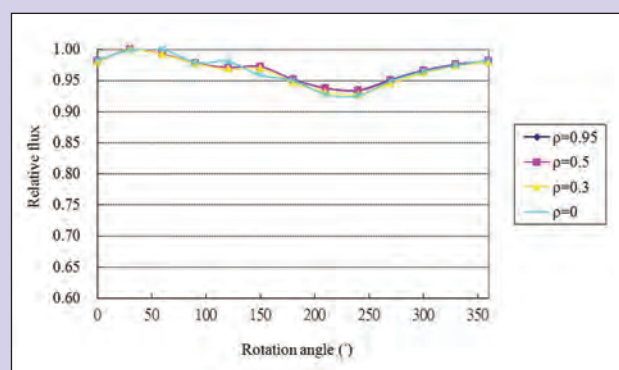


Figure 12. Results for different SLSs rear reflectance conditions.

directional light sources, such as the size and light distribution in the integrating sphere. By knowing the uniform region, the simulated and experimental results can decrease the measurement uncertainty. Many factors require further verification (from either simulation or experience), to correct the measurement results for a directional light source. In addition, a redesigned integrating sphere with suitable geometry could further improve the measurements of directional light sources.

5. Acknowledgement

The authors thank colleagues at the Korea Research Institute of Standards and Science (KRISS) for research consultation.

6. References

- [1] <http://www.light-measurement.com/ideal-integrating-sphere/>
- [2] International Commission on Illumination (CIE), “Measurement of LEDs,” *CIE 127*, 2007.
- [3] Y. Ohno, “Integrating sphere simulation: application to total flux scale realization,” *Appl. Optics*, vol. 33, no. 13, pp. 2637-2647, 1994.
- [4] Y. Ohno and R. Daubach, “Integrating sphere simulation on spatial nonuniformity errors in luminous flux measurement,” *J. IES*, vol. 30, no. 1, pp. 105-115, January 2001.
- [5] S. Park, J.-H. Jeon, N.-H Yoo, and S.-N Park, “Calculation of spatial response distribution function of an integrating sphere for LED total luminous flux measurement using a commercial Monte-Carlo ray-tracing simulator,” *Proceedings of the 26th Session of the CIE*, Beijing, China, pp. D2-37-D2-40, July 2007

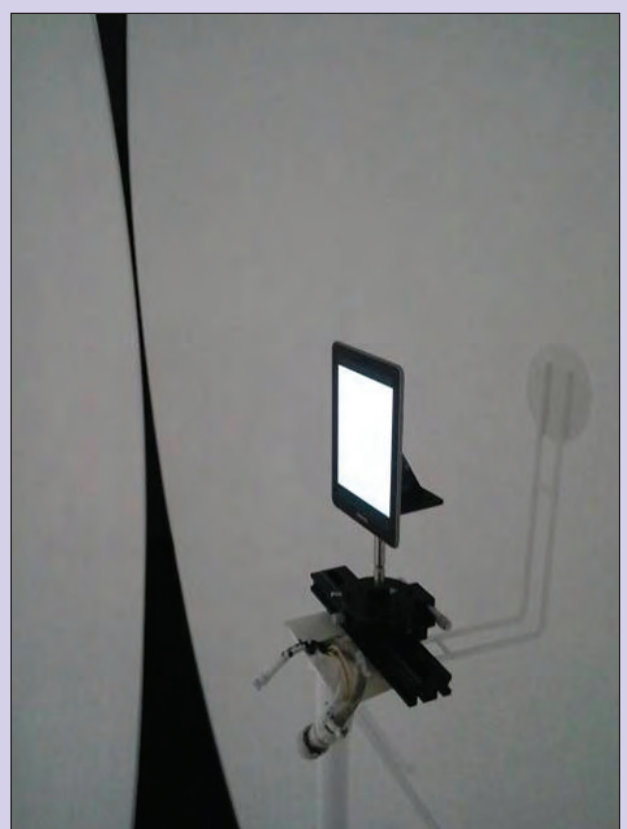


Figure 13. The setup of the tablet computer inside the sphere.

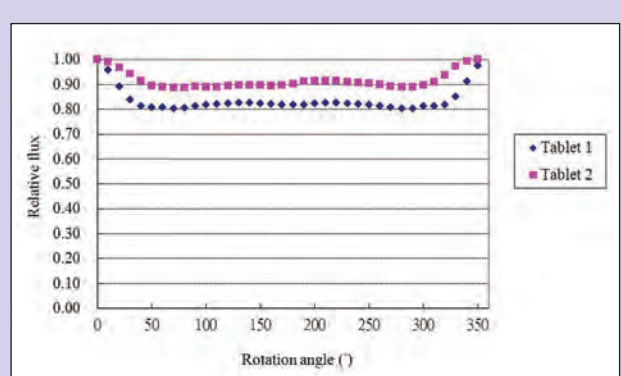


Figure 14. The measurement results for the tablet computers.

Two-Color One-Way Frequency Transfer in a Metropolitan Optical Fiber Data Network

Sven-Christian Ebenhag, Per Olof Hedekvist, and Kenneth Jaldehag

Abstract: Two-color one-way frequency transfer through one strand of optical fiber is an alternative method to two-way frequency transfer, and is useful if unknown asymmetries exist in the link due to different paths for each direction. The term “two-color” refers to the ability to send signals at two different wavelengths utilizing the same fiber in one direction. The method is suitable for implementation in existing urban Single Mode Fiber networks, for instance in networks that are utilized for data and television communication. It is therefore able to coexist with data channels in wavelength-division multiplexing (WDM) systems. It performs as a dynamical control of transit time and simultaneously enables a real-time phase stabilized output signal. This paper presents results from a comparison of two cesium beam frequency standards separated by about 3 km over an optical fiber network located in a metropolitan area in Sweden. The cesium standards were simultaneously compared to each other with a Global Positioning System (GPS) satellite link and over optical fibers, so that the optical fiber technique could be evaluated with respect to the GPS technique. The difference in frequency stability between the two methods is shown to be about 3×10^{-15} over an averaging interval of 10 000 s.

1. Introduction

The need for high accuracy time and frequency transfer has significantly increased over the last decade. Users with the most demanding requirements for the characterization of remotely located time and frequency standards are investigating the use of optical fibers, as the accuracy and stability of methods based on GNSS (Global Navigation Satellite Systems) such as Global Positioning System (GPS) appear to be reaching their limits. Recent work in the field of optical frequency transfer shows results with potential accuracies below 10^{-17} obtained in less than a day, demonstrating that the technique is useful for the comparison of optical frequency standards [1, 2]. Most of the optical frequency transfer methods or laser stabilizations [3] focus on two-way frequency transfer [4], whether it uses the optical phase [5-10] or intensity modulation at microwave frequencies [11], dark fiber, or data protocols utilized for timing in wavelength division multiplexing channels [12-14]. When two-way frequency transfer methods are used, there is a presumption that the signals delays are equivalent (symmetrical) in both directions, but in most cases the two counter wise transmission paths are asymmetrical and this introduces a

varying error. Solutions that use bidirectional signals in a single fiber results in a close to perfect match, but other limitations still occur [4].

For a solution utilizing one-way frequency transfer, it is therefore beneficial if the delay variations can be sufficiently compensated. Recent results have been presented using either a fiber based pre-compensation [15, 16], or an electronic post-compensation [17]. The pre-compensation uses a temperature controlled fiber as a part of the transmission and a feedback signal that adjusts the temperature to keep the phase difference constant between two propagated signals [15, 16]. The electronic post-compensation utilizes a model of the fiber to translate a phase difference between the two wavelengths into the corresponding delay in the fiber, and then adjusts an in-line delay unit accordingly [17].

This paper describes the results of an implementation of a one-way method utilizing propagation of two wavelengths that are compared against each other on the receiver side to create a correction algorithm for variable transit time. The algorithm is then used to control a fiber spool placed in a temperature chamber to counteract the temperature changes that affected the fiber between points of connection. This

is the first time known to the authors that such a one-way two-color transit time compensation system is implemented in an urban fiber networks for frequency comparisons between strategically placed clocks, applying the result of previous laboratory evaluations in a practical environment.

Authors

Sven-Christian Ebenhag ^{1,2}
sven-christian.ebenhag@sp.se

Per Olof Hedekvist ^{1,2}
per.olof.hedekvist@sp.se

Kenneth Jaldehag ¹
kenneth.jaldehag@sp.se

¹Department of Measurement Technology, Time and Frequency Lab
SP Technical Research Institute of Sweden, Borås, Sweden

^{1,2}Department of Microtechnology and Nanoscience, Photonics Lab
Chalmers University of Technology,
Göteborg, Sweden

The measurements presented in this paper were performed using signals with wavelengths separated by 8 nm propagated through a 3 km fiber in a metropolitan fiber network. The transmitter is located in an electromagnetically shielded room several meters below ground, while the receiver is in the entrance floor of an ordinary office building. Cesium frequency standards were located at each end of the fiber, and their frequency difference was estimated and compared using the one-way fiber link and a GPS carrier phase link.

2. Method Description

The successful distribution of a phase stabilized frequency over a one-way fiber optic connection relies on the unambiguous correlation between the dispersion and the group velocity in a single mode optical fiber. The variation in dispersion, as is detectable at the receiver, can be transformed to a corresponding change in delay through the fiber. This technique has previously been investigated in laboratory experiments [15-18].

An example of a one-way time and frequency transfer between two clocks, A and B , is illustrated in Fig. 1. The clocks are compared to each other by utilizing a time interval counter (TIC) that is located close to clock B . A predetermined signal, e.g. a 10 MHz sine wave, is transmitted from clock A at time $t_1(t_A)$, and when it arrives at clock B , the arrival time $t_1(t_B)$ is measured with respect to the local clock B ; $t_2(t_B)$. Therefore TIC_B is the measurement of clock A relative to clock B including the propagation delay ($\tau_A + \tau_{A,\text{det}}(t)$) in the transmission path as described by

$$TIC_B = (t_1(t_B) - t_2(t_B)) = (t_1(t_A) + \tau_A + \tau_{A,\text{det}}(t)) - t_2(t_B) \quad (1)$$

where τ_A is a constant and $\tau_{A,\text{det}}(t)$ indicates that the delay has a deterministically varying component.

The final frequency comparison between clocks A and B is achieved by estimating the slope of a series of time interval measurements as described by Eq. (2), which for an uncompensated link is affected by the varying propagation delay

$$t_1(t_A) - t_2(t_B) = TIC_B - \tau_A - \tau_{A,\text{det}}(t) \quad (2)$$

and accounting for possible ambiguities of the zero crossing dependent on the frequency of transmitted signal and relative frequencies of clocks A and B . Even though the average transit time delay can be estimated by calibration, the variation in the transit time will always affect the comparison unless it is continuously measured and compensated for.

To perform a time transfer between two points, a calibration must initially be performed of the transit time at starting point, τ_A , i.e. the time it takes for a given level of an edge of a signal or pulse to propagate between points A and B . Based on this reference, setting a starting value at the receiver clock, time is achieved by adding periods of a repetitive signal with known stability.

Several types of systems are utilized for one-way time and frequency transfer, including ground-based transmitters such as LORAN [19] (still operational in Europe and Asia), DCF77 [20], and satellite based systems such as GPS. A few of these systems do not compensate for variations in transit delays. In the proceeding analysis, the stability of the frequency, i.e. the operational part of time transfer, is characterized presuming alternative techniques for initialization.

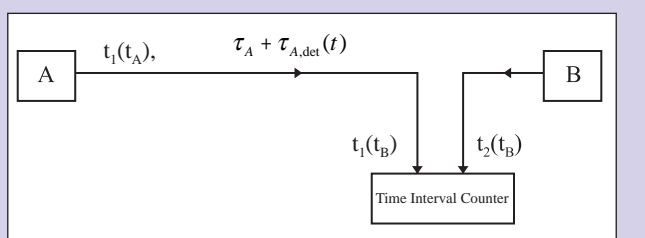


Figure 1. Schematic of an uncompensated one-way frequency transfer between clocks A and B . Time transfer is performed given that a initial calibration of the transit time in the path is performed.

When distance increases, and especially when a significant amount of the transmission media is outdoors, the temperature variations will affect the propagation properties of the media. For example, fiber located below ground is known to experience temperature variations of up to 20 °C during the year in inland regions [21], and if some sections of the fiber are installed outdoor above ground, the temperature variation will follow air temperature and the corresponding propagation delay variation will be even larger. In these cases, not only the propagation delay will change, but also the chromatic dispersion. The measurement technique for fiber dispersion is well known [22] and the variation with respect to temperature has been studied previously [23]. Nevertheless, the correlation to transit time delay has not yet been fully investigated or utilized for one-way two-color time and frequency transfer until the first presentations of this work [18].

The proposed method to solve for $(\tau_A + \tau_{A,\text{det}}(t))$ is to transmit two wavelengths through the same fiber and then detect the propagation delay differences between them [24-26]. The difference is then applied as a correction term for the delay variations in $(\tau_{A,\text{det}}(t))$. Development of this one-way frequency transfer method with enhanced stability is aimed to result in transfer quality comparable to well-established methods such as GPS [27], and TWSTFT (Two Way Satellite Time and Frequency Transfer) [28], i.e. on the order of 1 ns in time and 1×10^{-15} in frequency stability when averaging over one day. Furthermore, the proposed method operates within the C-band of commercial Dense Wavelength Division Multiplexing (DWDM) networks. The motive for using the C-band is that the commonly used Erbium Doped Fiber Amplifier (EDFA) has a flat gain spectrum between 1530 nm and 1560 nm that includes the C-band frequencies. The effect of transit time variations is greater when the two transmitted wavelength are far apart, while the availability to access channels in bright DWDM-fibers improves when the spacing is narrow. Previously published experiments [18] used two signals whose wavelengths were more than 18 nm apart, while this evaluation operates with signals separated by 8 nm. The utilized wavelengths correspond to International Telecommunication Union (ITU) channel 21 (1558.983 nm / 192.3 THz) and channel 41 (1550.918 nm / 193.3 THz) in a DWDM system. In a fully operational solution, the time or frequency from the master clock can be distributed to a network of slave clocks, with an uncertainty smaller than what would be the case if only a single wavelength was transmitted.

3. Dispersion Theory

The essential theory utilized in the one-way dual wavelength frequency transfer technique, aimed for creation of a compensation algorithm for

variable propagation delays, is based on dispersion in optical single-mode fiber (SMF) and how it relates to the signal transit time through the same fiber. Dispersion in SMF is divided into two main quantities: chromatic and polarization mode dispersion (PMD).

3.1 Chromatic Dispersion

Chromatic dispersion D_c is the sum of material dispersion, D_M and waveguide dispersion, D_w . Material dispersion arises from the variation of refractive index with wavelength while waveguide dispersion arises from the dependence of the fiber's waveguide properties with wavelength. Similar analysis has been previously presented [4] assuming the dispersion slope is not dependent on temperature and all variations can be linearly scaled from the change in zero-dispersion wavelength. Our model, however, is based on the simplified Sellmeier equations for material dispersion and the waveguide properties of a step-index fiber for waveguide dispersion, and the influence of temperature on these.

3.1.1 Material Dispersion

A wave packet propagates with a group velocity V_g as in Eq. (3) where ω is the angular frequency and β is the propagation constant,

$$V_g = \frac{d\omega}{d\beta}. \quad (3)$$

The group delay τ_g is the time delay per unit length L of a medium and is given by Eq. (4) where c is the speed of light in vacuum,

$$\tau_g = -\frac{\lambda^2 L}{2\pi c} \frac{d\beta}{d\lambda}, \quad (4)$$

which is the foundation for the utilized technique using two wavelengths of an optical fiber to determine changes in the dispersion along the path.

In a medium that is susceptible to material dispersion, the refractive index is itself a function of wavelength $n(\lambda)$ and the propagation constant β dependence on wavelength will determine the dispersion.

The free space propagation constant k is given by $2\pi/\lambda$ and the propagation constant in the medium is given by Eq. (5),

$$\beta = kn(\lambda) = \frac{2\pi n(\lambda)}{\lambda}. \quad (5)$$

It is possible to determine the group delay as a function of wavelength and refractive index in an arbitrary optical medium where refractive index is itself a function of wavelength, using Eq. (4) and (5). When applied on an optical fiber core with refractive index n_1 , the group delay, in terms of measurable physical quantities is given in Eq. (6) and the result is τ_m , the time (fiber version of τ_g) it takes for a pulse to propagate a distance L ,

$$\tau_m = \frac{L}{c} \left(n_1 - \lambda \frac{dn_1}{d\lambda} \right). \quad (6)$$

Assume now a source with a narrow band electrical signal modulated on two singular wavelengths with an optical spectral distance of $\Delta\lambda$ and a mean wavelength of λ . The phase shift due to material dispersion $\Delta\tau_m$ may then be found by expanding Eq. (6) using a Taylor series in which normally the first term is dominating. The result is given in Eq. (7),

$$\Delta_m = \Delta_\lambda \frac{d\tau_m}{d\lambda}. \quad (7)$$

Now, since the transfer technique is in need of a term that contains measurable attributes such as refractive index and wavelength, the first derivative of τ_m with respect to λ is obtained through the derivative of Eq. (6), i.e.

$$\frac{d\tau_m}{d\lambda} = -\frac{L\lambda}{c} \left(\frac{d^2 n_1}{d\lambda^2} \right). \quad (8)$$

The phase shift between two optical signals which are in phase at transmitter, due to material dispersion after a distance L is obtained by

$$\Delta_m \equiv \Delta_\lambda \frac{L}{c} \left| -\lambda \frac{d^2 n_1}{d\lambda^2} \right| = \Delta_\lambda L \cdot |D_M|. \quad (9)$$

The material dispersion, D_M , is finally defined by Eq. (10) and is usually presented in ps / (nm · km),

$$D_M = \frac{-\lambda}{c} \left(\frac{d^2 n_1}{d\lambda^2} \right). \quad (10)$$

3.1.2 Waveguide Dispersion

The evaluation of waveguide dispersion assumes that the cabling or mounting will stretch the fiber at increasing temperature, however leaving the volume intact. The variations in dimensions of the glass are assumed to be negligible. If the core of the fiber is modeled as a glass cylinder, of length L and diameter d , a geometrical approach gives that the variation in temperature will change the length with ΔL ($T - T_0$) and the diameter with Δd ($T - T_0$), such as

$$\frac{\Delta d(T - T_0)}{d} = -\frac{\Delta L(T - T_0)}{2L}, \quad (11)$$

where T is the temperature and T_0 is the temperature at starting point. This change in diameter will change the dispersion according to the variation in waveguide dispersion [29, 30] described as

$$D_w(\lambda) = -\frac{n_2 \Delta}{c \lambda} V \frac{d^2(Vb)}{dV^2}, \quad (12)$$

where n_2 is the refractive of the cladding and Δ is the relative difference of refractive index in the core and in the cladding. V and b are the normalized frequency and the normalized propagation constant, respectively, and can be found through

$$V = ka\sqrt{n_1^2 - n_2^2} \cong kan\sqrt{2\Delta}, \quad (13)$$

$$b = \frac{(\beta/k)^2 - n_2^2}{n_1^2 - n_2^2}, \quad (14)$$

where $a = d/2$ is the fiber core radius. From these equations it is apparent that fibers with notable waveguide dispersion, e.g. dispersion shifted fibers, dispersion compensating fibers, etc., will have different response to a change in diameter d compared to standard fibers where material dispersion is dominant. However, this response must be evaluated for each fiber design since the term $V(d^2(Vb)/dV^2)$ is between 0 and 1.2 with a maximum at $V \approx 1.2$. For a standard single mode fiber the operating range is $V = 2.0 - 2.4$ and results in $V(d^2(Vb)/dV^2)$ of 0.1 to 0.2 with $\Delta = 0.01$ and $n_2 = 1.5$ [30]. The waveguide dispersion for a 100 km SMF using the previous values inserted in Eq. (12) will result in a $D_w \approx 3$ ps / (nm · km), and the variation, caused by variation in n and in core diameter, is small in comparison to variations in D_M . This shows nevertheless that the system of detecting a variation in

transit time through a fiber with substantial waveguide dispersion is possible, but must be optimized for the actual fiber parameters.

According to ITU-T Rec. G.652 for single mode fiber the chromatic dispersion in the 1550 nm range should be less than 17 ps / (nm · km). It is important to note that both the material and waveguide dispersion are included in this value, and the waveguide dispersion is relatively linear while the material dispersion behaves non-linearly [30].

3.2 Polarization Mode Dispersion

The state of polarization is randomly changing along the fiber because it is not a perfectly uniform cylindrical medium, and also due to mechanical stress called birefringence. The group delay will be different for different polarizations which lead to pulse broadening due to PMD. A statistical analysis of the random differential group delay (DGD) results in [31]

$$\Delta\tau_{RMS} \equiv D_p \sqrt{z}. \quad (15)$$

In Eq. (15) D_p is the PMD parameter and have typical values in modern fibers between 0.05 to 1 ps / $\sqrt{\text{km}}$ and z is the fiber distance from start and L is total fiber length, both in kilometers. The average value of PMD is easily characterized but instantaneous PMD varies unpredictably and as a result it is difficult to compensate for. By inserting typical values for D_p and $z = 100$ km in Eq. (14), $\Delta\tau_{RMS} = 1$ ps is achieved.

The two wavelengths commonly used for this evaluation are 1551 nm and 1559 nm and if the chromatic dispersion, $D_c = 17$ ps / (nm · km) and the distance is 100 km the difference in transit time between the wavelengths will be 14 ns, which results that PMD is negligible.

3.3 Theory Evaluation

The theory for the presented one-way dual wavelength optical fiber frequency transfer technique is based on the transit time τ_m for propagation of a single mode in a fiber due to different kind of dispersions. The transit time τ_m in a fiber is dependent on the refractive index and the wavelength according to Eq. (6). The magnitude of temperature dependence of single mode fiber are shown in previous studies [21], and the property utilized in this technique. The dispersion causes two different wavelengths to propagate at different velocity in the same fiber and since the material dispersion is concluded to be dominant, the analysis focus on this. By calculating the derivative of Eq. (6) with respect to temperature, variations in both wavelength and refractive index will be taken into account as

$$\frac{d\tau_m}{dT}\Big|_{\lambda_N} = \frac{1}{c} \left(\frac{dL}{dT} \left(n_1 - \lambda \frac{dn_1}{d\lambda} \right) + L \left(\frac{dn_1}{dT} - \lambda \frac{d^2n_1}{d\lambda dT} \right) \right) \quad N = 1, 2. \quad (16)$$

The variation in transit time as a function of temperature can thus be calculated where λ_N with $N = 1, 2$ represents the two wavelengths. The equations for the two wavelengths are subtracted from each other, resulting in

$$\begin{aligned} \frac{d\tau_m}{dT}\Big|_{\lambda_1-\lambda_2} &= \frac{1}{c} \left(\frac{dL}{dT} \left((n_{\lambda_1} - n_{\lambda_2}) + \lambda_2 \frac{dn_{\lambda_2}}{d\lambda_2} - \lambda_1 \frac{dn_{\lambda_1}}{d\lambda_1} \right) + \right. \\ &\quad \left. L \frac{d}{dT} \left((n_{\lambda_1} - n_{\lambda_2}) + \lambda_2 \frac{dn_{\lambda_2}}{d\lambda_2} - \lambda_1 \frac{dn_{\lambda_1}}{d\lambda_1} \right) \right). \end{aligned} \quad (17)$$

Sellmeier Coefficient	Fitted constants (SiO_2)
A	$6.90754 \times 10^{-6}T + 1.31552$
B	$2.35835 \times 10^{-5}T + 0.788404$
C	$5.84758 \times 10^{-7}T + 1.10199 \times 10^{-2}$
D	$5.48368 \times 10^{-7}T + 0.91326$
E	100

Table 1. Empirically fitted values for Sellmeier coefficient.

This expression shows how the refractive indices of the two wavelengths are influenced by temperature, and, based on this, the variations in the transit time delay can be calculated. The frequency transfer technique uses the property that the variations are different, but correlated, which also is supported by experimental results given below.

The difference in transit time through the fiber will, as shown in Eq. (17) depend on the variation of length, L , and the variation in refractive index, n . Both these effects will affect the chromatic dispersion of the fiber, but through different properties.

The refractive index of the fiber can be described by the Sellmeier equation [32, 33],

$$n^2 = A + \frac{B}{1-C/\lambda^2} + \frac{D}{1-E/\lambda^2}, \quad (18)$$

where λ is the wavelength in μm and the Sellmeier coefficients A , B , C , D and E have been empirically estimated for different glasses. Empirical data for fused Silica [33] is used in Table 1.

The material dispersion can be calculated using Eq. (19) and corrected with respect to Ref. [33],

$$D_M(\lambda) = \frac{1}{cn} \left[-\frac{4}{\lambda^5} \left\{ \frac{BC^2}{(1-C/\lambda^2)^3} + \frac{DE^2}{(1-E/\lambda^2)^3} \right\} + \left(\frac{dn}{d\lambda} \right)^2 + 3n \frac{dn}{d\lambda} \right]. \quad (19)$$

The wavelength dependence of refractive index is given by the derivative of Eq. (19),

$$\frac{dn}{d\lambda} = -\frac{1}{n\lambda^3} \left(\frac{BC}{(1-C/\lambda^2)^2} + \frac{DE}{(1-E/\lambda^2)^2} \right). \quad (20)$$

Using these parameters, the material dispersion of SiO_2 is calculated at 20 °C and shown in Fig. 2. It may vary slightly in fibers where the silica is doped with small amount of other substances. Nevertheless the overall behavior is comparable.

Using the same model, the temperature dependence at a specific wavelength can be calculated. In Fig. 3, the material dispersion at 1530 nm is calculated over a temperature span of 40 °C, resulting in a slope of -0.0016 ps / (nm · km · °C), which is comparable to previously reported results -0.0025 ps / (nm · km · °C) for non-zero dispersion shifted fiber (NZDSF) and 0.0038 ps / (nm · km · °C) for large core fiber [21].

It is also possible to estimate the amount of transit time variations with respect to temperature. Assuming a fiber where material dispersion variation is the dominant effect (as is the case in standard single mode fiber), at a length of 20 km and measurement at 1530 nm and 1560 nm, the corresponding transit time is shown in Fig 4.

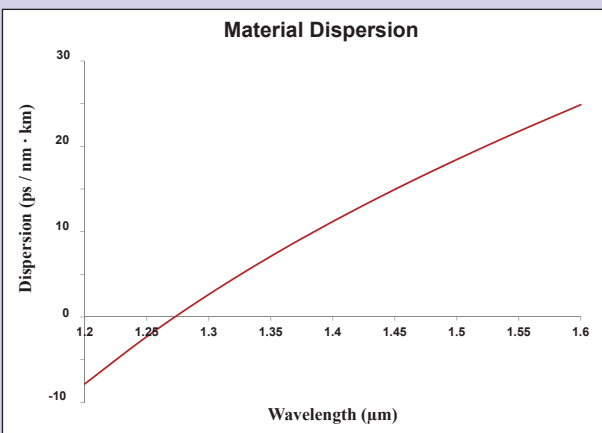


Figure 2. Calculation of material dispersion in Fused Silica at 20 °C.

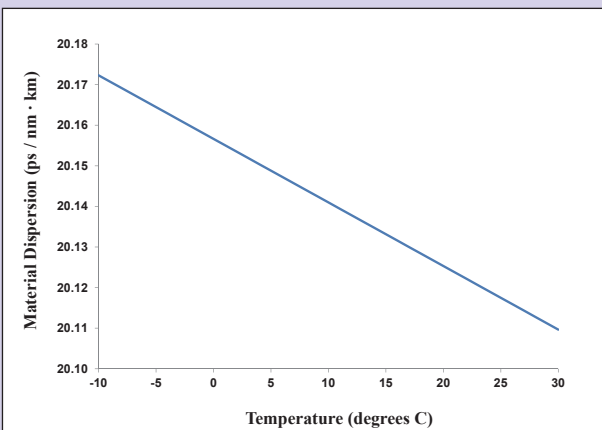


Figure 3. Temperature dependence of material dispersion in SiO.

The solid curve in Fig. 4 (left axis) shows the calculated transit time delay using Eqs. (16), (18) and (20) for a signal at 1530 nm, and the dashed curve shows the arrival transit time difference for two signals at 1530 nm and 1560 nm, using Eqs. (17), (18), and (20). Both curves are normalized with respect to the value at 20 °C, and it is apparent that the transit time delay within a single, 20 km long fiber varies with almost 0.25 μs when affected by 40 °C temperature difference. This variation can be detected and compensated for, using transmission at two wavelengths and a measurement system that can measure transit time variations on picoseconds level with sufficient precision.

3.4 Experimental Setup for Theory Evaluation

The theory was evaluated in a laboratory experiment with a setup shown in Fig. 5. The results are aimed at verifying the equations for material dispersion, and thereby presented as time resolved transit time variations compared with arrival time difference. Since no frequency stability is characterized in this experiment, no Allan deviations are calculated, and the same oscillator is used both at the transmitter and as the reference at the TIC at the receiver. This isolates the effects of the transmission of the fiber, with no errors from a reference system.

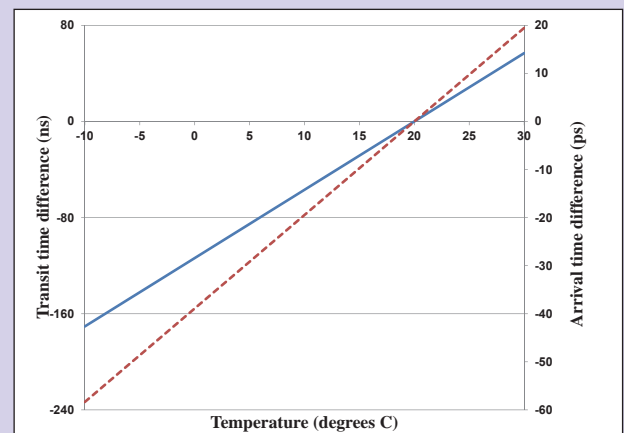


Figure 4. Temperature dependence of transit time (solid blue, left axis) and arrival time difference (dashed red, right axis).

A setup for verification of the proposed time and frequency transfer technique is shown in Fig. 5. Two continuous-wave lasers at wavelength 1551 nm and 1559 nm are after polarization controllers modulated with separate Mach-Zehnder modulators by a 10 MHz reference oscillator, after which the modulated light are launched into the SMF through a 50 / 50 power combiner. The reference oscillator is an active hydrogen maser steered in frequency using an Auxiliary Output Generator (AOG) which results in a stable and accurate reference signal. For evaluation of the method, the reference oscillator is also used as a time base for the Time Interval Counter (TIC). The total sum of the two spools of fiber that is in use was measured with an OTDR (optical time-domain reflectometer) to be 2×80 km. Added to this length is 188 m of fiber between the lab and the outdoor fiber spools. The fiber path starts and ends in the laboratory for evaluation. The use of several fiber spools instead of one creates a similar case to a commercial link, which will be assembled of multiple fibers spliced by connectors, and where there is no possibility to know the ageing of all optical fiber along the path.

At the receiving end the two wavelengths are separated in an 8-channel Dense Wavelength-Division Multiplexing Demultiplexer (DWDM DMUX), and detected in two 10 Gb / s P-I-N receivers. The signals are amplified and connected to the radio frequency (RF) ports of a double balanced mixer. One of the signals passes a power splitter that is connected to the TIC, which measures the total transit time as a reference for the evaluation. The output of the TIC is interpreted as the result of an uncompensated one-way frequency transmission.

By measuring the voltage changes from a mixer, a correction signal is achieved and can be used for a real-time delay control of the uncompensated signal. Most of the equipment is housed in a laboratory with controlled environment, except the spools of G.652-fiber which is placed outdoors inside a box for simulation of an actual environmental condition.

The 8-channel DWDM DMUX has a built in optical filter function that is used for separation of the two wavelengths. Measurement equipment detects the two 10 MHz sine waves after propagation through the fiber link, amplifies and compares with a reference signal. The results are extracted from a data set of eight days and are displayed in Fig. 6.

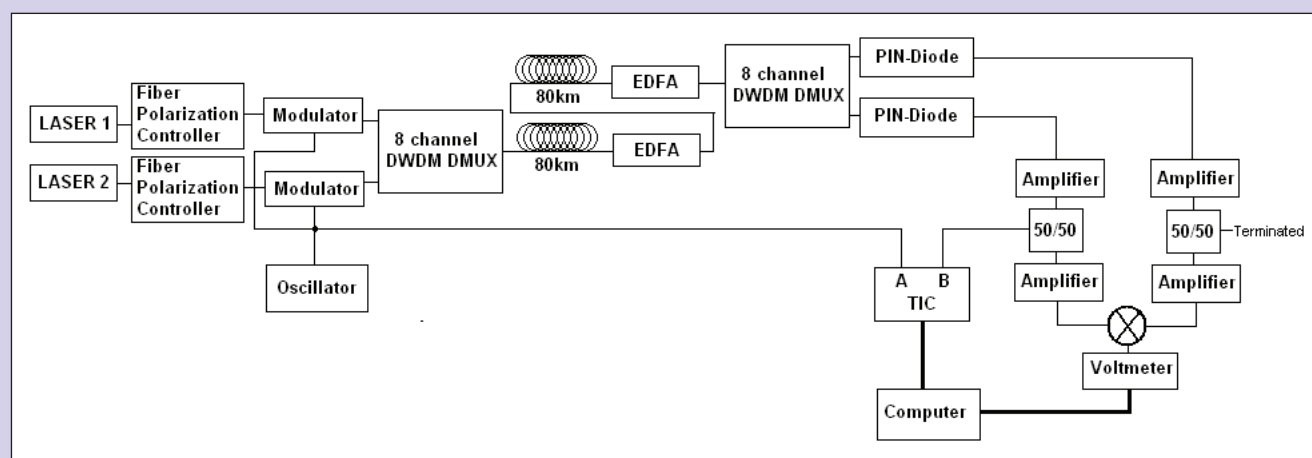


Figure 5. Experimental setup. The PIN-diode includes an electrical trans-impedance amplifier. Amplifiers are electrical amplifiers and TIC is a time interval counter.

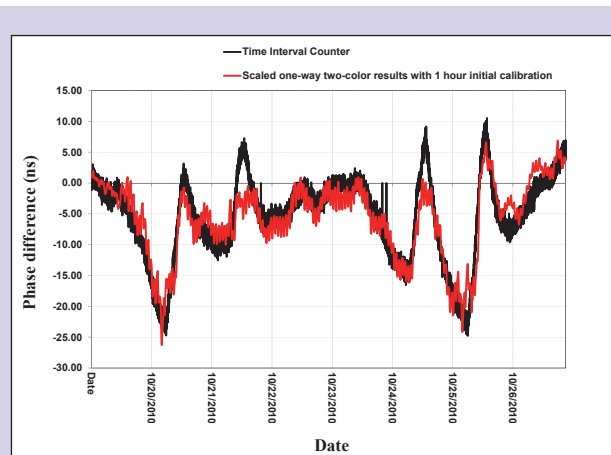


Figure 6. Data collected for theory evaluation from the outputs of the mixer (red curve) and the time interval data represented by the reference TIC (black) is plotted from data during eight days of measurement.

The mixer is set to have an initial calibration at the start to be able to calculate the fiber path parameters that would not be possible to measure in a system spread over a large distance. This calibration is presumed necessary for every individual system. The mixer in this experiment also set to have an initial startup period of 1 hour of which is used to create a running average, aimed to reduce the noise. Furthermore, the mixer solution is scaled to be able to be evaluated versus the TIC measurements and a graph displaying these data is shown in Fig. 6.

The standard deviation of the difference between the TIC data and the scaled one-way two-color technique result is 3.12 ns and the data showed temperature dependence in transit time of 6 ns / °C.

This experimental analysis demonstrates the main contributing effects of the difference in transit time and how it relates to the variations of transit time induced by temperature variations. In addition to the temperature dependence of group velocity and chromatic dispersion in the fiber, there are other effects that may influence the transit time of the signal. If these additional variations

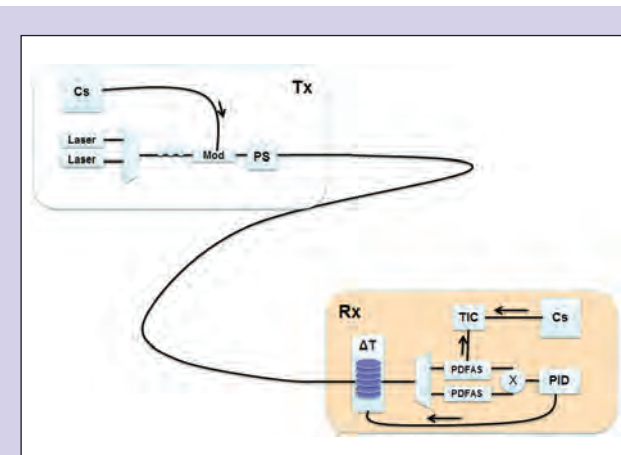


Figure 7. Frequency transfer setup. The transmitter includes a Cesium standard (Cs), two tunable lasers, a WDM multiplexer, a Mach-Zehnder optical modulator (Mod) which is preceded by a polarization controller (three circles) and followed by a polarization scrambler (PS). At the receiving end, ΔT illustrates a temperature controlled fiber spool, followed by a WDM demultiplexer, photo-detection, filter, amplification and splitting (PDFAS). The two outputs are mixed to achieve a difference signal for the PID regulator (PID) which controls the temperature box. The optical 10 MHz output from the fiber system is converted to electrical domain and measured against local cesium (Cs) standards by utilizing a time interval counter (TIC).

also vary linearly with temperature, they will be taken into account in the compensation created of empirical parameters.

The analysis enables a model for post-processing the data to compensate for transit time variations, but also enlightens the important parameters of the fiber if feedback compensation is implemented as shown in the next section.

4. Frequency Transfer Setup

The setup for the frequency transfer and the comparison of two cesium beam tube frequency standards is presented in Fig. 7. Two tunable lasers emitting light at different wavelengths 8 nm apart

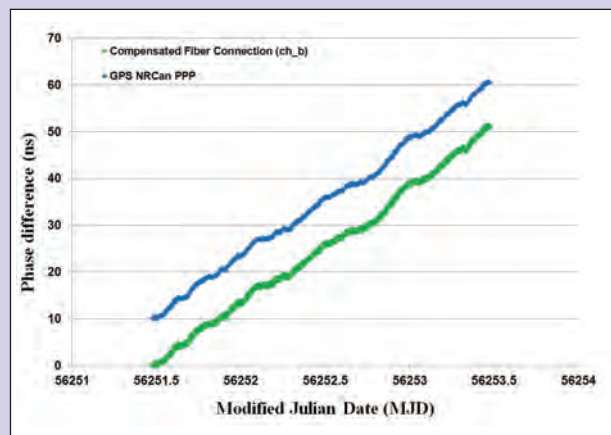


Figure 8. The phase difference between the two cesium beam standards that are compared, is presented for the period of fiber-compensation. In green utilizing the compensated fiber connection and in blue utilizing GPS NRCAn PPP. The results of the phase difference are presented with an arbitrary constant removed from the phase difference. The GPS NRCAn PPP solution has been given an extra offset of 10 ns for visualization.

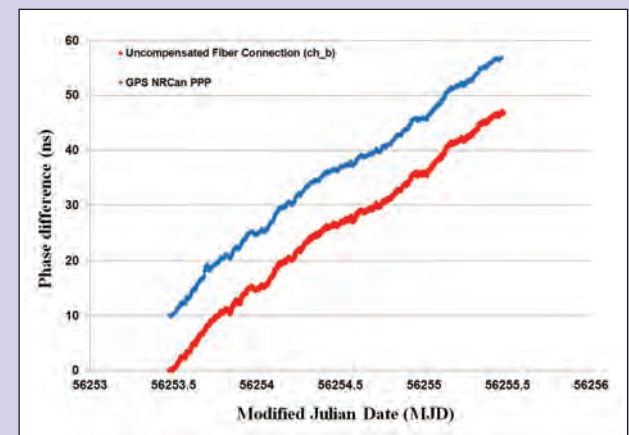


Figure 9. The phase difference between the two cesium beam standards that are compared, is presented for the period when the fiber were uncompensated. In red utilizing the uncompensated fiber connection and in blue utilizing GPS NRCAn PPP. The results of the phase difference are presented with an arbitrary constant removed from the phase difference. The GPS NRCAn PPP solution has been given an extra offset of 10 ns for visualization.

(1551 nm and 1559 nm) are combined in a WDM multiplexer and modulated by a 10 MHz sinusoidal signal from the Cesium clock (Cs). The modulated light is transmitted through a polarization scrambler, which varies the output polarization state controlled by four uncorrelated frequencies (each of the frequencies must not be a multiple of the others). The frequencies are therefore chosen as prime numbers of 7 Hz, 17 Hz, 37 Hz, and 71 Hz. The 3 km fiber between the transmitter and receiver is installed in tubing a few meters below city streets. At the receiver, the light is propagated through a 500 m standard single mode fiber (SMF) spooled on an aluminum cylinder and mounted in a thermally controlled box. At the output of this fiber, the light is split in a WDM demultiplexer and connected to P-I-N photodiodes for conversion to electrical signals. These signals are connected in parallel paths at equal length and attenuation to bandpass filters, amplifiers and power splitters (PDFAS), and finally combined in a mixer to generate a phase-difference detection (PDD) signal.

If the fiber in the temperature controlled box has the same characteristics as the fiber used in the transmission, the phase of the transferred signal is stable when the PDD signal is constant. The PDD signal is therefore connected to a proportional-integral-derivative (PID) regulator which controls the temperature of the box. Using this method for transit time compensation, all additional fiber effects with respect to temperature not included in the theory, will be compensated as well. The remaining error source is the difference between the fiber spool in the climate chamber, and the installed fiber in the network.

Both the master oscillator and slave oscillator are cesium frequency standards with high-performance beam tubes. The PDD signal emits a phase corresponding to the difference in the arrival time of the two signals. The present sensitivity using 10 MHz signals is 3.6 ° / ns and would be improved if a higher frequency were used. However, the use of 10 MHz is convenient because it is provided by the cesium standards as a standard output frequency, and no additional hardware is necessary.

The fiber is leased by the local network provider, which provides a passive fiber optic communications network within the Stockholm region. The network is open to all on equal terms and the network provider rents connections to anyone who wishes. Because only unlit or "dark" fiber is leased, customers are responsible for their own active equipment. It is used for transferring data, television and telephone signals, and more.

5. Results

The dataset of the controlled and compensated signal through the fiber was captured for a period of two days, followed by two days of an uncompensated fiber connection. The two cesium standards were simultaneously compared using the GPS Precise Point Positioning (PPP) technique, and data were processed using the NRCAn PPP software [27]. The first data set includes the phase difference between the cesium standards utilizing the compensated fiber connection and the GPS NRCAn PPP solution.

The calculated difference in phase between the cesium beam standards utilizing the compensated fiber connection that is presented in Fig. 8 shows an estimated frequency offset between the cesium clocks of $(3.0 \pm 0.4) \times 10^{-13}$ with $\sigma = 1$. The corresponding estimated offset for the GPS NRCAn PPP solution during the same time period is $(2.9 \pm 0.3) \times 10^{-13}$ with $\sigma = 1$. The rms difference between the techniques when using the compensated fiber connection is 156 ps.

The calculated difference in phase between the cesium beam standards utilizing the uncompensated fiber connection which is presented in Fig. 9 shows an estimated frequency offset between the cesium clocks of $(2.7 \pm 0.4) \times 10^{-13}$ with $\sigma = 1$. The corresponding estimated offset for the GPS NRCAn PPP solution during the same time period is $(2.7 \pm 0.3) \times 10^{-13}$ with $\sigma = 1$. The rms difference between the techniques when using the uncompensated fiber connection is 144 ps.

The frequency stabilities of the comparisons, as estimated with the overlapping Allan deviation, are shown in Figs. 10 and 11. Figure 12 presents the difference in frequency stability between the one-way

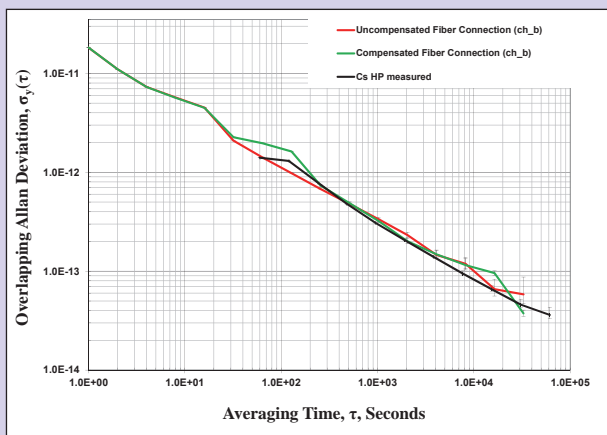


Figure 10. The frequency stability of the uncompensated frequency transfer utilizing fiber is presented in red and the real-time compensated frequency transfer utilizing fiber is presented in green. The black overlapping Allan Deviation line presents data sampled every 60 s between two high performance Cesium standards of the same type as used in the experiment.

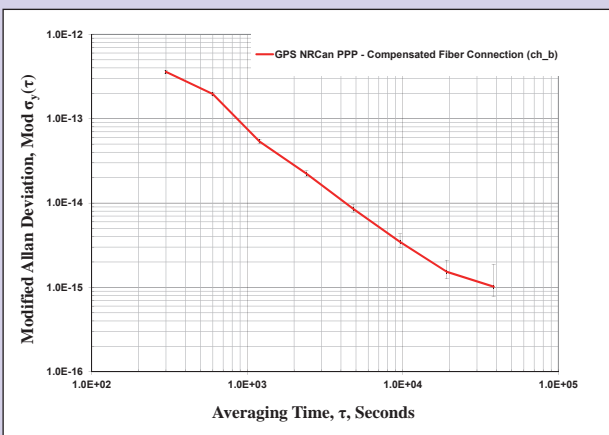


Figure 12. The Modified Allan deviation of the difference between the GPS PPP solution and the compensated one-way fiber is presented in red.

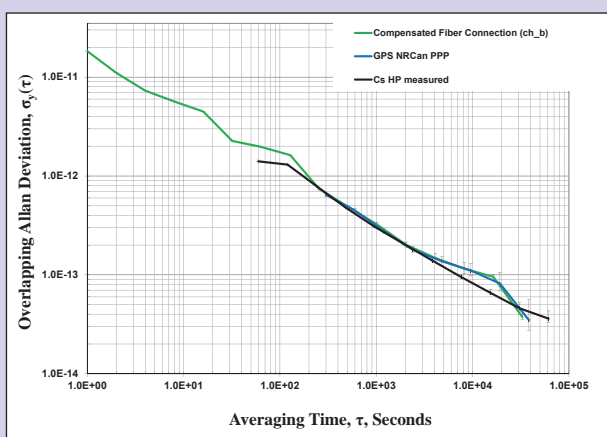


Figure 11. The frequency stability of the compensated frequency transfer utilizing fiber is presented in green and the simultaneous data for the GPS link is presented in blue. The black overlapping Allan Deviation line presents data sampled every 60 s between two high performance Cesium standards of the same type as used in the experiment.

two-color fiber based and GPS techniques estimated with Modified Allan deviation.

Time interval measurements for the compensated and uncompensated frequency transmissions are assembled with an existing multi-channel TIC with the measurement interval of 1 s at the receiver end. External temperature influence of an optical fiber is a longer process than 1 s, which means that if the time between measurements is in the 60 s range it is enough to create good propagation variation compensations. The overlapping Allan deviation is chosen to show the stability of the transmission since this is a better visualization than the TIC data when frequency stability is characterized.

From the overlapping Allan deviation graph shown in Fig.10, it is evident that improving the stability of the compensated fiber

connection is small. A small degradation at an averaging period of 100 s is expected, caused by the bandwidth of the feedback loop. The frequency stability of the link is approximately 3×10^{-13} for an average period of about 1000 s. The main improvement is expected over 10 000 s, which is slightly indicated in Fig. 10, but measurements over a longer period will be necessary to prove the full performance of the technique and would also serve the same purpose as more stable clocks to some extent.

During the time of the measurements the cesium standards were also monitored using GPS-receivers and data processed using NRCAN PPP software using rapid orbits.

Fig. 11 shows that the frequency stability of the compensated fiber was essentially equivalent to the GPS PPP link. The stability of both links was limited by the stability of the cesium clocks and the short dataset and more stable frequency standards are needed at both ends to fully evaluate the technique. Note that the GPS PPP data were sampled every 300 s. The two techniques are comparable at the level of 3×10^{-15} at 10 000 s, as shown in the Modified Allan deviation graph in Fig. 12.

6. Conclusion

The theory is experimentally verified, showing that it is possible to perform a one-way frequency transfer of optical single mode fiber with continuous real-time estimate of transit time variations. The technique is based on transmission utilizing two wavelengths, separated by 8 nm and both residing in the C-band of optical communication. By evaluating the phase difference between the transit time delays of the two signals the correction can be applied to compensate for the unwanted delay variations along the transmission path.

The improvement due to the real-time compensation in the one-way fiber frequency transfer method is substantial in lab experiments however small in the urban network installation. This fiber is more stable because it is located below ground and the duration of the measurements was too short to include large temporal variations in the transit time delay. The advantage gained over longer periods is presumed to be larger, but remains to be characterized. Furthermore, the evaluation of the technique requires more stable clocks on both sides since both links based on fiber and GPS seems to be limited by the instability of the cesium frequency standards.

To further improve the performance, the PID coefficients must be better optimized to reduce the noise at averaging intervals of 100 s, and the modulation frequency must be increased to enhance the PDD signal.

In conclusion, the experiment has been practically successful and has shown that the compensated one-way way fiber solution can be implemented in an existing metropolitan data network. The results shows the ability to transfer the frequency of a cesium beam frequency standard for distances of <10 km of buried fiber, and obtain accuracy comparable to GPS PPP even without delay compensation. For distances exceeding 10 km some compensation will be necessary.

Future improvements are related to size-reduction of the hardware and increased reliability of the transmitter and receiver. The setup is expected to work unsupervised in continuous long-term operation and to complement GPS frequency transfer.

7. Acknowledgements

This project was initiated and made possible thanks to the valuable support of Per-Olof Haettner at Swedish Defense Material Administration. GPS data was made available through Carsten Rieck at SP, NRCAN PPP software and the International GNSS Service (IGS). The NRCAN PPP software was kindly provided by Natural Resources Canada (www.nrccan.gc.ca).

8. References

- [1] C. Clivati, D. Calonico, C. Calosso, G. Costanzo, F. Levi, A. Mura, and A. Godone, "Time Transfer on Optical Fiber Development at INRIM," *Proceedings of the 26th European Frequency and Time Forum*, Gothenburg, Sweden, 2012.
- [2] O. Lopez, A. Amy-Klein, C. Daussy, Ch. Chardonnet, F. Narbonneau, M. Lours, and G. Santarelli, "86-km Optical Link With a Resolution of 2×10^{-18} for RF Frequency Transfer," *Eur. Phys. J. D*, vol. 48, no. 1, pp. 35-41, 2008.
- [3] F. Kéfélian, H. Jiang, P. Lemonde, and G. Santarelli, "Ultralow-Frequency-Noise Stabilization of a Laser by Locking to an Optical Fiber-Delay line," *Opt. Lett.*, vol. 34, no. 7, pp. 914-916, 2009.
- [4] A. Imaoka and M. Kihara, "Accurate Time/Frequency Transfer Method Using Bidirectional WDM Transmission," *IEEE T. Instrum. Meas.*, vol. 47, no. 2, pp. 537-542, 1998.
- [5] H. Jiang, F. Kéfélian, S. Crane, O. Lopez, M. Lours, J. Millo, D. Holleville, P. Lemonde, A. Amy-Klein, Ch. Chardonnet, and G. Santarelli, "Progress to a Full Optical Link on a Telecom Network," *Proceedings of the 22nd European Frequency and Time Forum*, Toulouse, France, 2008.
- [6] N. Newbury, P. Williams, and W. Swann, "Coherent Transfer of an Optical Carrier over 251 km," *Opt. Lett.*, vol. 32, pp. 3056-3058, 2007.
- [7] P. Williams, W. Swann, and N. Newbury, "High-Stability Transfer of an Optical Frequency over Long Fiber-Optic Links," *J. Opt. Soc. Am. B*, vol. 25, no. 8, pp. 1284-1293, 2008.
- [8] G. Grosche, B. Lipphardt, H. Schnatz, G. Santarelli, P. Lemonde, S. Bize, M. Lours, F. Narbonneau, A. Clairon, O. Lopez, A. Amy-Klein, and Ch. Chardonnet, "Transmission of an Optical Carrier Frequency over a Telecommunication Fiber Link," *Proceedings of Conference on Lasers and Electro-Optics (CLEO)*, CMKK1, Baltimore, Maryland, 2007.
- [9] O. Terra, G. Grosche, K. Predehl, R. Holzwarth, T. Legero, U. Sterr, B. Lipphardt, and H. Schnatz, "Phasecoherent Comparison of Two Optical Frequency Standards over 146 km Using a Telecommunication Fiber Link," *Appl. Phys. B*, vol. 97, no. 3, pp. 541-551, 2009.
- [10] O. Terra, G. Grosche, and H. Schnatz, "Brillouin Amplification in Phase Coherent Transfer of Optical Frequencies over 480 km Fiber," *Opt. Express*, vol. 18, no. 15, pp. 16102-16111, 2010.
- [11] F. Narbonneau, M. Lours, S. Bize, A. Clairon, G. Santarelli, O. Lopez, C. Daussy, A. Amy-Klein, and Ch. Chardonnet, "High Resolution Frequency Standard Dissemination via Optical Fiber Metropolitan Network," *Rev. Sci. Instrum.*, vol. 77, no. 6, pp. 064701 - 064701-8, 2006.
- [12] S. Jefferts, M. Weiss, J. Levine, S. Dilla, and T. Parker, "Two Way Time Transfer Through SDH and Sonet Systems," *Proceedings of the 10th European Frequency and Time Forum*, Brighton, United Kingdom, pp. 461-464, 1996.
- [13] M. Kihara, A. Imaoka, M. Imae, and K. Imamura, "Two Way Time Transfer Through 2.4 Gb/s Optical SDH Systems," *IEEE T. Instrum. Meas.*, vol. 50, no. 3, pp. 709-715, 2001.
- [14] R. Emardson, P. Hedekvist, M. Nilsson, S. Ebenhag, K. Jaldehag, P. Jarlemark, C. Rieck, J. Johansson, L. Pendrill, P. Löthberg, and H. Nilsson, "Time Transfer by Passive Listening over a 10 Gb/s Optical Fiber," *IEEE T. Instrum. Meas.*, vol. 57, no. 11, pp. 2495-2501, 2008.
- [15] J. Hanssen, S. Crane, and C. Ekstrom, "One way Temperature Compensated Fiber Link," *Proceedings of the Joint Conference of the IEEE Frequency Control Symposium and the 25th European Frequency and Time Forum*, San Francisco, California, pp. 1-5, 2011.
- [16] S. Ebenhag and P. Hedekvist, "Two Color One Way Time and Frequency Transfer in an Urban Optical Fiber Data Communication WDM Network," *Proceedings of the 44th Precise Time and Time Interval Systems and Applications Meeting*, Reston, Virginia, 2012.
- [17] S. Ebenhag, P. Hedekvist, and K. Jaldehag, "One Way Time Transfer Utilizing Active Detection of Propagation Delay Variations of Dual Wavelengths in an Optical Fiber Network," *Proceedings of the 43rd Precise Time and Time Interval Systems and Applications Meeting*, Long Beach, California, pp. 9-16, 2011.
- [18] S. Ebenhag, P. Hedekvist, and K. Jaldehag, "Fiber Based Frequency Distribution Based on Long Haul Communication Lasers," *Proceedings of the 41st Precise Time and Time Interval Systems and Applications Meeting*, Santa Ana Pueblo, New Mexico, pp. 57-65, 2009.
- [19] S. Yang, C. Lee, Y. Lee, J. Lee, Y. Kim and S. Lee, "Accuracy Improvement Technique for Timing Application of LORAN-C Signal," *IEEE T. Instrum. Meas.*, vol. 60, no. 7, pp. 2648-2654, 2011.
- [20] D. Engeler, "Performance Analysis and Receiver Architectures of DCF77 Radio-Controlled Clocks," *IEEE T. Ultrason. Ferr.*, vol. 59, no. 5, pp. 869-884, 2012.
- [21] A. Walter and G. Schaefer, "Chromatic Dispersion Variations in Ultra-Long-haul Transmission Systems Arising from Seasonal Soil Temperature Variations," *Proceedings of Optical Fiber Communication OFC02*, Atlanta, Georgia, pp. 332-333, 2002.

- [22] P. Vella, P. Garrel-Jones, and R. Lowe, "Measuring Chromatic Dispersion of Fibers," *United States Patent 4551019*, 1985.
- [23] W. Hatton and M. Nishimura, "Temperature Dependence of Chromatic Dispersion in Single Mode Fiber," *J. Lightwave Technol.*, vol. LT-4, no. 10, pp. 1552-1555, 1986.
- [24] L. Cohen and J. Fleming, "Effect of Temperature on Transmission in Lightguides," *Bell Syst. Tech. J.*, vol. 58, no. 4, pp. 945-951, April 1979.
- [25] L. Bergman, S. Eng, and A. Johnston, "Temperature Stability of Transmit Time Delay for a Single-Mode Fibre in a Loose Tube Cable," *Electron. Lett.*, vol. 19, no. 21, pp. 865-866, 1983.
- [26] K. Cochrane, J. Bailey, P. Lake, and A. Carlson, "Wavelength-Dependent Measurements of Optical-Fiber Transit Time, Material Dispersion, and Attenuation," *Appl. Optics*, vol. 40, no. 1, pp. 150-156, 2001.
- [27] J. Kouba and P. H'eroux, "Precise Point Positioning Using IGS Orbit and Clock Products," *GPS Solut.*, vol. 5, no. 2, pp. 12-28, 2001.
- [28] J. Levine, "A Review of Time and Frequency Transfer Methods," *Metrologia*, vol. 45, no. 6, pp. 162-174, 2008.
- [29] D. Gloge, "Dispersion in Weakly Guided Fibers," *Appl. Opt.*, vol. 10, no. 11, pp. 2442-2445, 1971.
- [30] G. Keiser, *Optical Fiber Communication*, McGraw-Hill, 2nd edition, 1991.
- [31] G. Agrawal, *Lightwave Technology: Telecommunication Systems*, Wiley-Interscience, 2005.
- [32] W. Sellmeier, "Zur Erklärung der Abnormen Farbenfolge im Spectrum Einiger Substanzen," *Annalen der Physik und Chemie* 219, pp. 272-282, 1871.
- [33] G. Ghosh, M. Endo, and T. Iwasaki, "Temperature-Dependent Sellmeier Coefficients and Chromatic Dispersions for Some Optical Fiber Glasses," *J. Lightwave Technol.*, vol. 12, pp. 1338 - 1342, 1994.

**2013
QUALITY
summit**

**Peak Performance for Today;
Future of Quality for Tomorrow.**

September 16 - 17, 2013
Laurel Manor Banquet & Conference Center
Livonia, Michigan

AIAG.org

The advertisement features a collage of images related to quality management and manufacturing, including a digital scale, a blueprint, a worker in a hard hat, and a robotic arm.

New for 2013! MEASUREMENT & METROLOGY Track!

Industry leaders will be on hand discussing
EVERYTHING METROLOGY - from the basics
to advanced!

Interested in exhibiting or sponsoring?
 Join sponsors GM, Toyota, Honda, Chrysler,
 Magna, and SAE International at this
 must-attend event! Contact Shannon Osburn
 at (248) 213-4642 or sosburn@aiag.org
 for details!

Register at:
[**http://bit.ly/aiagqs13**](http://bit.ly/aiagqs13)



Experimental and Simulation Study for a Time Transfer Service via a Commercial Geostationary Satellite

Jacqueline Walker and Marco Genova

Abstract: Time transfer over satellite links has been explored since the satellite era began. Currently, Two Way Satellite Time and Frequency Transfer (TWSTFT) is routinely used between national timing laboratories to align national timing standards, and the Global Positioning System (GPS) provides accurate timing signals in addition to its more familiar navigation solution. This paper reports on a method for transferring time from a reference clock over commercial geostationary satellite links with a specified low level of uncertainty at the receiving stations, using only the ephemeris information provided by the satellite operator. An initial experiment, reported here, showed that with one master station, measuring aggregate extraneous delays and transmitting positioning and delay data plus a correction factor to the slave stations, allowed transfer of a 1 pps (pulse per second) timing signal with a standard deviation of 72 to 98 ns and peak-to-peak variations of 500 to 600 ns, when measured against a GPS reference. Subsequent analysis of the experiment uncovered some issues with the implementation, suggesting that these results could be substantially improved upon. Furthermore, a simulation of the system that modeled the extraneous delays produced results similar to those obtained in the experiment.

1. Introduction

Time and frequency transfer is used to provide accurate time signals, synchronized to a reference clock, to locations distributed across a territory. The requirements of the implementation vary depending upon whether the need is to transfer time or frequency. For accurate transfer of time from a remote reference clock to a local clock, the path delay of the time signal must be known as accurately as possible, whereas for frequency transfer, the goal is to minimize the variation in the path delay [1]. Time and frequency transfer methods generally fall into three different categories: one-way methods, two-way methods, and common-view methods. In two-way time transfer, the delay is estimated based on measuring round trip delays between two stations. The path delay in each direction can be eliminated entirely if the paths between the two stations are symmetrical [2]. In common-view time transfer, two or more receiving stations measure the arrival time of a master timing signal from a common source then compare their measurements by subtracting them. To the extent that path delays and path delay

variations are common between the different paths, they will cancel out in the difference of two measurements, reducing the error in the time transfer [1].

Two-way time transfers over satellite links offer uncertainties on the order of nanoseconds, because most of the path delay cancels out [2]. Originally there were also significant disadvantages to this approach as it was expensive, both stations needing to transmit as well as receive, and it was more difficult to set up as a point-to-point procedure requiring calibration of equipment and careful measurement of delay components. However, TWSTT (two-way satellite time transfer) and TWSTFT (two-way satellite time and frequency transfer) are now routinely used to compare the reference clocks and time scales of national timing laboratories [3].

The simplest approach to time and frequency transfer might appear to be the one-way method, where the user requires only a receiver, and a master clock signal can be transmitted to many such receiving stations. However, for this approach to be successful, a good estimate of the delay and delay variation from transmitter to receiver must

be available [1]. One-way time transfer over geostationary satellite links has been explored since the satellite era began [4, 5]. However a geostationary satellite is not completely stationary but has a small, continuous variation in its position. References [4] and [5] represent early attempts to quantify the uncertainty in the received timing signal due to the resulting variation in the path delay between the sending and receiving stations. In [4], the position of the satellite is estimated

Authors

Jacqueline Walker
jacqueline.walker@ul.ie

Department of Electronic and
Computer Engineering
University of Limerick
Limerick, Ireland

Marco Genova
marco.genova@mixed-processing.ie

Mixed Processing Ltd.
Office 301, Shannon Airport House
Shannon, Ireland

from six orbital elements which are provided by the satellite operators and the delays thus calculated are compared with measured delays. In [5], the approach used is three station trilateration of the satellite position while simultaneously manually synchronizing the clocks.

A one-way time transfer approach which makes use of an existing signal, in this case a line in a standard television signal; was introduced in [6]. For time transfer between a reference station and a user station, the differential delay between the satellite and the two stations needed to be known as accurately as possible, and the uncertainty due to the variation in the satellite position was estimated at 2 to 3 μ s. Improvements to this approach were further described in [7, 8] where averaging was used to remove periodic components of the satellite motion, and the geometry of a known reference link was used to correct for the longitudinal drift. An alternative approach of fixing the position of the satellite was also described, although this required four stations as it used the differential delays.

The broadcast of Coordinated Universal Time as maintained by the National Physical Laboratory of India, UTC(NPLI), by use of the INSAT geostationary satellite system is described in [9]. In this system, the satellite position was calculated based on the six orbital elements received from the satellite operator once every seven to ten days. The results for the timing data showed a distinct diurnal variation and, in the absence of the orbital corrections, an increasing error up to $\pm 20 \mu$ s, which is reduced every time the orbital elements are updated by new information. In [10] a differential approach for reduction of diurnal residuals to within one microsecond accuracy is described. Another system that required differential measurements from four stations for input into an extended Kalman filter (EKF) to apply a dynamic model of the geostationary satellite orbit was claimed to improve the accuracy to within $\pm 0.025 \mu$ s across the Korean peninsula [11]. In [12], frequency transfer using a geostationary satellite was described. The approach required four reference stations with synchronized frequencies in order to determine the velocity vector of the satellite motion, and to provide a correction for the Doppler shift on the frequency at the receiver stations.

Currently, the most common one-way time transfer implementation using satellites is the Global Positioning System (GPS) [13, 14] in which the remote master device is an atomic clock located on board the navigation satellite. The delay from a GPS satellite to a receiver is large, about 65 ms, but the uncertainty in the delay, computed by the receiver using ephemeris information sent by the satellite, is just a small number of nanoseconds. However, components other than path delay uncertainty become just as important. Even though their individual absolute amounts may be quite small, the uncertainties involved in their estimates or measurements can still be significant [1].

For many years, the possibility of a commercial one-way timing service over satellite has been explored but apart from the GPS a commercial timing service product of this kind is not yet available. GPS provides excellent accuracy but from some points of view, it remains a technical and geopolitical risk because the system is managed by the defense department of a single country, the United States. These risks have been historically confirmed, for example, in the use of Selective Availability [15] where the system accuracy was intentionally degraded until the program was discontinued in May 2000. Consequently, as alternatives to GPS, there are similar projects under development, such as Galileo (EU), GLONASS (Russia), COMPASS (China) and IRNSS (India). Only one of these systems,

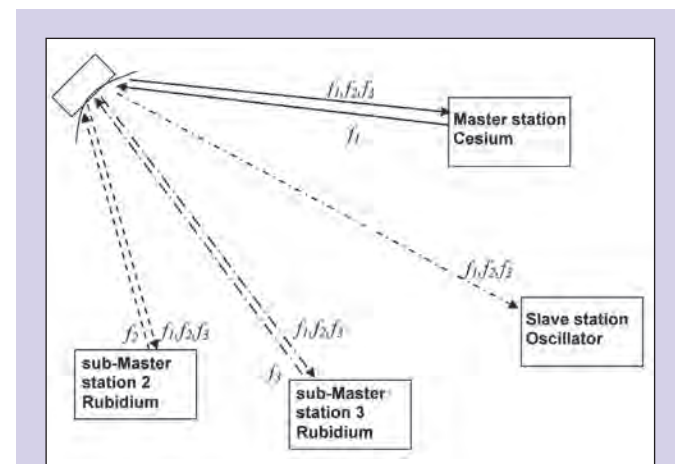


Figure 1. Proposed system for time transfer over satellite.

GLONASS, is currently fully available as an alternative, with the other systems projected to become operational progressively during the next decade. More recently, real concern has arisen over episodes of deliberate jamming of the GPS signal, usually in an attempt to block location information, sometimes with criminal intent [16]. In the current situation, if the quality of the GPS signal deteriorates, some of the main information and communications channels would not be usable in many countries, causing a wide range of problems [17].

This paper reports on the development of a system for time signal transfer from a reference clock over commercial satellite links. The system will aim to provide a specified low level of timing uncertainty of ± 50 ns at the receiving stations, making use only of the projected ephemeris information provided by the satellite operator. In the fully realized system, with a number of master stations using TWSTFT and exchanging timing information via satellite to track the satellite position, information transmitted concurrently with the reference timing signal will allow slave stations to adjust the timing signal to compensate for satellite motion. The paper is structured as follows: in Section 2, we present an overview of the time transfer system proposed by Mixed Processing Ltd., and of the experiment conducted as a proof of concept and a demonstration of the system. The analysis of the experiment and its results are also discussed. In Section 3, the development of a simulation of the experimental system and its results are presented. Finally, in Section 4 we present conclusions and a brief outline of the future development plans.

2. The Mixed Processing Time Transfer System

The time transfer system [18] now being developed by Mixed Processing Ltd. can provide a complete off-the-shelf system for transferring accurate time via satellite. The full system, shown schematically in Fig. 1, consists of three master stations used to fix the satellite position using triangulation, with the possibility of up to three more master stations for redundancy and failover. The master stations would communicate with each other and with the receive-only slave stations using bandwidth rented from a commercial satellite provider, such as Intelsat [19] or Eutelsat [20]. One master station will have a high performance clock, such as a cesium atomic clock. The two sub-master stations will have stable atomic clocks of lower performance, such as rubidium clocks. The master stations will align their clocks using TWSTFT and exchange satellite ranging data to allow the

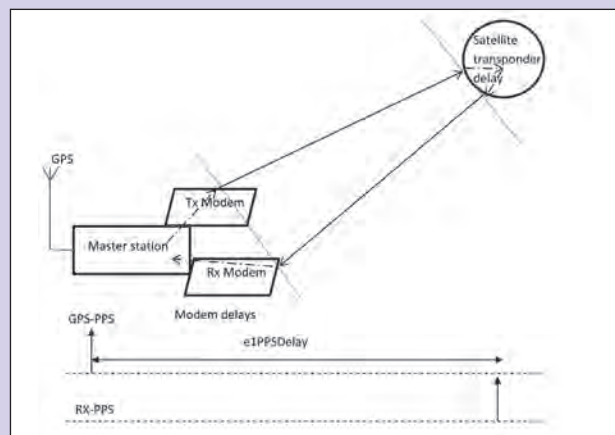


Figure 2. Diagram of procedure and measurements at master station.

master station to send real-time satellite ephemeris data to the slave stations. Each of the master stations, whether master or sub-master, will have a bidirectional link to the satellite. Finally, slave or receive-only stations will require only a unidirectional (receive-only) link with the satellite. Mixed Processing Ltd. has developed the satellite modem for the system using a field programmable gate array (FPGA) with a soft-core microprocessor. The RF transceiver functions in the L Band and is two-way only for the master stations, whereas it may be configured as receive-only for the slave stations. The satellite links are in the Ku Band.

In order to determine accurately the propagation time of signals between the master station and the slave stations it will be necessary to consider and correct errors due to:

- Errors in the satellite ephemeris.
- Relativistic effects, including the Sagnac effect.
- Delay variation due to the interaction of the signals with the troposphere and the ionosphere.
- Errors caused by the resolution of the transmitter and receiver system and by the noise of the PLL (phase locked loop) and DLL (delay locked loop).
- Temperature induced variations in cables and particularly in outdoor equipment.
- Generic statistical errors regarding the evaluation of distances and ground station position.

2.1 Proof of Concept Experiment

An experiment was conducted as a proof of concept of the system with a single master station broadcasting a 1 pps timing signal to three slave stations. The experiment was conducted in Italy with the master station located at Bresso, Lombardia and the three slave stations located at Asti, Piemonte; Treviso, Veneto; and Palermo, Sicilia. Satellite ephemeris data for Eurobird 3 (now known as Eutelsat E33A), a satellite used for the transmission of television signals, was obtained from the satellite operator [20]. The master station measured the round trip time to the satellite and broadcast the satellite coordinates, transmission delay information, and a correction factor to the slave stations so that they could adjust their expected arrival time of the 1 pps signal. Commercially available satellite

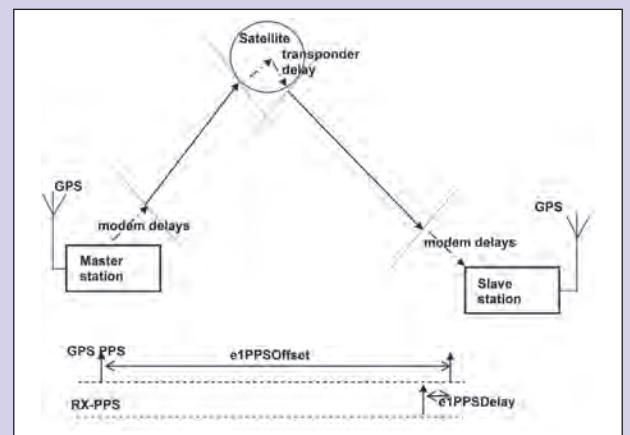


Figure 3. Diagram of procedure and measurements at slave station.

modems (Comtech CDM570 L band) were used at the stations and proprietary multi-source time and frequency equipment was used to provide a GPS 1 pps reference for the experiment and to implement the experimental algorithms. The GPS receiver in the equipment was a single frequency coarse acquisition (C/A) code receiver and the uncertainty of the GPS 1 pps was ± 50 ns. The 1 pps was encoded as the least significant bit (LSB) in channel 2 (Frame 0, Time Slot 1) of the multiframe E1 signal. As this was an initial experiment with such a system, the GPS 1 pps signal available at each station was used as a reference to measure the 1 pps timing signals transmitted from the master station to the slaves. The measurements were processed centrally at the master station equipment and stored in a spreadsheet for subsequent analysis.

The procedure carried out by the equipment at the master station is illustrated in Fig. 2 and is as follows:

- The expected path delay between the station position and the satellite position was calculated using the speed of light c , where the station position was that provided by the GPS receiver, and the satellite position was obtained from the operator provided ephemeris that had been interpolated to one second intervals.
- Measure e1PPSDelay: the time between the GPS PPS reference at the master station and the time the same PPS is received back at the master station following a round trip via the satellite.
- Calculate a correction factor: the difference between the predicted round trip time and the actual round trip time.
- Send the satellite coordinates, transmission delay and the correction factor to the slave stations.

From Fig. 2 and the sequence of steps performed at the master station, it can be seen that the calculation of the difference between the estimated round trip delay between master station and satellite and the actual measured delay will include all the extraneous delays such as the uplink and downlink satellite transponder delays, the delays through the ground equipment and cables, and delays due to atmospheric effects. The components of the extraneous delays such as the equipment and cable delays were not determined separately. In future development of the system, it is expected that these components will be measured allowing for more accurate adjustment of the delay between stations.

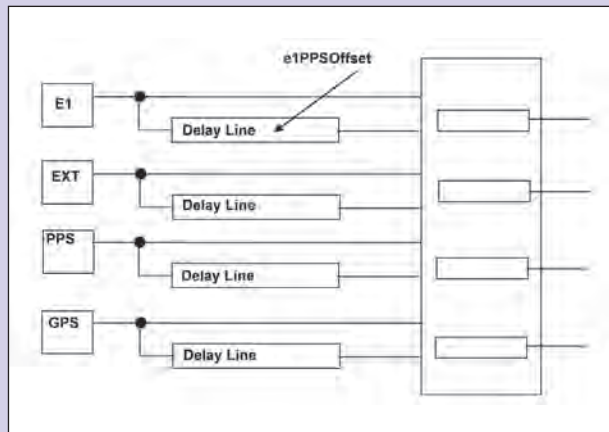


Figure 4. Schematic of timing signal regeneration using delay line.

The procedure carried out by the equipment in the slave stations (illustrated in Fig. 3), is as follows:

- Receive the satellite coordinates, transmission delay and the correction factor from the master station together with the 1 pps signal.
- Calculate the expected one-way delay between the slave station and the satellite using the known position of the slave station and the satellite coordinates.
- Calculate the expected one-way path-only receive delay from master to satellite to slave.
- Incorporate the correction factor and thus calculate the expected delay (e1PPSOffset) at the slave station for the 1 pps signal.
- e1PPSDelay is the time difference between the 1 pps signal received over the satellite link from the master and the GPS 1 pps reference available independently at the slave station which has been delayed by the e1PPSOffset in a delay line as shown in Fig. 4.

2.2 Experimental Results

The initial experiment demonstrated that, even with the simple protocol presented above, it was possible to transmit a 1 pps timing signal from a master station to slave stations dispersed over a large territory using a commercial geostationary satellite link with an accuracy of at worst 1 μ s. For this accuracy to be achieved, satellite ephemeris data from the satellite operator was interpolated to one second intervals and sent to the slave stations, along with the one-way transmit master to satellite delay calculated from the ephemeris data and a correction factor that accounts for all extraneous delays estimated from the measured round trip delay. At this initial stage of the project, the experiment did not use the measured round trip delay to improve the estimate of the satellite position because this is not possible without more master stations; for example, by using trilateration.

A number of problems arose in the initial experiment. These will be briefly described first and then the impact of each will be evaluated. The first issue was the occasional malfunctioning of the satellite modem used (not one developed by Mixed Processing Ltd). The malfunctions occurred three times at the master station and once at the Palermo slave station, where an interruption to the 1 pps transmission

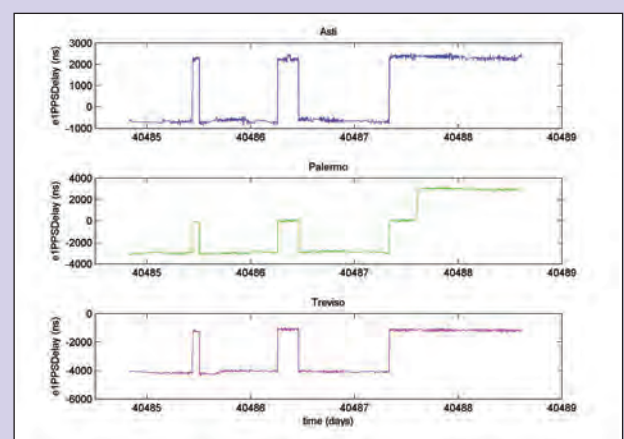


Figure 5. The measured time differences (e1PPSDelay) at the three slave stations.

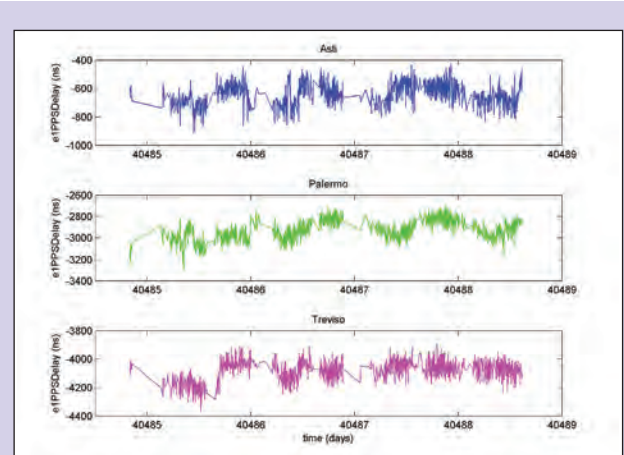


Figure 6. Adjusted e1PPSDelay at the three slave stations.

appears to have caused a phenomenon similar to a cycle slip and is the cause of the phase steps in the e1PPSDelay data seen in Fig. 5. A second issue is that the data recovered from the experiment are not continuous and have interruptions of varying duration. A third issue was that the ground station position coordinates obtained from the GPS equipment varied over time, affecting the calculations. A fourth issue was that an incorrect earth radius value was used which affected the calculation of the station to satellite path delays.

The e1PPSDelay was measured relative to the GPS 1 pps signal. In the evaluation of the e1PPSDelay, the phase steps in the data (Fig. 5) made it difficult to analyze the data. Thus, the phase steps, which were caused by resetting the communications link, were removed from the e1PPSDelay without shifting the data with respect to the x-axis (time of day) and the data were replotted. The results (called ‘adjusted e1PPSDelay’) for the three different slave stations are shown in Fig. 6. Note that in all figures showing data from the experiments, the horizontal axis shows time in days (represented as sequential date numbers in the format utilized by Microsoft Excel).

The adjusted e1PPSDelay values appear to show some quasi-periodic phase noise that is still somewhat obscured by the interruptions in the data collection, but is clearly present. It is seen

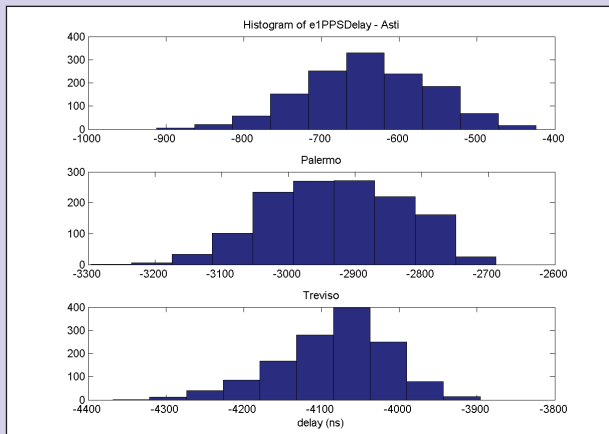


Figure 7. Histograms of adjusted e1PPSDelay.

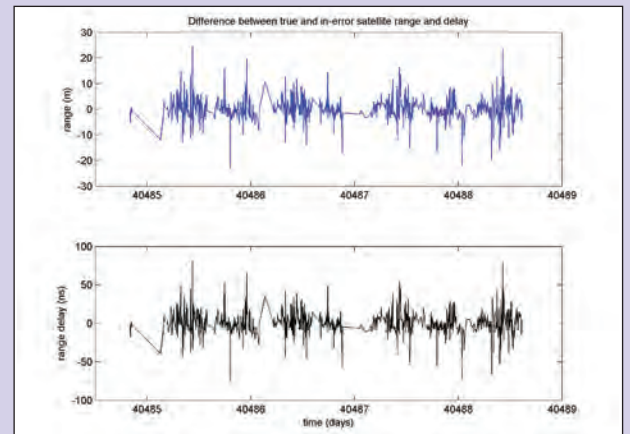


Figure 8. Range and delay variation due to time-varying satellite position.

	Asti (ns)	Palermo (ns)	Treviso (ns)
Mean	-642.5	-2927.0	-4083.4
Standard Deviation	78.5	98.6	72.0
Median	-648.0	-2928.0	-3896.0
Range	488.0	608.0	472.0

Table 1. Descriptive statistics for e1PPSDelay at slave stations.

most strongly in the Palermo data and is least visible in the Treviso data. Histograms of the e1PPSDelay distributions are shown in Fig. 7 and suggest an approximately normal distribution of the e1PPSDelay, with the station at Asti having the most normal distribution and the station at Treviso the least. Normal probability plots of the e1PPSDelay data (not shown) suggest that the major component of the e1PPSDelay is normally distributed phase noise due to a variety of causes including equipment noise, the path delay errors caused by using the time-varying GPS station location coordinates, and the impact of factors not used explicitly in the delay calculations such as atmospheric effects. However, there is some curvature in the normal probability plot suggesting that there are other sources of noise in the e1PPSDelay data, in particular a quasi-sinusoidal variation (wander) due to the satellite motion.

Descriptive statistics were also calculated for the adjusted e1PPSDelay. The results are summarized in Table 1, where the range characterizes the peak-to-peak variation of the time differences. The table also shows the mean, standard deviation, and median of the time differences. The range is due predominantly to the satellite motion and is largest at Palermo, the station which is the furthest from the master station.

2.3 Sources of Error in the Experiment

Apart from the issues with the modem discussed above, a further potential source of error in the experiment was that in the calculations of path delay, time-varying station position coordinates provided by the GPS portion of the equipment were used. Clearly, the ground station antenna position is not really varying and thus using time-

varying coordinates would be an uncertainty in the satellite path delay calculation and would add additional phase noise to the received timing signal. Errors in antenna coordinates are a common source of uncertainty in satellite time transfer measurements [8, 14] and the experience of the experiment highlights the importance of determining these as precisely as possible using a geodetic GPS receiver.

Even so, the analysis of the effect of using the varying ground station coordinates showed that it was not especially large. A comparison was made between the satellite ranges and range delays calculated using the time-varying position data and those that would have been calculated using a fixed value. The average of the time-varying positions was used as the fixed value for this comparison. The error plots for the range and delay resulting from using time-varying ground station positions are shown in Fig. 8, where it can be seen that the maximum absolute range error is approximately ± 25 m, the maximum absolute delay error was less than 100 ns, and the average delay was less than 10 ns.

A potentially more serious issue was that an error in the mean earth radius value was programmed into the software used to calculate the station to satellite ranges. Once this issue was discovered, extensive analysis was carried out investigating the effect of the error. The experiment was effectively re-run within a computer reconstructing the range and delay values using the satellite ephemeris data for the time period in question available from the satellite operator's archive [20]. These values were used to replicate the experiment results using the available measurement data, i.e. the actual measured master-to-satellite round trip delays from the experiment, for comparison with the experimental results. As a result of the analysis, it was established that the incorrect value used meant that the equipment consistently estimated the satellite as further away than it actually was. The net effect of the error was simply an additional delay with only a sub-nanosecond variation, as shown in Fig. 9.

3. Simulation

A simulation of the experiment using one master station and only one slave station was conducted. The aim of the simulation was to improve understanding of the limitations of the experiment by reproducing the transmission of the 1 pps signal from master to slave station. This was done by generating a 'ground truth' record of the satellite position and thus generating a set of measurements of the overall delay for

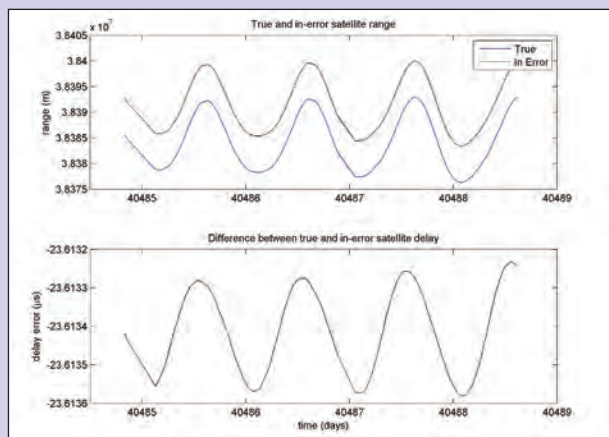


Figure 9. Difference in range and path delay due to radius error.

the transmission of the 1 pps signal from master to slave. The second step of the simulation was to reproduce the processing carried out at the master and slave stations in order to simulate the measurement of the difference (e1PPSDelay) between the GPS 1 pps and the received 1 pps sent over satellite.

In the simulation, the master station was placed at Bresso, as in the experiment, and the single slave station at Palermo. The satellite ephemeris data was downloaded as earth-centered earth-fixed (ECEF) Cartesian coordinates for the period covering the dates of the experiment from the satellite operator archive [20]. As it was archived satellite data, potentially corrected after observation of the satellite by the operator, it may be more accurate than the projected satellite ephemeris originally available at the time of the experiment, which makes it suitable for generating the ground truth track of the satellite for the simulation. However, the archived satellite ephemeris data is still available only at 30 minute intervals and had to be interpolated to one second intervals using splines as was done in the experiment. Using the station coordinates and the interpolated satellite coordinates, ground truth path delay values were calculated for the master and slave stations.

It was not possible to use the recorded correction factors from the experiment to simulate the measurements, because the correction factors are not available at one second intervals. Hence, an alternative approach was required to estimate the extraneous delays, providing us with the opportunity to use the simulation to determine how much these contributed to the observed results of the experiment. Two alternative approaches were used. In the first approach, the extraneous delays were modeled based on the statistics of the correction factor data from the experiment. In the second approach, the extraneous delays were modeled as a sum of the troposphere delay estimated from weather data and overall equipment delay modeled as a sum of white noise and diurnal wander. Satellite transponder delays are not included in the simulation calculations as no information was available to characterize these. The Sagnac effect is also not included in the simulation as it can easily be calculated and removed in practice [21].

The simulation records the reception of the 1 pps signal from the master at the slave by adding the generated measured overall master to slave transmission delay to an ‘ideal’ clock (i.e. a sequence of integers simulating an ideal one second period). This matches the procedure

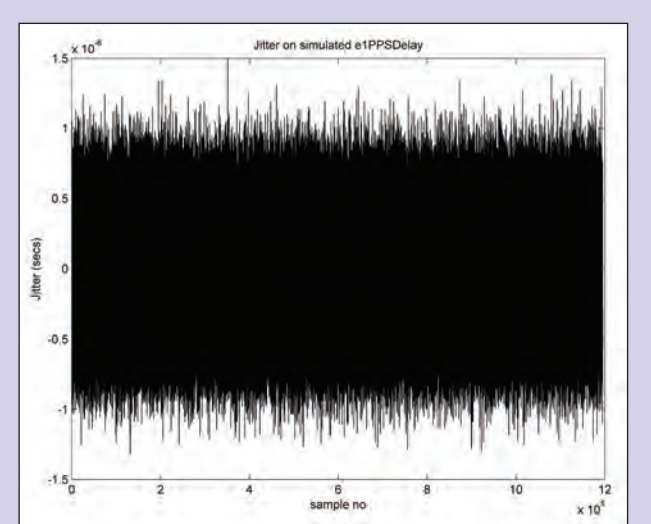


Figure 10. Simulation with equipment delay modeled using experimental statistics.

in the experiment where the GPS 1 pps was used as a reference and was assumed to not contribute any noise to the measurement. Then, following the procedure in the experiment, an estimate for the arrival time of the 1 pps at the slave is calculated (called ePPSOffset in the experiment) using the estimated path delays plus the station’s estimates of the correction factor. Again, as it was not possible to use the correction factor data from the experiments in the simulation, an alternative to the correction factor needed to be created for the simulation. The correction factor used in the simulation differed depending upon which approach was used to model the extraneous delays. The ePPSOffset is then subtracted from the 1 pps signal that ‘arrives’ at the slave station to generate the equivalent of the e1PPSDelay value in the experiment.

3.1 Modeling of Extraneous Delays

Two different approaches to modeling the extraneous delays were used in the simulation. In the first approach, the delays were modeled on the correction factor data from the actual measurements, by using a normal distribution based on the statistics of the collected data. In analysis of the measurement data, the correction factor values were found to be of bimodal or trimodal (Palermo station) distribution, but approximately normally distributed around each modal value. These distributions probably occurred due to the problems with the satellite modems, after each reset of the modem, a different mean delay was established. Thus, it was not necessary to model bimodal or trimodal distributions because these likely only arose due to the modem resets. Data sets of independent, normally distributed delays were generated for each mean and standard deviation value for each station, and then these were combined by averaging (of two data sets for Bresso and three data sets for Palermo). To prevent an increase in variance caused by the summation of n independent random variables, the standard deviation was then adjusted by multiplying by $1/\sqrt{n}$. Modeling the delays from the measurement data in this way means that the resulting values effectively include all extraneous delays, including atmospheric effects and the Sagnac effect, and that these delays do not have to be separately modeled.

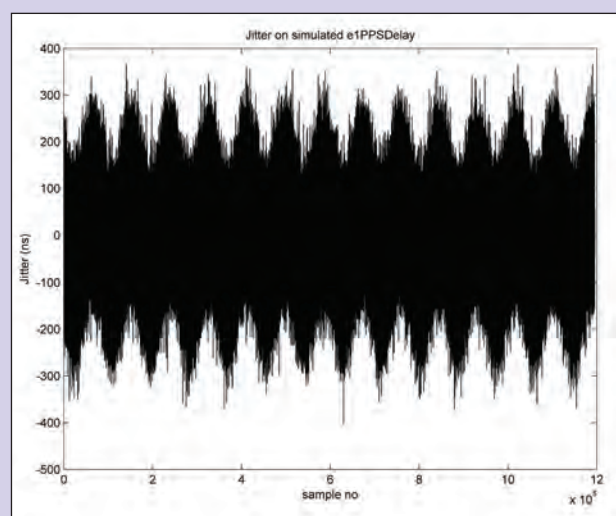


Figure 11. Simulation with equipment delay modeled using wander plus random noise.

When modeling equipment delay using data sets from the experimentally derived statistics, the results of the simulation were not as good as the actual measurements. In other words, the received 1 pps at the slave station was noisier in the simulation than it was during the actual measurement. The likely cause of this effect is that the noise produced by modeling the equipment delay based upon the statistics of the correction factor is too large. The standard deviation of the 1 pps signal received in the simulation at the slave station is 0.4 μ s and that of the resulting simulated e1PPSDelay at the slave station is 0.3 μ s. The peak-to-peak range of the simulated e1PPSDelay is $\pm 1.5 \mu$ s as shown in Fig. 10. The apparent poor performance of the system in simulation can be explained mainly by the difficulty of modeling the delays based on the correction factor statistics. The standard deviation used in the model based on the correction factor statistics is likely to be an overly pessimistic estimate, because of the bimodal and trimodal distributions and the effect of the problems experienced with the modem that occurred during the actual measurements.

The second approach of the simulation modeled the extraneous delays as a sum of troposphere delay and equipment delay. To model the troposphere delay, weather data were downloaded for the two locations from the historical weather data archive for Italy provided by ilMeteo.it [22] and used to estimate the 90 % of the troposphere delay due to the dry component using the dry model of Saastamoinen [23] for which barometric pressure is required. Where a barometric pressure reading for a day was missing (which occurred in one to three places within each file), it was replaced by the median value for the month. The dry component model value is also used as the station estimate of the mean troposphere delay. To add some uncertainty into the troposphere delay model, given that the stations would not be able to model the troposphere delay perfectly, the final value used in calculating the measured travel times of the signal also includes a random noise of average magnitude of 10 % of the troposphere delay due to the wet component. The variation in delay due to refraction and dispersion by the ionosphere is generally negligible at the frequencies used (uplink at 11.7 GHz, downlink at 14.4 GHz) [24] and is not modeled.

The equipment delay in this approach was modeled as a deterministic variation plus a random walk: a sum of a sinusoidal variation, modeling satellite motion and white noise. The values for the standard deviation of the Gaussian noise component and the random walk amplitude were then chosen by trial and error so that the simulation could reproduce the noise on the e1PPSDelay signal that was observed in the measurements. The final standard deviation values used were 45 to 55 ns and the amplitude of the diurnal variations was near 30 ns. For example, as shown in Fig. 11, these values generated a simulated e1PPSDelay signal with a peak-to-peak variation of about 500 to 600 ns and a standard deviation of 84 ns, comparable to the values found experimentally and shown in Table 1. The standard deviation of the received 1 pps signal after adjustment using knowledge of the path delays and estimates of the equipment delay and mean troposphere delay is 0.1 μ s, and the peak-to-peak range of the signal is less than 1.0 μ s.

4. Conclusions and Further Development

We have described a proposal by Mixed Processing Ltd. for an off-the-shelf system for transferring time signals via geostationary satellite. We have reported on the initial testing and simulation of the proposed system, which is under further development. Our experience has shown that developing such a system is within reach of a commercial operator but that careful attention must be paid to detail at every stage of development. An initial experiment, reported here, was successful in demonstrating the feasibility of the service as it succeeded in distributing a 1 pps timing signal across 900 km of territory (the baseline between Bresso and Palermo is approximately 889 km) with a peak-to-peak range of less than 1 μ s. The analysis of the experiment uncovered key issues which may have affected the performance of the timing signal transfer, suggesting that the results could have been substantially better. Working with the University of Limerick, simulations were developed which were able to replicate and explain the experimental results and were instrumental in uncovering some of the problems experienced. Simulations of the complete system are under further development to assist with the deployment and testing of the next stage of the system, which will incorporate a satellite modem designed and built by Mixed Processing Ltd. to use TWSTFT over the bidirectional links between the master stations.

5. References

- [1] J. Levine, "A review of time and frequency transfer methods," *Metrologia*, vol. 45, no. 6, pp. S162-S174, 2008.
- [2] D. Kirchner, "Two-way time transfer via communication satellites," *P. IEEE*, vol. 79, no. 7, pp. 983-990, July 1991.
- [3] H. Sun and Y. Li, "Analysis of two-way satellite time and frequency transfer system," *Proceedings of the Ninth International Conference on Electronic Measurement & Instruments*, pp. I-991-I-994, Beijing, China, 2009.
- [4] D. Hanson and W. Hamilton, "One-way time synchronization via geostationary satellites at UHF," *IEEE T. Instrum. Meas.*, vol. 20, no. 3, pp. 147-153, August 1971.
- [5] D. Hanson and W. Hamilton, "Clock synchronization from satellite tracking," *IEEE T. Aero. Elec. Sys.*, vol. 7, no. 5, pp. 895-899, September 1971.
- [6] F. Meyer, M. Brunet, M. Granveaud, F. Vernotte and M. Vincent, "Time transfer using a geostationary direct TV satellite,"

- Proceedings of the 5th European Frequency and Time Forum*, pp. 82-88, Besançon, Switzerland, March 1991.
- [7] F. Meyer, M. Granveaud, B. Laporte, F. Vernotte, and M. Vincent, "Improved time transfer using a geostationary direct TV satellite," *Proceedings of the 7th European Frequency and Time Forum*, pp. 129-134, Neuchâtel, Switzerland, March 1993.
- [8] F. Meyer, "One-way time transfer using geostationary satellite TDF2," *IEEE T. Instrum. Meas.*, vol. 44, no. 2, pp. 103-106, April 1995.
- [9] A. Sen Gupta, A. Hanjura, and B. S. Mathur, "Satellite broadcasting of time and frequency signals," *P. IEEE*, vol. 79, no. 7, pp. 973-981, July 1991.
- [10] A. Sen Gupta and B. Mathur, "Standard time and frequency signal broadcast via INSAT- accuracy improvements using differential mode," *IEEE T. Instrum. Meas.*, vol. 46, no. 2, pp. 212-215, April 1997.
- [11] J. Yoon, K. Lee, B. Lee, B. Kim, K. Choi, Y. Chang, Y. Chun, and S. Ra, "Geostationary orbit determination for time synchronization using analytical dynamic models," *IEEE T. Aero. Elec. Sys.*, vol. 40, no. 4, pp. 1132-1146, October 2004.
- [12] T. Morikawa, M. Aida, A. Otsuka, and C. B. Lee, "An Experiment on Frequency Transfer Using a Geostationary Broadcasting Satellite," *IEEE T. Instrum. Meas.*, vol. 46, no. 2, pp. 216-219, April 1997.
- [13] W. Lewandowski and C. Thomas, "GPS time transfer," *P. IEEE*, vol. 79, no. 7, pp. 991-1000, July 1991.
- [14] W. Lewandowski, G. Petit, and C. Thomas, "Precision and accuracy of GPS time transfer," *IEEE T. Instrum. Meas.*, vol. 42, no. 2, pp. 474-479, April 1993.
- [15] W. Lewandowski, J. Azoubib, and W. J. Klepczynski, "GPS : Primary tool for time transfer," *P. IEEE*, vol. 87, no. 1, pp. 163-172, January 1999.
- [16] C. Evans-Pughe, "GPS vulnerability to hacking," *Engineering and Technology Magazine*, vol. 6, no. 4, pp. 78-81, April 2011.
- [17] M. Lombardi, "Microsecond accuracy at multiple sites: is it possible without GPS?," *IEEE Instru. Meas. Mag.*, vol. 15, no. 5, pp. 14-21, October 2012.
- [18] M. Genova, "System for synchronizing signals on a telecommunication network," *European Patent (EP2420902 A2)*, February 22, 2012.
- [19] Intelsat Ephemeris Data, available at: <http://www.intelsat.com/resources/satellitedata/ephemeris.asp>
- [20] Eutelsat Group Extranet, available at: <https://services.eutelsat.fr/>
- [21] B. Dainty, J. Raquet, and R. Beckman, "Improving geostationary satellite GPS positioning error using dynamic two-way time transfer measurements," *Proceedings of the 39th Precise Time and Time Interval Meeting (PTTI)*, pp. 511-530, November 2007.
- [22] Archivio Meteo Storico, ilMeteo.it, available at: <http://www.ilmeteo.it/portale/archivio-meteo/>
- [23] J. Saastamoinen, "Atmospheric correction for troposphere and stratosphere in radio ranging of satellites," *Proceedings of the 3rd International Symposium on the Use of Artificial Satellites for Geodesy*, April 1971, [A.G.U. Monograph], pp. 247-252, 1972].
- [24] K. Davies and E. Smith, "Ionospheric effects on satellite land mobile systems," *IEEE Antenn. Propag. M.*, vol. 44, no. 6, pp. 24-31, December 2002.

A Survey of Time Transfer via a Bidirectional Fiber Link for Precise Calibration Services

Wen-Hung Tseng and Shinn-Yan Lin

Abstract: The aim of this survey is to prepare ourselves for the future need of precise time and frequency calibration services over fiber links. We study the accuracy requirements of some critical infrastructure timing applications, and review the development of time and frequency transfer via fiber. We also present results from a preliminary experiment on two-way time transfer through a 25 km optical fiber link. The fiber link is based on a common-path configuration that provides good reciprocity in both directions. Therefore, the propagation path delays in the fiber can be cancelled out almost entirely by employing the two-way method. The resulting data exhibit a time deviation of less than 7 ps for averaging periods ranging from one second to one day. A frequency stability of 1×10^{-16} at one day has also been demonstrated. The time calibration and residual non-reciprocity of bidirectional fiber links are also discussed in this paper.

1. Introduction

Time transfer is the practice of comparing the time and frequency of clocks that are separated by long distances. In recent years, precise comparison and synchronization of clocks have become important techniques, not only for measurement science, but also for daily life. In Taiwan, the demands of precise time synchronization have increased recently due to the next generation of telecommunication synchronization, the smart grid of electric power distribution systems, the practice of providing time stamps for financial networks, and science studies that are being conducted on some college campuses. Due to the long distances that often exist between clocks, time transfer must be carried out with the help of some type of communication medium.

Optical fibers are well suited for time transfer, because they have the characteristics of broad bandwidth and low transmission loss. Through a standard single mode fiber (SMF) [1], the light with 1550 nm wavelength has low dispersion and a loss of only 0.22 (dB/km), and the light with 1310 nm wavelength has zero dispersion and a loss of less than 0.35 (dB/km). Thus, the transmission distance can reach at least 55 km for an optical power budget of 20 dB. By employing optical amplifiers, we can extend the transmission distance to several

thousand kilometers [2]. Therefore, optical fiber is an ideal communication channel for the purpose of time and frequency transfer.

Some major timing institutes have devoted considerable effort to the study of time and frequency transfer over fiber optic links. Due to the environmental sensitivity of the optical fiber, there can be variations in propagation delay that cause time and frequency instability. The variations in propagation delay are introduced by both electric and optical equipment, and include the effects of noisy and unstable sources. These issues are important topics for future applications. Therefore, we have to evaluate these unstable sources and study the effective methods to cancel them. Moreover, the accuracy of time transfer depends on the measurement uncertainty of path delays. Unlike the scientific frequency transfer work (e.g., comparing primary frequency standards), the time transfer for industrial applications needs timing signals including not only the precise phase but also the exact timestamp. Then, the propagation delay can be measured and used to calculate a delay correction.

This paper begins by discussing the accuracy requirements of some critical infrastructure applications. Our goal is to design a dedicated time transfer system to meet the requirements of future calibration

services, especially for the reference clocks of the critical infrastructure systems. Following a brief review of time and frequency transfer techniques over fiber links, we present a preliminary experiment on two-way time transfer through a common-path optical fiber link. The common-path optical link can provide good reciprocity in both directions. Therefore, the propagation path delay in the fiber can be cancelled out almost entirely by employing the two-way method. Some brief discussions on calibration and unstable sources are also provided. This survey ends with a summary of most recent time transfer experiments over fiber links. The results obtained by the various groups around the world help us to understand the potential of precise calibration over dedicated fiber links.

Authors

Wen-Hung Tseng
whtseng@cht.com.tw

Shinn-Yan Lin
sylin@cht.com.tw

Telecommunication Laboratories
Chungwha Telecom Co., Ltd.
Taoyuan, Taiwan

2. Timing Accuracy Requirements for Critical Infrastructure Systems

The measurement of time has a wide range of applications. For many industrial applications, the need for accurate time synchronization is greater now than it has ever been in the past. The most notable applications include mobile phone networks, electrical power grid systems, and financial systems (Fig. 1).

Telecommunication systems usually require precise frequency synchronization (known as syntonization) to ensure the quality of data streams. Since mobile communications have been revolutionized by smart phones, the capacity of current networks cannot satisfy the consumer's need of mobile ultra-broadband Internet access. The mobile network is inevitably migrating towards the fourth generation (4G) standards. Time synchronization is typically required by the 4G systems. For example, base stations of a LTE-TDD (Long Term Evolution - Time Division Duplex) require frequency accuracy of 50 parts per billion (ppb) [3] and time accuracy of $\pm 1.5 \mu\text{s}$ ($< 3 \mu\text{s}$ phase difference for small cells) [4]. According to estimates, there were more than 25,000 3G base stations in Taiwan at the end of 2012. Since a large of small cells is vital for a 4G system to manage wireless spectrum more efficiently, accurate time synchronization between base stations is critical for future 4G mobile networks.

The electric power distribution grid needs accurate timing for fault detection, which requires the synchronization of phasor measurements. Devices called phasor measurement units (PMUs) are employed for precise grid measurements [5]. PMUs from multiple sites may yield inaccurate readings. At the 60 Hz power line frequency, time synchronization errors of $26 \mu\text{s}$ (a phase error of 0.57°) represent the maximum allowable tolerance. For a "Smart Grid" which enables real-time fault detection and network self healing, the desired accuracy is better than $1 \mu\text{s}$ [6].

Conventional financial trading activities are usually time stamped with a resolution of second or milliseconds. However, due to the impact of the "flash crash" on May 6, 2010, when stock prices in the United States fell by about 9 percent within 20 minutes [7], regulators are now aware that millisecond resolution is no longer enough for today's market. The risk arose from high frequency trading (HFT) which refers to a strategy where shares are bought and sold multiple

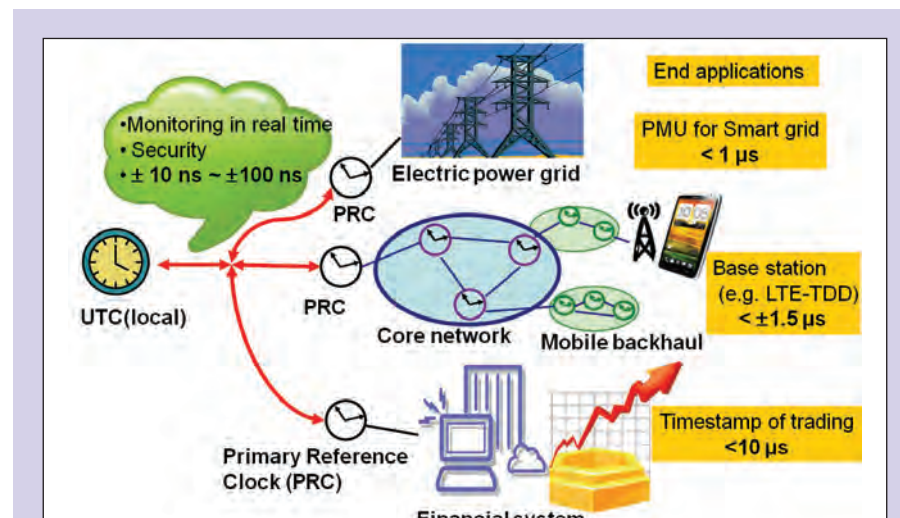


Figure 1. Time distribution networks for critical infrastructure applications.

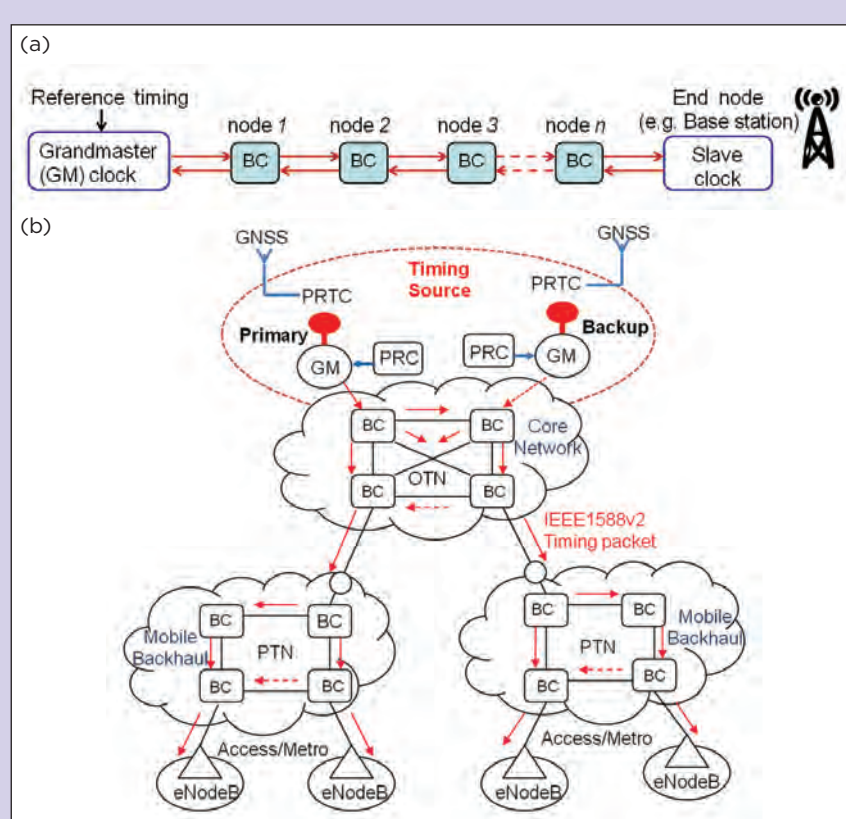


Figure 2. (a) A chain of boundary clocks. (b) Accurate time synchronization distribution with boundary clocks in future mobile networks (e.g. LTE). BC: boundary clock, PRC: primary reference clock, PRTC: primary reference time clock, GNSS (GPS, GLONASS, Galileo, Compass/BeiDou).

times within a short period of time, often within milliseconds [8]. HFT appears to make markets operate better (it can increase liquidity and price efficiency and reduce volatility), and has become a significant part of the market's operation. By some

estimates, HFT makes up over 50 % of the total volume on equity markets in the United States [9]. With the help of today's computer and communication technologies, HFT has pushed the speed of financial trading to near its theoretical limits. Huge amounts of

market data can be analyzed by high speed computers and transported between locations through fastest telecommunications links. In order to monitor “microsecond trading,” a time resolution of $10\text{ }\mu\text{s}$ is necessary for the stock market.

Currently, most critical infrastructure systems rely on Global Positioning System (GPS) signals, which can support sub-microsecond accuracy [10] for general receivers, and reach accuracies of about 5 ns with respect to Coordinated Universal Time (UTC) with calibrated dual frequency receivers specially designed for timekeeping purposes [11]. Although time synchronization requirements can be easily satisfied by using GPS signals, the reception of GPS may be difficult at some locations. For example, the facilities of a hydraulic power plant might be under or near high mountains, which may block the GPS reception. A more serious concern is that the reliability of GPS systems can be threatened by jamming and spoofing of the signal [12].

To provide redundancy in the event of GPS failures, alternative timing systems based on Synchronous Ethernet (Sync-E) [13] and the IEEE-1588 protocol [14] are now used in critical infrastructure applications. Since a large number of sites are required both for PMUs in a smart grid and base stations in a LTE network, a network timing synchronization solution would be cost effective and easier to manage. Many working groups sponsored by IEEE and ITU-T have made a considerable effort to advance this technology in recent years. A key development has involved realizing precise time synchronization on a wide area network with the help of boundary clocks and transparent clocks [15]. As illustrated in Figure 2(a), if a boundary clock (BC) is implemented in every network node and the link delay asymmetry of each direction between two adjacent BCs is relative small, the time difference between BCs can be estimated and calibrated. By the timing distribution chain, the precise reference timing can transfer from a grandmaster clock to slave clocks at application nodes. A mobile backhaul may be synchronized to the accuracy of 100 ns by means of enhanced G-PON (based on G.984.3 Amendment 2 [16]) in cooperation with IEEE-1588v2 (i.e., 2008 version). Accordingly, the GPS receivers can move from base stations to the backhaul network, and then to the core network. Figure 2(b) shows a prospective architecture for time synchronization distribution in mobile networks. Ideally, the reference clocks of the core network need to be calibrated and monitored in real-time by a national metrology institute (NMI). Considering the time uncertainty budgets required for complicated distribution networks and end applications (e.g., PMUs and base-stations), the primary reference clocks will require accuracies of 100 ns, and some of them possibly need accuracy up to 10 ns. A dedicated fiber link is one of the few possible solutions that can allow us to develop a service to calibrate these reference clocks. Let us now briefly review the development of time and frequency transfer over fiber links.

3. A Brief Review of Time and Frequency Transfer Methods Over Fiber Links

The first example of delivering radio frequency (RF) reference signals through optical fibers occurred in the early 1980s [17, 18]. The stable reference signals generated by a hydrogen maser clock were distributed over optical fibers to multiple antenna sites at the National Aeronautics and Space Administration (NASA). The technique was rapidly found to be a good choice for transmitting RF signals over long distances. Since the stability of optical and microwave

frequency standards has greatly improved during the past 20 years, the transfer stability of the fiber links has become a critical technique for comparing these frequency standards. To avoid the degradation of frequency due to the instability in the prorogation delay, active noise cancellation is implemented to improve the transfer stability of the fiber link [19, 20]. For compensating the delay variation of the outdoor optical fiber paths, a phase correction is employed by means of the phase information of the round trip signal. The scheme of phase correction can be classified as either optical compensation or electrical compensation system. The former system includes the use of a temperature compensated fiber reel, a piezoelectric fiber stretcher, optical tunable delay line, and an acousto optic modulator (AOM). The electrical compensation system includes a dual mixing scheme with voltage controlled crystal oscillator (VCXO) [21, 22] and controlled electronic delay lines with application specific integrated circuits (ASIC) [23].

During recent years, ultra stable frequency transmission over an optical fiber link has been accomplished by some major laboratories in the United States, Europe and Japan. These links are: the Joint Institute for Laboratory Astrophysics (JILA) – National Institute of Standards and Technology (NIST) in the United States, Physikalisch Technische Bundesanstalt (PTB) – Max Planck Institute for Quantum Optics (MPQ) in Germany, Observatoire de Paris (SYRTE) – Laboratoire Parole et Langage (LPL) in France, and National Institution of Information and Communication Technology (NICT) – National Metrology Institute of Japan (NMIJ) – University of Tokyo (UT) in Japan. An RF transfer using amplitude modulation of the laser carrier has demonstrated frequency stability of 10^{-15} at a 1 s averaging period and near 10^{-18} at one day [22-24]. An optical carrier frequency transfer can reach stabilities below 10^{-18} after 1000 s [25-27]. In addition, the recorded distance for frequency transfer has increased from 251 km in 2007 [28] to 920 km in 2011 [29] with 10^{-19} relative accuracy. In China, there have already been regular frequency comparisons between the National Institute Metrology (NIM) and Tsinghua University (THU) via the 80 km urban telecommunication fiber network in the Beijing area. A frequency dissemination stability of 7×10^{-15} at 1 s and 4.5×10^{-19} at 10^5 s has been demonstrated [30].

Although precision optical fiber frequency transfer links via an urban network setting have received a lot of interest recently, the methods require bidirectional access to the fiber. However, telecom fiber networks are inherently unidirectional. For the application purpose of the remote frequency users, a simple and economic frequency dissemination method by using the current synchronous optical fiber communication networks has been considered [31]. The method provides an uncertainty of less than 1×10^{-12} at an averaging period of one day, which is suitable for most applications. On the other hand, a one-way two-color fiber link for frequency transfer has been introduced recently [32, 33]. In this system, two separate wavelengths are sent in the same direction along a fiber network. This work may benefit future applications.

Unlike frequency transfer, time transfer over fiber requires all delays to be calibrated. Several laboratories have published studies [34-37]. Most of them employ the two-way method to cancel the major delays and to address the residual delay asymmetry, e.g., chromatic dispersion. However, for a long distance time transfer, the absolute delay calibration is very important for verifying some relativity effects, such as the Sagnac effect. Currently, a GPS-based

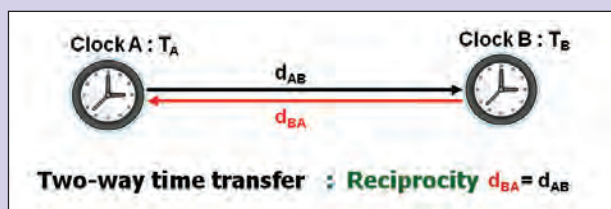


Figure 3. Two-way time transfer method.

time calibration is still the best way to verify the absolute calibration of a time transfer system over fibers [38]. Nevertheless, it is expected that the absolute time calibration via an optical fiber link will soon be utilized as an independent method with less uncertainty than the satellite links.

4. Use of Bidirectional Common-Path Optical Link

4.1 Two-way time transfer method

Two-way time transfer is generally used to compare two geographically separated clocks [34], as illustrated in Fig. 3. In a bidirectional link, the two clocks at each end transmit the time of the local clock, and simultaneously receive the time of the remote clock. Each clock then measures the difference between the local clock (T_A) and the remote clock (T_B) and the delay (d_{BA}). The readings of time interval counters at sites A and B are $TIC_A = T_A - T_B + d_{BA}$, and $TIC_B = T_B - T_A + d_{AB}$, respectively. Assuming that the path from the remote site to the local site is reciprocal with the path from the local site to the remote site, i.e., $d_{BA} = d_{AB}$, the path delay effects are then removed. The time difference between clocks can be expressed as

$$T_A - T_B = \frac{1}{2}(TIC_A - TIC_B). \quad (1)$$

4.2 Bidirectional Common-Path Optical Link

We employ two optical circulators and two pairs of optical transceivers (i.e., E/O and O/E) to construct a bidirectional common-path optical link. The RF signals are modulated to optical signals on the same light wavelength, and are transmitted bidirectionally along a single fiber. Thus, the common-path link can avoid the non-reciprocity of path.

Figure 4 shows the block diagram of a common-path optical link [39]. It is composed of 1310 nm directly modulated lasers, photodetectors, optical circulators, and single mode fibers. The optical circulators utilize the Faraday effect to route light from port 1 to port 2, and port 2 to port 3, and are used here for bidirectionally transmission. They also have the characteristics of low insertion loss and high isolation. Thus, the signal to noise ratio will be kept high and the reflected signal will be isolated to a large extent.

An intermediate frequency (IF) of 70 MHz from a timing modem is converted to an optical signal by the directly modulated laser, and then is transmitted to the remote side through optical links. At the receiver site, a photodetector converts the optical signal to the IF signal. The same procedure is also operated in the reverse direction through the same fiber with the same light wavelength. Therefore, the reciprocity of the optical link is ensured.

The timing modem is the other key part of a time transfer system. A modem should be synchronous to its reference clock and can generate timing signals that are usually coded and modulated for transmitting through a communication channel. A modem needs at least one

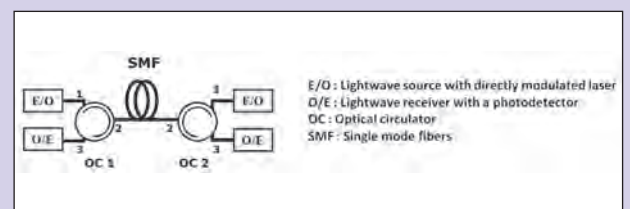


Figure 4. Block diagram of a common-path optical link.

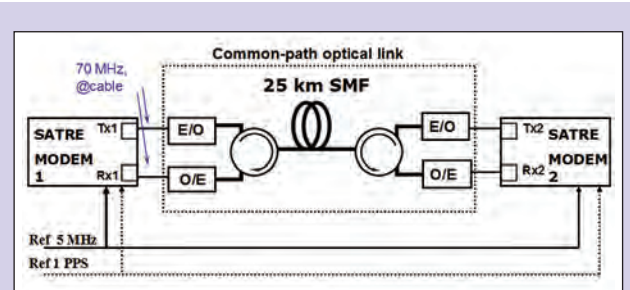


Figure 5. Setup of the two-way time transfer experiment via a 25 km fiber.

receiver to demodulate the timing signal from remote sites and to measure the time delay with a low uncertainty.

5. Measurements

5.1 Experimental Setup

Figure 5 shows the experimental configuration. We used two-way time transfer modems (Timetech SATRE, [40]) that were driven from a common clock to conduct a two-way test. The bidirectional propagation delays through the common-path optical link were investigated. In the measurement, we employed pseudorandom noise (PRN) coded signals of 20 Mcps (MHz chip rate) and added 3 Hz and 7 Hz offsets to the 70 MHz carrier frequency at both sites to avoid the possible beat note with the modem reference frequency [41]. The coaxial cables that connected the modem and optical transmitter/receiver were chosen to be as short as possible. The experiment took place indoors at a temperature of 24.5 ± 1.5 °C. The length of the single mode fiber used here was 25 km and the temperature coefficient of the fiber was about 38 ps/(km·°C).

5.2 Calibration: Comparison between a short fiber and a 25 km fiber
For the purpose of time calibration, we needed to determine the modem's time delay with respect to its reference clock, the internal delays of modems, delays of the connected coaxial cables, fiber pigtails, and other optical components. Since the system was placed at the same location at the beginning, we replaced the 25 km fiber with a 10 m fiber pigtail, and then measured the initial total differential delays in a common clock condition. The differential delay was 13.444 ns (a 120 s averaging value) for the system with the short fiber pigtail. When the two nodes were separated by the 25 km fiber (connected to a 25 km long spool of fiber), the measured differential delay was 13.375 ns. This value differs from that of 10 m fiber pigtail by only 69 ps. The two differential delays were measured within an interval of 15 minutes.

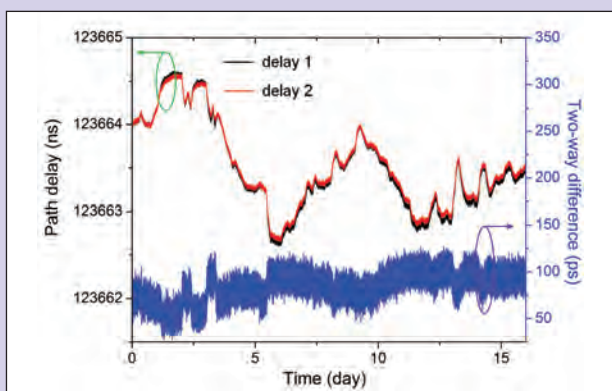


Figure 6. Forward and backward path delays via a common-path optical link and their two-way difference. The delay 1 (backward, red line) and delay 2 (forward, black line) were measured by SATRE 1 and SATRE 2, respectively. The delay data were corrected by the initial calibration.

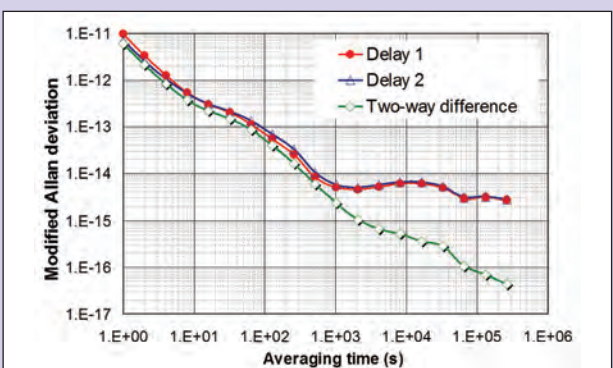


Figure 8. Frequency stabilities of the delay 1, delay 2 and their two-way time difference.

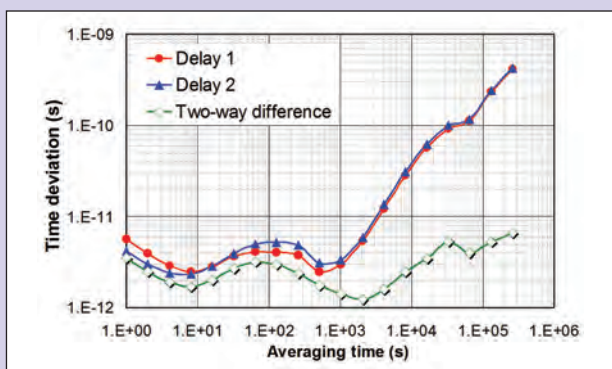


Figure 7. Time stabilities of the delay 1, delay 2 and their two-way time difference.

We may consider that the small difference is caused by the non-reciprocity of the 25 km SMF fiber. One of the non-reciprocity sources may be due to the chromatic dispersion. Nevertheless, the effect should be relatively small for the light sources around 1310 nm (zero dispersion for fibers). Due to the Sagnac effect induced by the earth rotation [42-43], the time difference between the forward and backward fiber paths may be

$$\Delta t = \frac{4NA_E\Omega}{c^2}, \quad (2)$$

where the fiber was wound onto a circular coil with N turns, A_E is the perpendicular projection of the area of the fiber coil onto the equatorial plane, Ω is the rotation rate of the Earth, and c is the speed of light. In our experiment, the 25 km spool of fiber with an average 20 cm coil diameter was placed on a table top located at a latitude of 24.95° N. Then, NA_E is about 1133 m^2 , and the time difference induced by the Sagnac effect was about 9.2×10^{-19} s. This non-reciprocity term was negligible in the common clock test.

Because the laser sources we used had slightly different optical powers, and the absorption, reflection and scattering in both directions of the fiber were different, the received RF power levels consequently

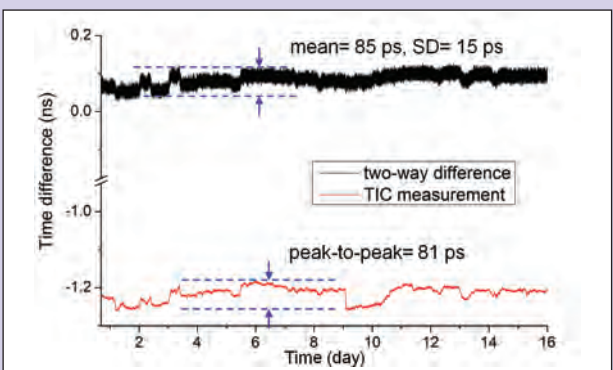


Figure 9. Comparison between the common-clock two-way difference over the 25 km common-path optical link and the TIC measurement of the time difference between two modems.

differed by 6 dB between both sides. In addition, the different received levels would lead to slightly variant results for delay measurements in modems [35]. If the received power is kept constant, the non-reciprocity of the 25 km fiber can be less than 69 ps.

5.3 Results of Two-Way Time Difference

Figure 6 shows the path delay data measured by the internal counter of the SATRE modems. The trends of the two curves are similar, and the variation during the period of 16 days (in December 2011) is up to 2 ns. The two-way time difference (i.e., one half of the time difference between the forward and backward delays) is shown in the same plot, and its variation range becomes only 83 ps. This result indicates that the delay variation can be cancelled out to a certain extent.

Figure 7 shows the time stability of the bidirectional delays and their two-way time difference. The curves of delays represent time transfer results through the one-way fiber link. The time instability is below 1 ns at averaging periods around 10^5 s. After employing the two-way method to cancel out the delay variation, the time instability can be below 7 ps at an averaging period of 10^5 s. Figure 8 shows the corresponding frequency stability of the one-way delays and their two-way difference. At an averaging period of one day, the modified Allan deviation of the one-way delay is 3×10^{-15} , while that of the two-way difference is 1×10^{-16} .

Method	Equipment, Signal Type	Fiber link, Distance @Place Wavelength	Time stability (TDEV)	Uncertainty estimation	Conformity to GPS PPP	Reference
Time: two-way	SATRE modem, PRN, 20 Mcps	Dark fiber 73 km @Germany 1550 nm	< 6 ps	74 ps	0.72 ns	Rost [44]
Time and frequency dissemination: round trip + link stabilized by ASIC	Dedicated hardware, 1 pps modulated on square wave	Dark fiber >420 km @Poland 1550 nm	< 1 ps @ 1 d	112 ps	1.5 ns	Śliwczynski [45]
Time: two-way and optical frequency transfer: round trip + link stabilized by AOM	SATRE modem, PRN, 20 Mcps	Dark channel 540 km @France 1550 nm	< 20 ps	250 ps	N/A	Lopez [46]
Time: two-way	SATRE modem, PRN, 20 Mcps	Fiber spool 25 km @indoor 1310 nm	< 7 ps	100 ps	N/A	This paper

Table 1. Summary of the most recent time transfer experiments over fiber links.

In the short term ($\tau < 10$ s), the performance of the optical link is limited by the resolution of the measurement method. When using the 20 Mcps PRN coded signals, the resolution is several picoseconds. The actual resolution value is also related to the C/N_0 ratio. The overall time deviation of the transfer over the common-path fiber link can be under 7 ps for averaging periods from one second to one day. Thus, time transfer over fiber has considerable potential as a method for next generation applications.

5.4 A Comparative Experiment

Although our experiment was carried out by the common clock method (the same reference clock was used for both nodes), some system noise may still be present due to the instability in the modem. To help us understand this influence, we performed a comparative test by using an additional time interval counter (TIC, Stanford Research SR-620) to directly measure the time difference between the 1 pps (pulse per second) outputs of two modems. Figure 9 shows the comparison of the two-way difference over the 25 km common-path optical link and the TIC measurement of the time difference between two modems. The two curves in the plot are highly correlated. This result represents the basic limit of accuracy in this time transfer experiment. Although the two modems were connected with the same reference signal, there were still slight variations (peak-to-peak value up to 81 ps) between their timing systems. The variation, possibly caused by the thermal sensitivity of the time transfer equipment (e.g., ≤ 30 ps/K in specification [40]), resulted in the residual instabilities. If this variation cannot be cancelled, it will affect the time comparison results of two remote clocks.

In conclusion, the absolute time calibration can be conducted by means of the initial measurement of total differential delay in a common clock condition. When two time transfer systems were separated by the 25 km fiber link, a slight non-reciprocity term (i.e., 69 ps measured in the beginning) is induced probably by the change of received power levels in the fiber link. By combining this with variation terms including the synchronization difference - between the clocks and timing modems and the uncancelled fiber

delay fluctuation, the mean common clock difference was 85 ps with a standard deviation of 15 ps (see Fig. 9). Then, the uncertainty was estimated to be 100 ps. The error is small enough to meet the requirements of most applications. However, for better precision, we may use external counters to monitor the difference between the modem and its reference clock, or put the equipment in a more stable temperature environment.

6. Discussion

We have evaluated a two-way time transfer experiment over a 25 km fiber spool. Before making further investment in a dedicated fiber network, it is worthwhile to check the most recent studies on time transfer which have been successfully performed through communication fiber links. Table 1 summarizes the newest relevant research from the past year [44-46]. A two-way time transfer link between Braunschweig and Hannover in Germany was established by using a dark fiber over a distance of 73 km [44]. During a common clock experiment at PTB, the calibration uncertainty was estimated as 74 ps. The results agreed within the 0.72 ns uncertainty of the GPS link results. An optical link for time and RF frequency dissemination between Warsaw and Borowiec in Poland was installed over a distance of 421.4 km (most of the length was based on dark fiber) [45]. Its estimated uncertainty is 112.3 ps and the difference between the results of the fiber link and of the GPS link is 1.5 ns. In both of these cases, the results obtained via the fiber links agree within 1.5 ns of the GPS results, suggesting that the long distance optical link through the dark fiber can provide small enough uncertainties for our time transfer purposes. Another recent work demonstrated accurate time transfer via a dedicated dark channel in a public telecommunication optical fiber network [46]. The uncertainty of 250 ps over the 540 km fiber link demonstrates the potential of time transfer over long distance fiber links carrying Internet data.

The uncertainty of the two-way time transfer method is highly dependent on the residual non-reciprocity terms. The identified terms for non-reciprocity over fiber links may be grouped into three categories: the internal differential delays of the transmission and

reception paths in both sites (including modems, coaxial cables, fiber pigtails, and optical components), the bidirectional asymmetry of a fiber link, and the synchronization difference between the timing modems and clocks. It is simple to measure the internal differential delays if the equipment of both sites could be located in the same place, so we can measure the total delay difference before the equipment is installed at the remote sites.

When considering the optical signals passing through a fiber link, the differential delay between bidirectional paths is caused by chromatic dispersion, the Sagnac effect, and birefringence of fiber. Because the last two terms (i.e. Sagnac effect and birefringence) were evaluated at the level of a few picoseconds [45], we may focus on the chromatic dispersion, which results in the difference of propagation delays of two lasers with different wavelengths. In our experiment, the light sources around 1310 nm with zero dispersion have small influence. However, for distances longer than 50 km, the 1550 nm light source is more suitable, not only for the lowest loss in fiber, but also for more available optical amplifiers (e.g., Erbium Doped Fiber Amplifiers (EDFA)) in this spectrum. The typical dispersion of SMF-28 is 17.5 ps/(nm·km) at 1550 nm [1]. For a distance of 100 km, the accuracy requirement of 1 ns may allow a wavelength difference of 0.5 nm, which can be determined by employing an optical spectrum analyzer. Nevertheless, the delay of bidirectional optical amplifiers should be taken into account for the transmission over the 100 km distance.

Finally, we need to address two issues related to the timing modem, which may affect the performance of time transfer. These issues are the synchronization with respect to the modem's reference clock, and the resolution of the time interval measurement provided by the modem. The timing modem developed specifically for optical fiber links will be an important topic for future applications. The research presented in [45] used dedicated hardware to enhance the resolution and enable the real-time calibration. A software-radio based modem has been developed and been successfully applied on the two-way satellite time transfer experiment [47]. The modem can be refined and placed into the apparatus for measuring the fiber delay. We may also evaluate the timing equipment in cooperation with the IEEE-1588v2 protocol in future studies.

The demonstrated fiber system can provide more precision than the requirement of nowadays industrial applications. This implies there is still a range to reduce the system cost. Otherwise, we may consider that precise time synchronization technique will enable the new services that we have not imaged.

7. Conclusions

We have conducted a two-way time transfer experiment by employing a bidirectional common-path optical link. The experiment over a 25 km fiber produced promising results; the time deviations were below 7 ps for averaging periods ranging from 1 s to 1 day. However, our experiment was only performed in an indoor environment. Therefore, this survey ends with a summary of most recent time transfer experiments over fiber links. The results obtained by the various groups around the world confirm the potential of precise time transfer over dedicated fiber links between remote clocks.

Because the optical fiber network is expected to be part of many future applications, some power companies already have its own fiber links along the power transmission system, and the dark fibers or

dark channels may be available for telecom companies. Moreover, an investment in timing distribution fiber links will be cost effective for some large financial companies and regulators. Thus, we hope to extend the time transfer service to other remote institutes in Taiwan. A study on remote two-way time transfer experiments with the common-path optical links will be carried out in the near future.

8. References

- [1] Corning SMF-28 single-mode optical fiber, <http://ece466.groups.et.byu.net/notes/sm28.pdf>
- [2] G. Agrawal, *Fiber-Optic Communication Systems*, John Wiley & Sons, 3rd ed., 2002.
- [3] 3GPP, "Evolved Universal Terrestrial Radio Access (E-UTRA); TDD Home eNode B (HeNB) Radio Frequency (RF) requirements analysis," *3GPP TR 36.922*, v. 10.0.0, 2011.
- [4] 3GPP, "Evolved Universal Terrestrial Radio Access (E-UTRA); Requirements for support of radio resource management," *3GPP TS 36.133*, v. 10.1.0, 2011.
- [5] R. Pirret, "Testing and calibration of Phasor Measurement Units," *NCSLI Measure J. Meas. Sci.*, vol. 7, no. 2, pp. 36-42, 2012.
- [6] K. Moslehi and R. Kumar, "A reliability perspective of the Smart Grid," *IEEE T. Smart Grid*, vol. 1, no. 1, pp. 57-64, June 2010.
- [7] D. Schneider, "Trading at the speed of light," *IEEE Spectrum*, vol. 48, no. 10, pp. 11-12, October 2011.
- [8] J. Brogaard, "High frequency trading and its impact on market quality," *Working paper*, Northwestern University, 2010.
- [9] D. Schneider, "The microsecond market," *IEEE Spectrum*, vol. 49, no. 6, pp. 66-81, June 2012.
- [10] M. Lombardi, "Microsecond accuracy at multiple sites: is it possible without GPS?," *IEEE Instru. Meas. Mag.*, vol. 15, no. 5, pp. 14-21, October 2012.
- [11] D. Piester, M. Rost, M. Fujieda, T. Feldmann, and A. Bauch, "Remote atomic clock synchronization via satellites and optical fibers," *Adv. Radio Sci.*, vol. 9, pp. 1-7, 2011.
- [12] N. Tippenhauer, C. Popper, K. Rasmussen, and S. Capkun, "On the Requirements for Successful GPS Spoofing Attacks," *Proc. 18th ACM Conference on Computer and Communications Security*, pp. 75-86, Chicago, Illinois, October 2011.
- [13] J. Ferrant, M. Gilson, S. Jobert, M. Mayer, M. Ouellette, L. Montini, S. Rodrigues, and S. Ruffini, "Synchronous ethernet: a method to transport synchronization," *IEEE Commun. Mag.*, vol. 46, no. 9, pp. 126-134, 2008.
- [14] J. Ferrant, M. Gilson, S. Jobert, M. Mayer, L. Montini, M. Ouellette, S. Rodrigues, and S. Ruffini, "Development of the first IEEE 1588 telecom profile to address mobile backhaul needs," *IEEE Commun. Mag.*, vol. 48, no. 10, pp. 118-126, 2010.
- [15] M. Ouellette, K. Ji, S. Liu, and H. Li, "Using IEEE 1588 and boundary clocks for clock synchronization in telecom networks," *IEEE Commun. Mag.*, vol. 49, no. 2, pp. 164-171, 2011.
- [16] ITU, "Gigabit-capable Passive Optical Networks (G-PON): Transmission convergence layer specification Amendment 2: Time-of-day distribution and maintenance updates and clarifications," *ITU-T G.984.3 AMD 2*, 2009.
- [17] L. Primas, R. Logan, and G. Lutes, "Applications of ultra-stable fiber optic distribution systems," *Proceedings of 43rd Annual Symposium on Frequency Control*, Denver, Colorado, pp. 202-211, 1989.

- [18] L. Maleki, "The optoelectronic oscillator," *Nat. Photonics*, vol. 5, no. 12, pp. 728–730, 2011.
- [19] L. Ma, P. Jungner, J. Ye, and J. Hall, "Delivering the same optical frequency at two places: accurate cancellation of phase noise introduced by an optical fiber or other time-varying path," *Opt. Lett.*, vol. 19, no. 21, pp. 1777-1779, 1994.
- [20] J. Ye, J. Peng, R. Jones, K. Holman, J. Hall, D. Jones, S. Diddams, J. Kitching, S. Bize, J. Bergquist, L. Hollberg, L. Robertsson, and L. Ma, "Delivery of high-stability optical and microwave frequency standards over an optical fiber network," *J. Opt. Soc. Am. B*, vol. 20, no. 7, pp. 1459-1467, 2003.
- [21] F. Narbonneau, M. Lours, S. Bize, A. Clairon, G. Santarelli, O. Lopez, Ch. Daussy, A. Amy-Klein, and Ch. Chardonnet, "High resolution frequency standard dissemination via optical fiber metropolitan network," *Rev. Sci. Instrum.*, vol. 77, no. 6, pp. 064701-064708, 2006.
- [22] M. Kumagai, M. Fujieda, S. Nagano, and M. Hosokawa, "Stable radio frequency transfer in 114 km urban optical fiber link," *Opt. Lett.*, vol. 34, no. 19, pp. 2949-2951, 2009.
- [23] L. Śliwczynski, P. Krehlik, Ł. Buczek, and M. Lipiński, "Active propagation delay stabilization for fiber optic frequency distribution using controlled electronic delay lines," *IEEE T. Instrum. Meas.*, vol. 60, no. 4, pp. 1480-1488, 2011.
- [24] O. Lopez, A. Amy-Klein, M. Lours, C. Chardonnet, and G. Santarelli, "High-resolution microwave frequency dissemination on an 86-km urban optical link," *Appl. Phys. B*, vol. 98, no. 4, pp. 723-727, 2010.
- [25] H. Jiang, F. Kéfélian, S. Crane, O. Lopez, M. Lours, J. Millo, D. Holleville, P. Lemonde, Ch. Chardonnet, A. Amy-Klein, and G. Santarelli, "Long-distance frequency transfer over an urban fiber link using optical phase stabilization," *J. Opt. Soc. Am. B*, vol. 25, no. 12, pp. 2029-2035, 2008.
- [26] G. Grosche, O. Terra, K. Predehl, R. Holzwarth, B. Lipphardt, F. Vogt, U. Sterr, and H. Schnatz, "Optical frequency transfer via 146 km fiber link with 10^{-19} relative accuracy," *Opt. Lett.*, vol. 34, no. 15, pp. 2270-2272, 2009.
- [27] M. Fujieda, M. Kumagai, S. Nagano, A. Yamaguchi, H. Hachisu, and T. Ido, "All-optical link for direct comparison of distant optical clocks," *Opt. Express*, vol. 19, no. 17, pp. 16498-16507, 2011.
- [28] N. Newbury, P. Williams, and W. Swann, "Coherent transfer of an optical carrier over 251 km," *Opt. Lett.*, vol. 32, no. 21, pp. 3056-3058, 2007.
- [29] K. Predehl, G. Groschel, S. Raupach, S. Droste, O. Terra, J. Alnis, Th. Legero, T. Hänsch, Th. Udem, R. Holzwarth, and H. Schnatz, "A 920-Kilometer optical fiber link for frequency metrology at the 19th decimal place," *Science*, vol. 336, no. 6080, pp. 441-444, April 2012.
- [30] B. Wang, C. Gao, W. Chen, J. Miao, Y. Bai, T. Li, and L. Wang, "Fiber-based time and frequency dissemination between THU and NIM," *Proceedings of 2012 IEEE International Frequency Control Symposium*, Baltimore, Maryland, pp. 1-4, May 2012.
- [31] M. Amemiya, M. Imae, Y. Fujii, T. Suzuyama, and S. Ohshima, "Simple time and frequency dissemination method using optical fiber network," *IEEE T. Instrum. Meas.*, vol. 57, no. 5, pp. 878-883, 2008.
- [32] S. Ebenhag, P. Hedekvist, and K. Jaldehag, "Active detection of propagation delay variations in single way time transfer utilizing dual wavelengths in an optical fiber network," *Proceedings of 2011 Joint Conference of the IEEE International Frequency Control and the European Frequency and Time Forum (FCS)*, San Francisco, California, pp. 1-6, May 2011.
- [33] J. Hanssen, S. Crane, and C. Ekstrom, "One-way two-color fiber link for frequency transfer," *Proceedings of 2012 IEEE International Frequency Control Symposium*, Baltimore, Maryland, pp. 1-4, May 2012.
- [34] S. Jefferts, M. Weiss, J. Levine, S. Dilla, E. Bell, and T. Parker, "Two-way time and frequency transfer using optical fibers", *IEEE T. Instrum. Meas.*, vol. 46, no. 2, pp. 209-211, April 1997.
- [35] M. Rost, M. Fujieda, and D. Piester, "Time transfer through optical fibers (TTTOF): progress on calibrated clock comparisons," *Proceedings of 24th European Frequency and Time Forum*, Noordwijk, The Netherlands, April 2010.
- [36] P. Hedekvist and S.-C. Ebenhag, "Time and frequency transfer in optical fibers," Chapter 17 in *Recent Progress in Optical Fiber Research*, InTech, January 25, 2012.
- [37] L. Śliwczynski, P. Krehlik, and M. Lipiński, "Optical fibers in time and frequency transfer," *Meas. Sci. Technol.*, vol. 21, no. 7, pp. 075302-075312, 2010.
- [38] D. Matsakis, private communication, May 2012.
- [39] W. Tseng, M. Li, and C. Liao, "Two-way time transfer via common-path optical link," *Proceedings of Asia-Pacific Radio Science Conference (AP-RASC'01)*, Tokyo, Japan, p. 50, 2001.
- [40] Satellite Time and Ranging Equipment (SATRE), Timetech website: <http://www.timetech.de>
- [41] W. Tseng and H. Lin, "The influence of IF offset on the modem delay measurement," *Proceedings of Asia-Pacific Workshop on Time and Frequency (ATF 2001)*, Xi'an CSAO, China, October 2001.
- [42] O. Celikel and S. San, "Establishment of all digital closed-loop interferometric fiber-optic gyroscope and scale factor comparison for open-loop and all digital closed-loop configurations," *IEEE Sens. J.*, vol. 9, no. 2, pp. 176-186, 2009.
- [43] P. Krehlik, L. Śliwczynski, Ł. Buczek, and M. Lipiński, "Fiber-optic joint time and frequency transfer with active stabilization of the propagation delay," *IEEE T. Instrum. Meas.*, vol. 61, no. 10, pp. 2844-2851, 2012.
- [44] M. Rost, D. Piester, W. Yang, T. Feldmann, T. Wübbena, and A. Bauch, "Time transfer through optical fibers over a distance of 73 km with an uncertainty below 100 ps," *Metrologia*, vol. 49, no. 6, pp. 772-778, 2012.
- [45] L. Śliwczynski, P. Krehlik, A. Czubla, Ł. Buczek, and M. Lipiński, "Dissemination of time and RF frequency via a stabilized fibre optic link over a distance of 420 km," *Metrologia*, vol. 50, no. 2, pp. 133-145, April 2013.
- [46] O. Lopez, A. Kanj, P. Pottie, G. Rovera, J. Achkar, C. Chardonnet, A. Amy-Klein, and G. Santarelli, "Simultaneous remote transfer of accurate timing and optical frequency over a public fiber network," *Appl. Phys. B*, vol. 110, no. 1, pp. 3-6, January 2013.
- [47] W. Tseng, Y. Huang, T. Gotoh, T. Hobiger, M. Fujieda, M. Aida, T. Li, S. Lin, H. Lin, and K. Feng, "First international two-way satellite time and frequency transfer experiment employing dual pseudo-random noise codes," *IEEE T. Ultrason. Ferr.*, vol. 59, no. 3, pp. 531-538, March 2012.

NEW PRODUCTS AND SERVICES

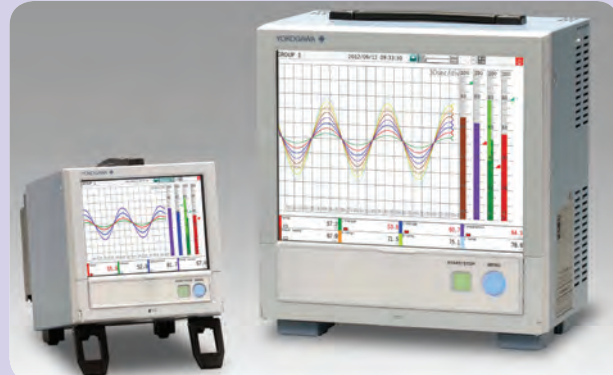
Hexagon Metrology Releases PC-DMIS Gear 2.5



Hexagon Metrology, the largest software developer in the metrology industry, has announced the release of PC-DMIS Gear 2.5, a sophisticated software module designed for basic and advanced gear measurement applications. The new version simplifies measurement routines by using a parameter-driven graphical interface to speed inspections of helical spur, bevel gears and pinions. PC-DMIS Gear 2.5 software is compatible with standard Coordinate Measuring Machines (CMMs), eliminating the need to invest in separate gear measurement equipment. The software also runs on vision CMMs for inspection applications of small spur gears. PC-DMIS is an integrated metrology system used for developing inspection routines, measuring parts, managing data, evaluating and reporting results.

► For more information, visit: www.pcdmis.com

New Yokogawa SMARTDAC+ GP Series Data Acquisition Stations



The new GP series data acquisition stations incorporate Yokogawa's all-new SMARTDAC+ Smart User Interface, Smart Architecture, and Smart Functionality design principles. GP users can measure more input signals, save data for longer time periods, and access that data more readily via touch display screens and an all-new real-time web browser interface. There are two GP models, the large GP20 with a 12.1 in touchscreen and up to 100 input channels, and the smaller GP10 with a 5.7 in touchscreen and up to 30 input channels. Both are portable bench-top units that share the same performance specifications and standard high capacity SD flash memory data storage. These units can be used in a wide range of lab and test applications that require measurement and recording of temperature and other DC sensor input signals at fast sampling rates.

► For more information, visit: www.smartdacplus.com

Rotronic Now Distributes RH Systems Model 473 Dew Point Hygrometer



Rotronic Instrument Corporation is one of the world leaders in providing solutions for measuring, monitoring, and controlling

relative humidity. Rotronic is now representing RH Systems 473 dew point hygrometer throughout the Americas. RH Systems are a world renowned developer of precision chilled mirror hygrometers that are used by standards laboratories and research organizations' worldwide. The Model 473 is a portable instrument equipped with a separate measuring head for both spot and continuous measurement of Dew/Frost point and temperature in air and gas mixtures. Based on the chilled mirror principle, the 473 ensures direct and accurate humidity measurement. and accurate humidity measurement.

► For more information, contact Rose Mannarino: rose@rotronic-usa.com

Fluke Introduces 9190A Ultra-Cool Field Metrology Well



The new Fluke 9190A Ultra-Cool Field Metrology Well is ideal for pharmaceutical, biomedical and food processing applications that demand strict quality control and regulatory process compliance, including on-location validation and calibration of RTDs, thermocouples, thermometers, and other temperature sensors. The 9190A conforms to EURAMET cg-13 guidelines for best measurement practices for temperature dry-block calibrators. This ensures that the 9190A specifications for accuracy, stability, axial (vertical) uniformity, radial (well-to-well) uniformity, loading, and hysteresis have been thoroughly and carefully defined and tested. It has a wide temperature range (-95 to 140 °C) to cover the coldest and warmest temperatures required in pharmaceutical, biomedical and food processing applications, and can operate at ultra-cold temperatures not typically available with a calibration bath.

- ▶ For more information about the Fluke Calibration 9190A Ultra-Cool Field Metrology well, call: 1-877-355-3225

A2LA Accredits Forensic Drug Testing Laboratory

The American Association for Laboratory Accreditation (A2LA) is proud to announce the accreditation of Western Slope Laboratory of Troy, Michigan, as part of the A2LA forensic accreditation program. Western Slope Laboratory performs controlled substances testing and was found through onsite assessment to meet the requirements of ISO/IEC 17025 as well as A2LA's supplemental document, "R221-Specific Requirements: Forensic Examination Accreditation Program - Testing." Western Slope Laboratory (www.westslopelabs.com) received its initial accreditation on May 1st, 2013. Erica A. Guice, Western Slope's director of research and development, commented that "The Western Slope Laboratory team takes great pride in having made a true commitment to the provision of quality testing services and even greater pride in having that effort formally recognized via accreditation by The American Association for Laboratory Accreditation as having met the ISO/IEC 17025:2005 standard. Being the first forensic drug testing laboratory to be accredited by A2LA gives us further gratification given A2LA's substantial role in providing world class accreditation services."

- ▶ For more information about the A2LA Forensic Examination Accreditation Program, contact Karin Athanas at: kathanas@A2LA.org

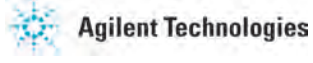
Measurements International introduces new 10 and 20 Channel Coaxial High Resistance Matrix Scanners



MI is proud to announce the latest addition to its line of Matrix Scanners. Designed specifically for use in high resistance measurements, the 4610A (10 Channel) and 4620A (20 Channel) scanners are an ideal addition to any high resistance measurement system whether it be a single input Teraohmmeter device or a high accuracy Dual Source Bridge. The scanners improve high resistance measurement efficiency by eliminating the need to continually change leads when measuring groups of resistors. The input channels can be manually selected from the front panel or via the standard IEEE488 Interface when used in an automated system. The proprietary design employs a completely coaxial sample path from input to output. This ensures leakage paths are minimized allowing measurements up to 1T Ohms with no noticeable uncertainty contribution.

- ▶ For more information, call: 866-684-6393 or email sales@mintl.com

ADVERTISERS' INDEX

Additel www.additel.com	Page 19	
Agilent Technologies www.agilent.com	Page 10	
AIAG www.aiag.org	Page 61	
AssetSmart www.assetsmart.com	Inside Back Cover	
CPEM www.inmetro.gov.br/cpem2014	Page 39	
Collége Français De Metrologie www.metrologie2013.com	Page 45	
Essco Calibration Laboratory www.esscolab.com	Page 11	
FasTest www.fastestinc.com	Page 12	
Fluke Calibration www.fluke.com	Page 6	
Guildline www.guildline.com	Page 13	
Isotech North America www.isotechna.com	Page 17	
Martel Electronics www.martelcalibrators.com	Page 12	
Measurements International www.mintl.com	Page 9	
Mensor Corporation www.mensor.com	Page 5	
Morehouse Instrument Company www.mhforce.com	Page 15	
2014 NCSLI Call for Papers www.ncsl.org	Page 32	
2014 NCSLI Workshop & Symposium www.ncsl.org	Back Cover	
Northrop Grumman www.northropgrumman.com	Inside Front Cover	
Ohm-Labs, Inc. www.ohm-labs.com	Page 23	
Rotronic www.rotronic-usa.com	Page 22	
Thunder Scientific Corporation www.thunderscientific.com	Page 27	
Vaisala www.vaisala.com	Page 15	

Visit AssetSmart at NCSLI Booth 412 / 414

***Think Outside the Boxes.
All of Your Calibration Boxes!***

SMART | CMS

The Corporate Calibration/Maintenance Management System

- ✓ Save Money**
- ✓ Get Better Control**
- ✓ Apply Uniform Metrics**
- ✓ Connect Your Labs**

Now That's SMART.

AssetSmart®
smart asset management software

By PMSC

August 3 - August 7, 2014
Walt Disney World Swan & Dolphin
Orlando, Florida

WORKSHOP SYMPORIUM

and

MEASUREMENT SCIENCE AND THE ENVIRONMENT

